

LUIGI VANVITELLI UNIVERSITY OF
CAMPANIA

DOCTORAL THESIS

Manifestation of cluster structure
of weakly bound light nuclei in
direct nuclear reactions

Author:

Bakytzhan URAZBEKOV

Supervisor:

Prof. Nunzio ITACO

Co-Supervisor:

Prof. Andrey DENIKIN

Department of Mathematics and Physics



Università
degli Studi
della Campania
Luigi Vanvitelli

Declaration of Authorship

I, Bakytzhan URAZBEKOV, declare that this thesis titled, “Manifestation of cluster structure of weakly bound light nuclei in direct nuclear reactions” and the work presented in it are my own. I confirm that:

- This work was done wholly or mainly while in candidature for a research degree at this University.
- Where any part of this thesis has previously been submitted for a degree or any other qualification at this University or any other institution, this has been clearly stated.
- Where I have consulted the published work of others, this is always clearly attributed.
- Where I have quoted from the work of others, the source is always given. With the exception of such quotations, this thesis is entirely my own work.
- I have acknowledged all main sources of help.
- Where the thesis is based on work done by myself jointly with others, I have made clear exactly what was done by others and what I have contributed myself.

Signed:

Date:

*“By the love of God, the nations are created, and you love them like yourself.
Love people as brothers, like freedom, then truth and life are for you. ”*

Abay Qunanbayev

LUIGI VANVITELLI UNIVERSITY OF CAMPANIA

Abstract

Department of Mathematics and Physics

Doctor of Philosophy

Manifestation of cluster structure of weakly bound light nuclei in direct nuclear reactions

by Bakytzhan URAZBEKOV

In this work, the following light weakly bound atomic nuclei are studied: ${}^6\text{He}$, ${}^6\text{Li}$ and ${}^9\text{Be}$. A three-body model $\alpha + 2\text{N}$ for ${}^6\text{He}$ and ${}^6\text{Li}$, and $2\alpha + \text{N}$ model for ${}^9\text{Be}$ are applied. The wave function of the three-body system is obtained within the framework of variational calculations based on the Gaussian basis. The interaction potentials for three-body systems have a Pauli projector, which excludes forbidden states. An analytical expression is obtained for the density distribution function of nuclear matter using the three-body wave function. The root-mean-square matter radii of the ${}^6\text{He}$, ${}^6\text{Li}$, ${}^9\text{Be}$ nuclei are calculated and given comparisons with other sources.

The interactions of ${}^6\text{He}$, ${}^6\text{Li}$ and ${}^9\text{Be}$ with the simplest particles, such as α , d , ${}^3\text{He}$ are studied in detail. On the basis of the calculated density distribution functions of the complex projectiles nuclear matter, the folding interaction potentials are obtained, and the comparison with global optical potentials are performed. The resulting folding interaction potential is applied to calculate the differential cross sections of elastic scattering. Using the Coupled Channels approach for the ${}^9\text{Be}$ induced reactions role of different reaction channels is studied, and deformation parameters are derived. Comparisons of theoretical cross sections with experimental data in inelastic channels for nuclear reactions $\alpha + {}^9\text{Be}$, $d + {}^9\text{Be}$ are given. Within the framework of the Coupled Reaction Channels method, the cross sections for nuclear reactions of single-nucleon and cluster transfers are calculated taking into account the internal structure of the ${}^6\text{He}$, ${}^6\text{Li}$ and ${}^9\text{Be}$ nuclei . The mechanisms are revealed providing the contribution to the transfer of clusters and nucleons in the reactions induced by the ${}^6\text{He}$, ${}^6\text{Li}$ and ${}^9\text{Be}$.

Acknowledgements

I believe that if it were not for these people, then the thesis in the form, in which you are reading it, would not have taken place.

I am very grateful to my scientific supervisors Prof. Nunzio Itaco and Prof. Andrey Denikin, who gave a great chance to implement my scientific ideas. Their suggestions, ideas and comments always gave me goals, raised my understanding of science higher and higher.

Undoubtedly, I think it is worthwhile to thank the staff of the Department of Physics and Astronomy and the CIRCE laboratory: Prof. D'Onofrio, Prof. Gialanella, Giuseppe Porzio, Liz, and all members.

In addition, I would like to express my gratitude to Prof. Vladimir Kukulin (Moscow State University), who gave advice on a scientific career, Prof Sayabek Sakhiyev (Abay State University), who gave not only scientific guides but also about life.

I also want to thank my dear friends Riccardo Mancino and Felice Pignatelli, without whom I could not just cope with simple life questions in Caserta.

Thanks to Prof. Ian Thompson (LLNL) for explaining the input file for the FRESCO code, Prof. Alexandr Volya (MSU), for providing the values of the spectroscopic amplitudes of alpha particles for p-shell nuclei.

I also dedicate my big thanks to my wife Mervet, who has always supported me at all stages of my scientific career, and my newborn daughter Dina, who has been a source of strength and positiveness.

Contents

Declaration of Authorship	i
Abstract	iii
Acknowledgements	iv
Introduction	1
1 The three body model	5
1.1 The basis function	6
1.2 Transformation of the basis function	7
1.3 Overlap matrix elements	8
1.3.1 Partial wave expansion	9
1.3.2 Projection into T matrix	11
1.4 Normalization and correlation density of the three-body wave function	11
1.5 The density distribution function of nuclear matter	12
2 Theoretical models describing nuclear reactions	16
2.1 Description of elastic scattering	16
2.2 The coupled channels method for inelastic scattering	18
2.3 The coupled-reaction-channels method for the transfer reactions	21
2.4 Distorted Wave Born Approximation	23
2.5 Spectroscopic Amplitudes within the Shell Model	25
2.6 Interaction potentials. The double folding model	28
3 Results and discussions	31
3.1 The three-body wave function	31
3.2 The density distribution function of nuclear matter	34
3.3 The $\alpha + {}^6\text{He}$ nuclear reactions	37
3.3.1 Elastic scattering	37
3.3.2 Elastic transfer	39
3.4 The $\alpha + {}^6\text{Li}$ nuclear reactions	41

3.4.1	Elastic scattering	41
3.4.2	Elastic transfer	42
3.5	The d + ${}^9\text{Be}$ nuclear reactions	45
3.5.1	The elastic channel	45
3.5.2	Inelastic scattering	46
3.5.3	One-nucleon transfer reactions	48
3.5.4	Cluster-transfer reaction	52
4	Key findings and Conclusion	57
A	Some aspects from the quantum theory of angular momenta	58
B	Parameters of the three body wave function	61
B.1	Helium-6	61
B.2	Lithium-6	68
B.3	Beryllium-9	76
	Bibliography	84

List of Figures

1	Schematic representation of the cluster structure of some nuclei, and their half-life, if unstable. Alpha particle, proton and neutron are marked in yellow, red and orange, respectively. The allocation of ${}^6\text{He}$, ${}^6\text{Li}$ and ${}^9\text{Be}$ nuclei means the selected as objects of study. Read the text for more details..	2
1.1	The schemes of Jacobi coordinate sets for the three body system.	6
1.2	The (k, pq) scheme of Jacobi coordinate sets for calculation of the density distribution function of nuclear matter in the framework of the three body system.	13
1.3	The (p, qk) scheme of Jacobi coordinate sets for calculation of the density distribution function of nuclear matter in the framework of the three body system.	14
2.1	An incoming plane wave scattering off a body making a distorted wave . .	17
2.2	The arrangement of radial vectors in the DWBA on example of the $A + b \rightarrow a + B$ nuclear reaction. Here $A = a + \nu$ and $B = b + \nu$	24
2.3	Radius vectors for the double folding model.	29
3.1	The correlation function $W(x, y)$ of the three-body wave function of the ground state of ${}^6\text{He}$ in the a) 3D-Plot and b) contour-plot.	33
3.2	The same caption as in the Fig.3.1, but for ${}^6\text{Li}$	33
3.3	The same caption as in the Fig.3.1, but for ${}^9\text{Be}$	34
3.4	The density distribution function of nuclear matter $\rho(R) = \rho_{\alpha}^{(k)} + \rho_N^{(p)} + \rho_N^{(q)}$ illustrated with the densities of the ${}^6\text{He}$ constituents.	34
3.5	The same caption as in Fig. 3.4, but for ${}^6\text{Li}$	35
3.6	The density distribution function of nuclear matter $\rho(R) = \rho_N^{(k)} + \rho_{\alpha}^{(p)} + \rho_{\alpha}^{(q)}$ illustrated with the densities of the ${}^9\text{Be}$ constituents.	35
3.7	The folding potential $V^{DF}(r)$ in the framework of the three-body model. The potential is for the interaction of the α particle with the constituents of ${}^6\text{He}$	38

3.8	<i>a)</i> The differential cross section of the elastic scattering of ${}^6\text{He}$ by α -particles at $E_{lab} = 151\text{MeV}$ with the different potentials: the double folding potential (blue solid), the WS2 (gray dashed) [59] and WS1 (gray dotted) [59]. <i>b)</i> The cross sections of the elastic transfer reaction in terms of the transfer mechanisms: elastic scattering (solid gray), simultanious transfer of $2N$ (gray dashed), sequaential transfer of $2N$ (dotted) and teit coherent sum (solid blue). Experimanetal data taken from [59].	39
3.9	Schematic representation of the elastic transfer nuclear reaction, on the left - the simultaneous transfer of two nucleons, on the right - the sequential transfer of two nucleons.	40
3.10	The folding potential $V^{DF}(r)$ in the framework of the three-body model. The potential is for the interaction of the α particle with the constituents of ${}^6\text{Li}$	41
3.11	<i>a)</i> The differential cross section of the elastic scattering of ${}^6\text{Li}$ by α -particles at $E_{lab} = 166\text{MeV}$ with the different potentials: the double folding potential DF- ${}^6\text{Li}$ (blue solid), the WS1- ${}^6\text{Li}$ (gray dashed) [59]. <i>b)</i> The cross sections of the elastic transfer reaction are represented in terms of the transfer mechanisms: elastic scattering (solid gray), simultanious transfer of d (gray dashed), sequential transfer of $2N$ (dotted) and their coherent sum (solid blue). Experimanetal data taken from [59].	42
3.12	Schematic representation of the elastic transfer nuclear reaction, on the left - the simultaneous transfer of two nucleons, on the right - the sequential transfer of two nucleons.	43
3.13	The angular distribution of elastic scattering data of d from ${}^9\text{Be}$ at laboratory energy 19.5 MeV in comparison with theoretical calculations within the OM (solid curve).	45
3.14	The cross sections of inelastic scattering ${}^9\text{Be}(d, d){}^9\text{Be}^*$ ($E_{exc}=2.43$ MeV) at laboratory energies 19.5 MeV (full circle) and 35 MeV (full triangle). Theoretical curves are described in the text.	47
3.15	The target coupling schemes in the ${}^9\text{Be}(d, p){}^{10}\text{Be}$ (upper) and the ${}^9\text{Be}(d, t){}^8\text{Be}$ (lower) nuclear reactions. The bold two-headed arrows indicate $E\lambda$ transitions. The spin re-orientation effects are indicated as back-pointing arrows.	47
3.16	Differential cross sections for the ${}^9\text{Be}(d, p){}^{10}\text{Be}^*$ reactions at 19.5 MeV leading to different final states (labelled in the figure) in ${}^{10}\text{Be}$. The experimental data are shown in comparison with theoretical results obtained within the CRC method.	49

3.17 Differential cross sections for the ${}^9\text{Be}(d,t){}^8\text{Be}^*$ reactions at 19.5 and 35 MeV leading to different final states (labelled in the figure) in ${}^8\text{Be}$. The experimental data are shown in comparison with theoretical results obtained within the CRC method.	50
3.18 The scheme illustrates the reaction mechanisms taken into account in CRC calculations of the cross sections for ${}^9\text{Be}(d,\alpha){}^7\text{Li}$ reaction.	53
3.19 Differential cross sections for the ${}^9\text{Be}(d,\alpha){}^7\text{Li}$ reactions measured at 19.5 MeV and 35 MeV energy with the ${}^7\text{Li}$ observed in the ground or low-lying excited states in the exit channels.	54
3.20 The scheme illustrates the energy balance of the different intermediate stages for the two-step mechanisms of ${}^9\text{Be}(d,\alpha){}^7\text{Li}$ transfer reaction. The Q -values for the different intermediate channels are shown near the corresponding lines. The numbers near the arrows correspond to the spectroscopic amplitudes of the heaviest reaction participants. For example, spectroscopic amplitude for the ${}^9\text{Be} = {}^8\text{Li} + p$ configuration is equal $S = -0.947$	55
3.21 Contributions of the different mechanisms to the cross section of the ${}^9\text{Be}(d,\alpha){}^7\text{Li}_{g.s.}$ reaction. See Fig. 3.18 for explanation of the curve notations.	56

List of Tables

2.1	Parameters of the M3Y-Paris [50] NN-potential used in double-folding calculations.	30
3.1	Results of the search for the minimum energy of three-body systems found by means of the variational approach: ${}^6\text{He}$, ${}^6\text{Li}$ and ${}^9\text{Be}$. The obtained minimum energy E_{min} , used set of quantum numbers $\gamma \equiv \lambda L S$, the dimension D and the probability P of each γ are listed.	32
3.2	Comparisons of the binding energies obtained by means of variational approach BE_{min} with the experimental data BE_{exp} and the rms matter radii $\langle R_m^2 \rangle^{\frac{1}{2}}$ with other sources.	36
3.3	The parameters of the potentials used in OM calculations for both $\alpha + {}^6\text{He}$ and $\alpha + {}^6\text{Li}$ nuclear reactions. For more details, see the text	40
3.4	Parameterized double-folding potentials of the $d+{}^9\text{Be}$ system used in the OM, CC and DWBA calculations.	46
3.5	Spectroscopic amplitudes used in CRC calculations for the Composite = Core + Nucleon system. The one-nucleon spectroscopic amplitudes have been calculated by means of the <i>ANTOINE</i> code [70]. The alpha spectroscopic amplitudes were taken from [72, 73].	51
B.1	The three-body wave function parameters found by means of variational approach for the ground state of ${}^6\text{He}$	61
B.2	The three-body wave function parameters found by means of variational approach for the ground state of ${}^6\text{Li}$	68
B.3	The three-body wave function parameters found by means of variational approach for the ground state of ${}^9\text{Be}$	76

List of Abbreviations

OM	optical model
DF	double folding
CC	coupled channel
CRC	coupled reaction channels
DWBA	distorted wave Born approximation
SA	spectroscopic amplitude
cm	center of mass

Physical Constants

Speed of Light $c_0 = 2.997\,924\,58 \times 10^8 \text{ m s}^{-1}$ (exact)

Constant Name *Symbol* = *ConstantValue* with units

List of Symbols

Symbol	Name	Unit
ω	angular frequency	rad

to my mom

whom we had immeasurable love of mother and child...

Introduction

Humanity has always been interested in the structure of the Universe - how it works, what it consists of. The understanding and naming of modern objects such as molecules and atoms began in ancient antiquity. The meaning of the word atom, in Greek *ατομος*, is an indivisible, or uncut particle of matter. Modern science has gone much deeper and determined that the atom is actually a complex particle. According to the standard model, the fundamental particles are now six quarks, six leptons and their corresponding anti-particles and so on (for more details, see [1–3]). All this is due to the development of integrated complex technology and detection systems designed to detect even the smallest details in fundamental interactions. Particularly, in the modern nuclear physics the experimental techniques have also been successfully developed in the field of the production of secondary beams. Secondary beams, being rare and unstable nuclei, allow studying the properties and characteristics of the dripline nuclei, challenging the nuclear physics.

In recent years, the study of light weakly bound nuclei has not lost interest due to the successful development of experimental facilities [4–8]. It is known that in nuclei the nucleons tend to group into clusters. A well known manifestation of the cluster structure in heavy nuclei is the α -decay of ^{238}U , first experimentally discovered by E. Rutherford [9]. The α -decay means that it can be formed in the uranium nucleus as an individual subsystem. The first quantitative theory of α -decay was developed by G. Gamov (see [10]). In addition to α -decay, there is also the cluster decay, where the emitted particle can be a heavy nucleus, for example – ^{12}C [11].

In light nuclei, the cluster structure can often be clearly manifested in the dripline region of the nuclear map. These series include such nuclei as ^6He , ^{11}Li , ^{12}Be and other exotic nuclei. However, there are also stable nuclei with prominent cluster structures. These include such nuclei as ^6Li , ^9Be , ^{11}B and others. Numerous experimental data [12–14] allow us to treat such nuclei as multi-cluster systems, including tightly bound α -clusters and valence nucleons

A visual representation of how these nuclei are arranged in the cluster model is illustrated in Fig 1. For these nuclei the relative motion of internal subsystems determines the property and mechanisms of nuclear reactions. In the figure,

we see that the simplest nuclei with a cluster structure are ^6He , ^6Li and ^9Be . Their structure is ideally suited to consideration within the framework of the three-body model. The model has well-known many works on the theoretical approach. Moreover, it should be noted that the interaction of pairs inside these nuclei is also well known, which can be used in constructing a solution to the Schrödinger equation. An important factor is also the number of scattering experiments made to study these nuclei.

There are many theoretical approaches [15–19] devoted to studying the structure of exotic nuclei. In particular, the nuclear excitation function for light exotic nuclei is well reproduced by the No Core Shell Model (NCSM) method [20–23]. The method uses one-particle basis function of the harmonic oscillator, realistic NN, NNN interactions. This method is reduced to solving the A -nucleon Schrödinger equation on a basis containing all possible configurations of A -nucleon oscillator functions. However, the size of the basis grows rapidly with the number of nucleons, the reliability of the NCSM model calculations decreases in the case of heavy nuclei. At present, the capabilities of modern computational machines make it possible to calculate with sufficient accuracy of nuclei with masses $A \leq 16$. For example, in Ref. [21] within the framework of this model, the excitation spectrum of the one-particle basis for the ^9Be nucleus is in good agreement with the experimental data.

The microscopic description, that is, taking into account the NN effective potential, of the break-up reaction was presented in the Resonating Group Method (RGM) [24–26]. Generalization of the RGM consists in constructing overall

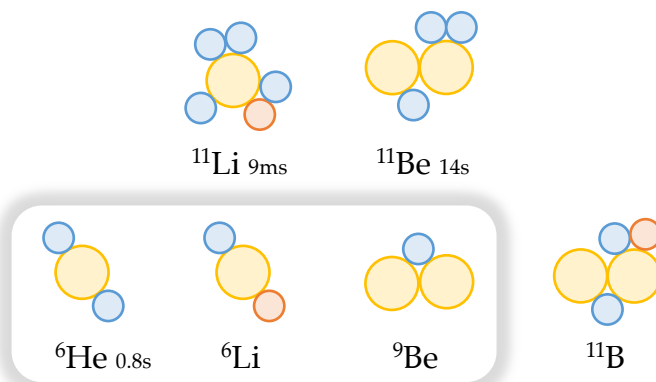


FIGURE 1: Schematic representation of the cluster structure of some nuclei, and their half-life, if unstable. Alpha particle, proton and neutron are marked in yellow, red and orange, respectively. The allocation of ^6He , ^6Li and ^9Be nuclei means the selected as objects of study. Read the text for more details..

mathematically equivalent methods for the simultaneous calculation in the nuclear structures and nuclear reactions. The practical application of this method is also limited in the region of the lightest nuclei due to the lack of computational power in the antisymmetrization process. In the work [27] the algebraic RGM was successfully applied in describing the internal structure ${}^6\text{He}$, ${}^6\text{Li}$ and ${}^8\text{He}$ nuclei, calculated their rms matter and proton and neutron radii, as well as nuclear matter distribution density. Also the fusion reactions at low energies participating ${}^6\text{He}$ were presented.

Similar to the RGM [24], is the Generator Coordinate Method (GCM), if one takes the full model space of the basis Bloch-Brink wave functions [28]. In the framework of the GCM it is possible to carry out calculations for the nuclei with medium masses implementing many clusters. Microscopic three-body calculations for two valence neutrons around a core nucleus have been achieved by many groups to investigate the neutron halo and two-neutron correlation in drip-line nuclei such as ${}^6\text{He}$ and ${}^{14}\text{Be}$ [29, 30]. The ${}^{12}\text{Be}$ using the GCM has been studied [15]. In this work a negative-parity band was found, electromagnetic transition probabilities and partial widths of molecular states were calculated.

In addition to the above theoretical approaches, there is a variational method [31–34]. The method uses the Gaussian function as a basis function, which is convenient for analytical deriving matrix elements of the Hamiltonian. The corresponding Hamiltonian contains a Pauli projector [35], that removes forbidden states. The variational method describes well the internal structures of ${}^6\text{He}$, ${}^6\text{Li}$ and ${}^9\text{Be}$ [32–34]. In particular, the electromagnetic properties, geometric parameters and configuration weights are in good agreement with the methods, where they are obtained by real solutions of three-body problems.

To describe the elastic scattering in the field of a complex potential, one usually uses the Optical Model, first presented in Ref. [36]. Within the framework of this model, the nucleus is considered as a transparent substance that has the ability to absorb. In practice, this method describes the experimental data well providing the direct information on the nucleus-nucleus interaction potential. However, the ambiguity of the optical potential parameters reduces the merits of optical model.

To study the inelastic channels, transfer reactions and their use to describe experimental data the Distorted Wave Born Approximation (DWBA) method has been successfully applied [37]. The DWBA method proved to be appropriate and successful in describing the cross section of nuclear reactions involving ground and low-lying excited nuclear states of single particle type as well as collective nature. The method becomes inadequate, since the reaction leads to

the broad or strongly overlapped final states. In this case the couples channel formalism has to be applied.

Chapter 1

The three body model

The wave function for the three-body system in the current work was calculated within the model proposed in Ref. [31]. The work based on the three body model provides great progress in understanding the structure and properties of the light weakly bound nuclei, like ^6He , ^6Li , ^9Be nuclei. In addition, a lot of research has been done in different directions of physics [31–34, 38–43] using this wave function. Below we list some of them:

- electromagnetic properties;
- low lying excitation spectra;
- root-mean-square charge radii $\langle r_{ch} \rangle^{1/2}$, magnetic μ , quadrupole Q and octupole Ω moments;
- processes of ^6Li interaction with hadrons, including quasi-elastic scattering $(\alpha, 2\alpha)$, (p, d) and $(p, p\alpha)$;
- high energy proton and the lightest nuclei scattering on ^6Li
- scattering of π^\pm -mesons and μ -capture by ^6Li
- parameters of β -decay of ^6He ;
- the thermonuclear reactions in the $\text{D}-^3\text{He}-^9\text{Be}$ plasma;
- properties of the six-quark dibaryons in nuclei with $A=6$ and *etc.*

Since this wave function was widely used, we chose it as the wave function to describe the three-body system in this work.

1.1 The basis function

The three-body wave function of the ${}^9\text{Be}$ nucleus with total spin J and spin projection M_J is represented as

$$\Psi^{JM_J} = \sum_i C_i \psi_i^{JM_J} (k, pq). \quad (1.1)$$

For simplicity the Jacobi coordinates \mathbf{x}_k and \mathbf{y}_k are down, the symbols k , p and q comply with the cluster indices (see Fig. 1.1), and the combination of indices (k, pq) corresponds to a certain choice of Jacobi coordinates \mathbf{x}_k and \mathbf{y}_k of the three-body system, where \mathbf{x}_k is a vector of the relative distance between the pair of particles pq and k , and \mathbf{y}_k is the vector of the relative distance between the center of mass of the pair pq and the particle k . The coefficients C_i in Eq. (ref totwf) are the parameters of the wave function expansion and are found as a result of solving the generalized eigenvalue problem.

The explicit form of the basis functions $\psi_i^\gamma (k, pq)$ is chosen in the form of the multiplication of the spatial and spin wave functions:

$$\psi_i^{JM_J} (k, pq) = [\phi_i^\gamma (k, pq) \times \chi^S]_{JM_J}, \quad (1.2)$$

here the index γ includes the quantum numbers $L\lambda l$. The spatial part $\phi_i^\gamma (k, pq)$ of the wave function (1.2) is constructed using the Gaussian functions:

$$\phi_i^\gamma (k, pq) = x_k^\lambda y_k^l \exp \left(-\frac{1}{2} \alpha_i^{(k)} x_k^2 - \frac{1}{2} \beta_i^{(k)} y_k^2 \right) [Y_\lambda (\hat{\mathbf{x}}_k) \times Y_l (\hat{\mathbf{y}}_k)]_{LM_L}, \quad (1.3)$$

where L and M_L are the total orbital momentum of the system and its projection, λ , l are the orbital moments conjugated to the coordinates \mathbf{x}_k and \mathbf{y}_k respectively, $\alpha_i^{(k)}$, $\beta_i^{(k)}$ are the linear parameters of the three-body wave function.

In order to describe the three-body system within the model [31] one uses three pair pseudo-potential, taking into account forbidden states by the Pauli

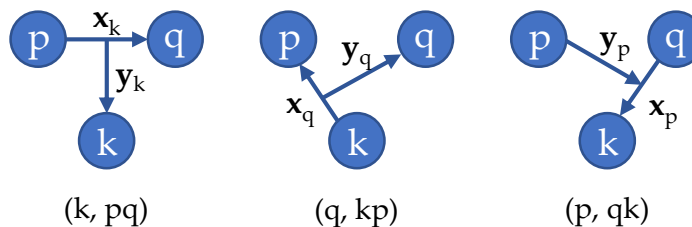


FIGURE 1.1: The schemes of Jacobi coordinate sets for the three body system.

principle:

$$\tilde{V}_{kp} = V_{kp} + \Delta_{kp}, \quad (1.4)$$

where V_{kp} is an interaction potential of kp subsystem, $\Delta_{kp} = \lambda\Gamma$ is an orthogonalizer, λ – constant and Γ is a projector, which for forbidden state f reads:

$$\Gamma = \Gamma(f) = \sum_{m_f} |\phi_{fm_f}(\mathbf{x})\rangle\langle\phi_{fm_f}(\mathbf{x}')|\delta(\mathbf{y} - \mathbf{y}'). \quad (1.5)$$

The Pauli principle plays a huge role in the structure of the nucleus, particularly it does not allow overlapping of two constituent particles.

The three body pseudo-Hamiltonian including kinetic energy and pseudo potentials looks like this

$$\tilde{H} = H_0 + \sum_{k < p} \tilde{V}_{kp}. \quad (1.6)$$

This approach, so-called the method of orthogonalizing pseudo-potentials, was previously developed by the group of V. Kukulin [35], and is widely used not only in the construction of the wave function of the bound state, but also in the scattering theory [44, 45].

1.2 Transformation of the basis function

The main advantage of the basis function (1.2) ofrm is the simplicity of the wave function transformation to an alternative set of Jacobi coordinates. This transformation may be expressed as follows:

$$\begin{pmatrix} \mathbf{x}_k \\ \mathbf{y}_k \end{pmatrix} = \mathbf{T}^{(kq)} \begin{pmatrix} \mathbf{x}_q \\ \mathbf{y}_q \end{pmatrix}, \quad (1.7)$$

where, the $\mathbf{T}^{(kq)}$ matrix reads

$$\mathbf{T}^{(kq)} = \begin{pmatrix} T_{11}^{(kq)} & T_{12}^{(kq)} \\ T_{21}^{(kq)} & T_{22}^{(kq)} \end{pmatrix} = \begin{pmatrix} -\frac{m_p}{m_p+m_q} & 1 \\ -\frac{m_q(m_k+m_p+m_q)}{(m_p+m_q)(m_k+m_q)} & -\frac{m_k}{(m_k+m_q)} \end{pmatrix}. \quad (1.8)$$

The transformation of the spatial part of the wave function from the set (k, qp) into the set (q, kp) can be expressed in the following way [46, 47]

$$\phi_i^\gamma(k, pq) = \sum_{\tilde{\gamma}} A_{\tilde{\gamma}\gamma}^{\mathbf{T}^{(kq)}} \phi_i^{\tilde{\gamma}}(q, kp), \quad (1.9)$$

where the sum is over quantum numbers of the $\tilde{\gamma}$ new set, and the new basis function is

$$\begin{aligned}\phi_i^{\tilde{\gamma}}(q, kp) = & x_q^{\tilde{\lambda}} y_q^{\tilde{l}} \exp\left(-\frac{1}{2}\alpha_i^{(q)}x_q^2 - \frac{1}{2}\beta_i^{(q)}y_q^2 - \rho_i^{(q)}\mathbf{x}_q \cdot \mathbf{y}_q\right) \times \\ & \times [Y_{\tilde{\lambda}}(\hat{\mathbf{x}}_q) \times Y_{\tilde{l}}(\hat{\mathbf{y}}_q)]_{LM_L},\end{aligned}\quad (1.10)$$

where new parameters of the wave function are given by

$$\begin{pmatrix} \alpha_i^{(q)} & \rho_i^{(q)} \\ \rho_i^{(q)} & \beta_i^{(q)} \end{pmatrix} = (\mathbf{T}^{(kq)})^T \begin{pmatrix} \alpha_i^{(k)} & \rho_i^{(k)} \\ \rho_i^{(k)} & \beta_i^{(k)} \end{pmatrix} \mathbf{T}^{(kq)}. \quad (1.11)$$

Note, that for the (k, pq) coordinate set the radial wave function (1.3) does not include the scalar product $\mathbf{x}_k \cdot \mathbf{y}_k$, which means $\rho_i^{(k)} = 0$. For the transformation of basis functions (1.9) the coupling coefficient $A_{\tilde{\gamma}\gamma}^{\mathbf{T}^{(kq)}}$ is defined as follow

$$\begin{aligned}A_{\tilde{\gamma}\gamma}^{\mathbf{T}^{(ka)}} = & \sum_{\lambda_1\lambda_2l_1l_2} \left(\mathbf{T}_{11}^{(kq)}\right)^{\lambda_1} \left(\mathbf{T}_{12}^{(kq)}\right)^{\lambda_2} \left(\mathbf{T}_{21}^{(kq)}\right)^{l_1} \left(\mathbf{T}_{22}^{(kq)}\right)^{l_2} \times \\ & \times E_{\tilde{\lambda}\tilde{l}}^{\lambda_1\lambda_2\lambda l_1l_2lL} \mathcal{D}(\lambda, \lambda_1, \lambda_2) \mathcal{D}(l, l_1, l_2),\end{aligned}\quad (1.12)$$

where, $E_{\tilde{\lambda}\tilde{l}}^{\lambda_1\lambda_2\lambda l_1l_2lL}$ and $\mathcal{D}(\lambda, \lambda_1, \lambda_2)$ come from re-coupling of spherical harmonic functions, which are explicitly given in Appendix A in equations (A.10) and (A.14). The summation is satisfied to the conditions: $\lambda_1 + \lambda_2 = \lambda$, $l_1 + l_2 = l$ and $\lambda + l = \tilde{\lambda} + \tilde{l}$.

1.3 Overlap matrix elements

Within the (k, pq) scheme an overlap matrix element, in particular for the space part $\phi_i^{\gamma}(k, pq)$ of the basis function, is expressed by

$$\begin{aligned}\langle \phi_i^{\gamma}(k, pq) | \phi_j^{\gamma'}(k, pq) \rangle = & \int \int d\mathbf{x}_k d\mathbf{y}_k \phi_i^{\gamma}(k, pq) \left(\phi_j^{\gamma'}(k, pq)\right)^* = \\ = & \int_0^\infty \int_0^\infty dx_k dy_k x_k^{2\lambda+2} y_k^{2l+2} \exp\left(-\frac{1}{2}\alpha_{ij}^{(k)}x_k^2 - \frac{1}{2}\beta_{ij}^{(k)}y_k^2\right) \delta_{\gamma\gamma'} = \\ = & \mathcal{I}_1\left(2\lambda+2, \alpha_{ij}^{(k)}\right) \mathcal{I}_1\left(2l+2, \beta_{ij}^{(k)}\right),\end{aligned}\quad (1.13)$$

where $\alpha_{ij}^{(k)} = \alpha_i^{(k)} + \alpha_j^{(k)}$ and $\beta_{ij}^{(k)} = \beta_i^{(k)} + \beta_j^{(k)}$, the table integral \mathcal{I}_1 may be expressed as

$$\mathcal{I}_1(\lambda, \alpha) = 2^{1+\lambda} \frac{\Gamma(1+\lambda)}{(\alpha)^{1+\lambda}}. \quad (1.14)$$

According to the Eq. 1.10, the new basis function contains the $\rho_i^{(q)} \mathbf{x}_q \cdot \mathbf{y}_q$ scalar product. In order to treat this problem, in this section the overlap matrix elements of the basis functions for the (q, kp) scheme are given by means of two methods. The first is based on the expansion of the exponential function [46], another is in the implementing of $\rho_i^{(q)}$ into the rotation matrix \mathbf{T} [47]. Both methods give the same result. It is important to present these two methods, since both will be used further to derive the density distribution function of nuclear matter in the three-body system.

1.3.1 Partial wave expansion

Overlap matrix elements of the basis functions for the (q, kp) scheme may be written as

$$\langle \phi_i^{\tilde{\gamma}}(q, kp) | \phi_j^{\tilde{\gamma}'}(q, kp) \rangle = \int \int d\mathbf{x}_k d\mathbf{y}_k \phi_i^{\tilde{\gamma}}(q, kp) \left(\phi_j^{\tilde{\gamma}'}(q, kp) \right)^*. \quad (1.15)$$

One must handle with the scalar product $\exp(-\rho \mathbf{x} \cdot \mathbf{y})$ in Eq. (1.10), in which radial and angular parts are mixed. It gives a problem in integration procedure, consequently, special mathematical techniques must be applied. Thus, the expansion of exponential function is given by

$$\exp(-\rho \mathbf{x} \cdot \mathbf{y}) = 4\pi \sum_{nm} \sqrt{2n+1} \epsilon(n, \rho) i_n(|\rho|xy) Y_{nm}(\hat{\mathbf{x}}) Y_{nm}(\hat{\mathbf{y}})^* \quad (1.16)$$

where $i_n(x)$ – modified spherical Bessel function of the first kind, $\epsilon(n, \rho) = (-1)^n$ for $\rho \leq 0$, otherwise it equals to 1. Once radial part is separated, then it can be defined as

$$\begin{aligned} \int_0^\infty \int_0^\infty dx dy x^{2\lambda+n+2} y^{2l+n+2} \exp\left(-\frac{1}{2}\alpha x^2 - \frac{1}{2}\beta y^2\right) i_n(|\rho|xy) = \\ = \mathcal{I}_2(\lambda, l, n, \alpha, \beta, |\rho|) \end{aligned} \quad (1.17)$$

where, the integral \mathcal{I}_2 has analytical form as

$$\begin{aligned} \mathcal{I}_2(\lambda, l, n, \alpha, \beta, |\rho|) = & \sqrt{\frac{\pi}{8}} (2l)!! \Gamma(l + n + \frac{3}{2}) |\rho|^n \beta^{-l-n-\frac{3}{2}} \times \\ & \times \sum_{\kappa=0}^l \frac{\Gamma(\kappa + \lambda + n + \frac{3}{2})}{\kappa!(l-\kappa)!\Gamma(\kappa + n + \frac{3}{2})} \left(\frac{\rho^2}{2\beta}\right)^\kappa \left(\frac{\alpha}{2} - \frac{\rho^2}{2\beta}\right)^{-\kappa-\lambda-n-\frac{3}{2}}. \end{aligned} \quad (1.18)$$

Integration over angular variables can be expressed analytically in the following way

$$\int \int d\hat{\mathbf{x}} d\hat{\mathbf{y}} Y_{00}^{(\kappa\kappa)}(\hat{\mathbf{x}}, \hat{\mathbf{y}}) Y_{L'M'L'}^{(\lambda'l')}(\hat{\mathbf{x}}, \hat{\mathbf{y}}) \left(Y_{LM_L}^{(\lambda l)}(\hat{\mathbf{x}}, \hat{\mathbf{y}}) \right)^* = E_{\lambda l}^{\kappa\kappa 0\lambda' l' LL} \delta_{LL'} \quad (1.19)$$

Using the property of the 9-j symbol with one of the moments equals to zero, $E_{\lambda l}^{\kappa\kappa 0\lambda' l' LL}$ can be reduced as

$$E_{\lambda l}^{\kappa\kappa 0\lambda' l' LL} = U(\lambda L \kappa l'; l \lambda') \frac{\mathcal{C}(\lambda', \lambda, \kappa) \mathcal{C}(l', l, \kappa)}{\sqrt{(2L+1)(2\kappa+1)}}. \quad (1.20)$$

Here, $U(\lambda L \kappa l'; l \lambda')$ – the Racah coefficient (see definition in Appendix A, Eq. A.4).

The Jacobian matrix $\mathbf{J}^{(kq)}$ for transformation from the $\mathbf{x}_k, \mathbf{y}_k$ coordinates to the $\mathbf{x}_q, \mathbf{y}_q$ coordinates gives the $\mathbf{T}^{(kq)}$ matrix

$$\mathbf{J}^{(kq)} = \begin{pmatrix} \frac{\partial \mathbf{x}_k(\mathbf{x}_q, \mathbf{y}_q)}{\partial \mathbf{x}_q} & \frac{\partial \mathbf{x}_k(\mathbf{x}_q, \mathbf{y}_q)}{\partial \mathbf{y}_q} \\ \frac{\partial \mathbf{y}_k(\mathbf{x}_q, \mathbf{y}_q)}{\partial \mathbf{x}_q} & \frac{\partial \mathbf{y}_k(\mathbf{x}_q, \mathbf{y}_q)}{\partial \mathbf{y}_q} \end{pmatrix} = \mathbf{T}^{(kq)}. \quad (1.21)$$

Accordingly, the determinant $|\mathbf{J}^{(kq)}|$ is a determinant of the $\mathbf{T}^{(kq)}$ matrix, which equals to 1:

$$|\mathbf{J}^{(kq)}| = |\mathbf{T}^{(kq)}| = 1. \quad (1.22)$$

Therefore, the integration variables in Eq. (1.15) can be changed without any factorization.

Finally, an expression for the overlap matrix element of the (q, kp) coordinate sets (1.15) can be determined as follow

$$\begin{aligned} \langle \phi_i^{\tilde{\gamma}}(q, kp) | \phi_j^{\tilde{\gamma}'}(q, kp) \rangle &= \int \int d\mathbf{x}_k d\mathbf{y}_k \phi_i^{\tilde{\gamma}}(q, kp) \left(\phi_j^{\tilde{\gamma}'}(q, kp) \right)^* = \\ &= 4\pi \sum_{\tilde{\gamma}\tilde{\gamma}'} A_{\gamma\tilde{\gamma}}^{T^{(kq)}} A_{\tilde{\gamma}'\tilde{\gamma}'}^{T^{(kq)}} \sum_{\kappa} \sqrt{2\kappa+1} \epsilon(\kappa, \rho) E_{\lambda l}^{\kappa\kappa 0\lambda' l' LL} \times \\ &\quad \times \mathcal{I}_2 \left(\frac{\tilde{\lambda}+\tilde{\lambda}'-\kappa}{2}, \frac{\tilde{l}+\tilde{l}'-\kappa}{2}, \kappa, \alpha_{ij}^{(q)}, \beta_{ij}^{(q)}, |\rho_{ij}^{(q)}| \right), \end{aligned} \quad (1.23)$$

where, $\rho_{ij}^{(q)} = \rho_i^{(q)} + \rho_j^{(q)}$.

1.3.2 Projection into T matrix

In this approach the rotation matrix \mathbf{Q} , projecting the scalar product in the radial part of the wave function, is implemented by

$$\mathbf{Q}_i^{(kq)} = \mathbf{T}^{(kq)} \times \begin{pmatrix} 1 & -\frac{\rho_i^{(q)}}{\alpha_i^{(q)}} \\ 0 & 1 \end{pmatrix}. \quad (1.24)$$

Consequently, the radial part of the wave function can be rewritten with no scalar product term as

$$\begin{aligned} \phi_i^{\tilde{\gamma}}(q, kp) = & x_q^{\tilde{\lambda}} y_q^{\tilde{l}} \exp \left(-\frac{1}{2} \alpha_i^{(q)} x_q^2 - \frac{1}{2} \left(\beta_i^{(q)} - \frac{(\rho_i^{(q)})^2}{\alpha_i^{(q)}} \right) y_q^2 \right) \times \\ & \times [Y_{\tilde{\lambda}}(\hat{\mathbf{x}}_q) \times Y_{\tilde{l}}(\hat{\mathbf{y}}_q)]_{LM_L}. \end{aligned} \quad (1.25)$$

One can get easily the expression of the overlap matrix element for the (q, kp) coordinate sets (1.15) can be determined as follow

$$\begin{aligned} \langle \phi_i^{\tilde{\gamma}}(q, kp) | \phi_j^{\tilde{\gamma}'}(q, kp) \rangle = & \int \int d\mathbf{x}_k d\mathbf{y}_k \phi_i^{\tilde{\gamma}}(q, kp) \left(\phi_j^{\tilde{\gamma}'}(q, kp) \right)^* = \\ = & \sum_{\tilde{\gamma}\tilde{\gamma}'} \left(A_{\gamma\tilde{\gamma}}^{\mathbf{Q}_{ij}^{(kq)}} \right)^2 \mathcal{I}_1 \left(2\tilde{\lambda} + 2, \alpha_{ij}^{(q)} \right) \mathcal{I}_1 \left(2\tilde{l} + 2, \left(\beta_{ij}^{(q)} - \frac{(\rho_{ij}^{(q)})^2}{\alpha_{ij}^{(q)}} \right) \right) \delta_{\tilde{\gamma}\tilde{\gamma}'}. \end{aligned} \quad (1.26)$$

Analogously, changing the integration variables is carried out with no factorizations due to the $|\mathbf{Q}_i^{(kq)}| = 1$. Notably, in this case of the rotation matrix \mathbf{Q}_{ij} the coefficient $A_{\gamma\tilde{\gamma}}^{\mathbf{Q}_{ij}^{(kq)}}$ becomes depended on the ij indexes as well.

1.4 Normalization and correlation density of the three-body wave function

Using the overlap matrix elements the normalization of the total three-body wave function is given by

$$\begin{aligned} \mathcal{N}^{(k)} = & \langle \Psi^{JM_J} | \Psi^{JM_J} \rangle = \sum_{\gamma} \mathcal{N}_{\gamma}^{(k)}, \\ \mathcal{N}_{\gamma}^{(k)} = & \sum_{ij} C_i C_j \mathcal{I}_1 \left(\lambda, \alpha_{ij}^{(k)} \right) \mathcal{I}_1 \left(l, \beta_{ij}^{(k)} \right). \end{aligned} \quad (1.27)$$

For the alternative set of Jacobi coordinates the overlap of the total wave function is given by

$$\mathcal{N}^{(q)} = \langle \Psi^{JM_J} | \Psi^{JM_J} \rangle = \sum_{\gamma} \sum_{\gamma'} \mathcal{N}_{\gamma\gamma'}^{(q)} \quad (1.28)$$

According to the Eq. (1.19) the sum in the latter expression is limited with the condition $\delta_{LL'}$ only. Using the analytical form of overlap matrix element (1.18), $\mathcal{N}_{\gamma\gamma'}^{(q)}$ can be given by

$$\begin{aligned} \mathcal{N}_{\gamma\gamma'}^{(q)} = & 4\pi \sum_{ij} C_i C_j \sum_{\tilde{\gamma}\tilde{\gamma}'} A_{\gamma\tilde{\gamma}}^{\mathbf{T}(kq)} A_{\gamma'\tilde{\gamma}'}^{\mathbf{T}(kq)} \times \\ & \times \sum_{\kappa} \sqrt{2\kappa + 1} \epsilon(\kappa, \rho_{ij}^{(k)}) E_{\lambda l}^{\kappa\kappa 0\lambda' l' LL} \times \\ & \times \mathcal{I} \left(\frac{\tilde{\lambda} + \tilde{\lambda}' - \kappa}{2}, \frac{\tilde{l} + \tilde{l}' - \kappa}{2}, \kappa, \alpha_{ij}^{(q)}, \beta_{ij}^{(q)}, |\rho_{ij}^{(q)}| \right), \end{aligned} \quad (1.29)$$

or using the Eq. (1.26)

$$\begin{aligned} \mathcal{N}_{\gamma\gamma'}^{(q)} = & \sum_{ij} C_i C_j \sum_{\tilde{\gamma}} \left(A_{\gamma\tilde{\gamma}}^{\mathbf{Q}_{ij}^{(kq)}} \right)^2 \times \\ & \times \mathcal{I}_2 \left(\tilde{\lambda}, \tilde{l}, \alpha_{ij}^{(q)}, \left(\beta_{ij}^{(q)} - \frac{(\rho_{ij}^{(q)})^2}{\alpha_{ij}^{(q)}} \right) \right). \end{aligned} \quad (1.30)$$

A correlation density function of the total wave function (1.1) can be expressed in the following way

$$\begin{aligned} W(x_k, y_k) &= \sum_{\gamma} W_{\gamma}(x_k, y_k) \\ W_{\gamma}(x_k, y_k) &= \sum_{ij} C_i C_j x_k^{2+2\lambda} y_k^{2+2l} \exp \left(-\frac{1}{2} \alpha_{ij}^{(k)} x_k^2 - \frac{1}{2} \beta_{ij}^{(k)} y_k^2 \right). \end{aligned} \quad (1.31)$$

1.5 The density distribution function of nuclear matter

An operator of matter density distribution of the three body system takes the sums of all three clusters and brings it from the center of system mass (see. Fig. 1.2, 1.3)

$$\rho(R) = \sum_{i=k,p,q} \rho_{\iota}^{(i)}(R), \quad (1.32)$$

where ι stands for the α particle or the nucleon inside the three-body system.

In this work the valence nucleons are treated like structureless body, while the α -cluster has own density distribution function of nuclear matter in a form

$$\rho_\alpha(r) = \rho_0 \exp(-\gamma_0 r^2) \quad (1.33)$$

where parameters $\gamma_0 = 0.7024$, $\rho_0 = 0.4229$ [48]. Corresponding matrix elements of the density function for both the nucleon and the α -cluster, which are spectators in the three-body system (k , pq), can be written as

$$\begin{aligned} \rho_N^{(k)}(R) &= \sum_{\gamma} \sum_{ij} \langle \varphi_i^\gamma(k, pq) | \delta(\mathbf{R} - y_0^{(k)} \mathbf{y}_k) | \varphi_j^\gamma(k, pq) \rangle \\ \rho_\alpha^{(k)}(R) &= \sum_{\gamma} \sum_{ij} \langle \varphi_i^\gamma(k, pq) | \rho_\alpha(\mathbf{r}) | \varphi_j^\gamma(k, pq) \rangle \end{aligned} \quad (1.34)$$

Here \mathbf{r} is the radius-vector, shown in Figures 1.2 and 1.3.

Using the basis function in the (k , pq) coordinate set, one can express the density function of the spectator of the three body system (p , qk), i.e. of the p -particle within the (p , qk) scheme, using the transformation (1.9) into the (p , qk) set as follows:

$$\begin{aligned} \rho_N^{(q)}(R) &= \sum_{\gamma\tilde{\gamma}} \sum_{ij} \left(A_{\gamma\tilde{\gamma}}^{\mathbf{Q}_{ij}} \right)^2 \langle \varphi_{\tilde{\gamma}}(q, kp) | \delta(\mathbf{R} - \mathbf{y}_q) | \varphi_{\tilde{\gamma}}(q, kp) \rangle \\ \rho_\alpha^{(q)}(R) &= \sum_{\gamma\tilde{\gamma}} \sum_{ij} \left(A_{\gamma\tilde{\gamma}}^{\mathbf{Q}_{ij}} \right)^2 \langle \varphi_{\tilde{\gamma}}(q, kp) | \rho_\alpha(\mathbf{r}) | \varphi_{\tilde{\gamma}}(q, kp) \rangle. \end{aligned} \quad (1.35)$$

The superscript (kq) in the rotation matrix $\mathbf{Q}_{ij}^{(kq)}$ is omitted here, and it will be done further for simplicity. With the properties of the spherical functions, partial expansion of the exponent function (1.16) and pre-defined table integrals

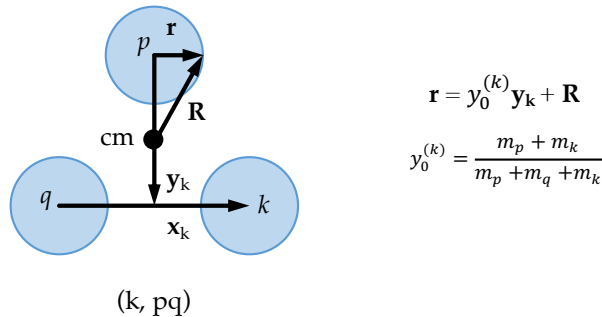


FIGURE 1.2: The (k , pq) scheme of Jacobi coordinate sets for calculation of the density distribution function of nuclear matter in the framework of the three body system.

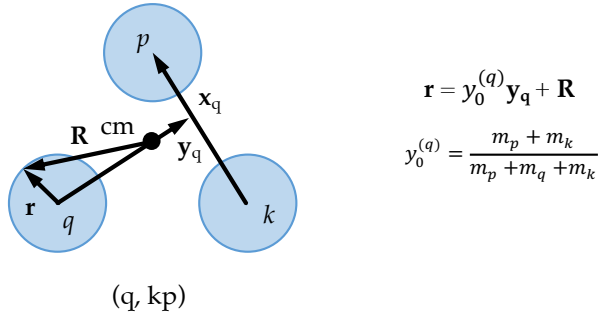


FIGURE 1.3: The (p, qk) scheme of Jacobi coordinate sets for calculation of the density distribution function of nuclear matter in the framework of the three body system.

(1.18) and (1.14) above mentioned six and eight dimensional integrals may be expressed analytically. In particular, for the spectators in the (k, qp) set the density functions are defined like

$$\begin{aligned} \rho_k^{(N)}(R) &= \sum_{\gamma} \sum_{ij} C_i C_j R^{2+2l} \mathcal{I}_1 \left(2 + 2\lambda, \alpha_{ij}^{(k)} \right) \exp \left(-\frac{1}{2} \beta_{ij}^{(k)} \left(y_0^{(k)} R \right)^2 \right) \\ \rho_k^{(\alpha)}(R) &= (4\pi)^2 \rho_0 \exp(-\gamma_0 R^2) \sum_{\gamma} \sum_{ij} \mathcal{I}_1 \left(2 + 2\lambda, \alpha_{ij}^{(k)} \right) \times \\ &\quad \times \mathcal{I}_2 \left(l, 0, (\beta_{ij}^{(k)} + 2\gamma_0) \left(y_0^{(k)} \right)^2, 2\gamma_0 R \right). \end{aligned} \quad (1.36)$$

The density distribution function of the nuclear matter for the N spectators in the (p, qk) three-body system can be written as follow

$$\begin{aligned} \rho_q^{(N)}(R) &= \sum_{\gamma\tilde{\gamma}} \sum_{ij} C_i C_j \tilde{A}_{\gamma\tilde{\gamma}}^{(N)}(\mathbf{Q}_{ij}, R)^2 \times \\ &\quad \times \exp \left(-\frac{1}{2} \left(\beta_{ij}^{(q)} - \frac{(\rho_{ij}^{(q)})^2}{\alpha_{ij}^{(q)}} \right) \left(y_0^{(q)} R \right)^2 \right) \end{aligned} \quad (1.37)$$

The coefficient of transformation of the basis function (1.12) now depends on R and it has form as

$$\begin{aligned} \tilde{A}_{\gamma\tilde{\gamma}}^{(N)}(\mathbf{Q}_{ij}, R) &= \sum_{\lambda_1 \lambda_2 l_1 l_2} (Q_{11})^{\lambda_1} (Q_{12})^{\lambda_2} (Q_{21})^{l_1} (Q_{22})^{l_2} \times \\ &\quad \times E_{\tilde{\lambda}\tilde{l}}^{\lambda_1 \lambda_2 \lambda l_1 l_2 l L} \mathcal{D}(\lambda, \lambda_1, \lambda_2) \mathcal{D}(l, l_1, l_2) \times \\ &\quad \times R^{\lambda+l-\ell/2} \mathcal{I}_1 \left(\ell + 2, \alpha_{ij}^{(q)} \right)^{1/2}, \end{aligned} \quad (1.38)$$

where $\ell = \lambda_1 + \lambda_2 + l_1 + l_2$, and the sum is carried out in conditions: $\lambda_1 + \lambda_2 = \lambda$, $l_1 + l_2 = l$ and $\lambda + l = \tilde{\lambda} + \tilde{l}$.

The density distribution function of the nuclear matter for the α spectator in the (p, qk) scheme has the form

$$\rho_q^{(\alpha)}(R) = \sum_{\gamma\tilde{\gamma}} \sum_{ij} C_i C_j \tilde{A}_{\gamma\tilde{\gamma}}^{(\alpha)}(\mathbf{Q}_{ij}, R)^2 \times \\ \times \exp(-\frac{1}{2}\gamma_0 R^2) \quad (1.39)$$

where its transformation coefficient also depends on R , and turns to

$$\tilde{A}_{\gamma\tilde{\gamma}}^{(\alpha)}(\mathbf{Q}_{ij}, R) = \sum_{\lambda_1 \lambda_2 l_1 l_2} (Q_{11})^{\lambda_1} (Q_{12})^{\lambda_2} (Q_{21})^{l_1} (Q_{22})^{l_2} \times \\ \times E_{\tilde{\lambda}\tilde{l}}^{\lambda_1 \lambda_2 \lambda l_1 l_2 l L} \mathcal{D}(\lambda, \lambda_1, \lambda_2) \mathcal{D}(l, l_1, l_2) \times \\ \times \mathcal{I}_2 \left(\lambda + l - \frac{1}{2}\ell, 0, \left(\left(\beta_{ij}^{(q)} - \frac{(\rho_{ij}^{(q)})^2}{\alpha_{ij}^{(q)}} \right) + 2\gamma_0 \right) y_0^{(q)2}, 2\gamma_0 R \right)^{1/2} \times \\ \times \mathcal{I}_1 \left(\ell + 2, \alpha_{ij}^{(q)} \right), \quad (1.40)$$

where $\ell = \lambda_1 + \lambda_2 + l_1 + l_2$, and the sum is carried out in conditions: $\lambda_1 + \lambda_2 = \lambda$, $l_1 + l_2 = l$ and $\lambda + l = \tilde{\lambda} + \tilde{l}$.

Chapter 2

Theoretical models describing nuclear reactions

2.1 Description of elastic scattering

Descriptions of the scattering of two nuclei are considered in this chapter when the interaction between them is a potential U which may depend on the spins of the two nuclei but not on their internal coordinates. Thus, it cannot excite the nuclei internally or cause the transfer between them. It can only change their relative motion and, perhaps, reorient spins to each other or to the orbital motion. In general, U will be complex.

In the case of the colliding the $a + A$ particles without spin the potential $U(r)$ is central, depending only on the magnitude of the channel coordinate \mathbf{r} . The corresponding Shrödinger equation may be written explicitly

$$\left(E + \frac{\hbar^2}{2\mu} \nabla^2 - U(r) \right) \chi(\mathbf{r}) = 0 \quad (2.1)$$

where μ is the reduced mass of the $a+A$ system, E is the energy in the centre-of-mass system. The $\chi(\mathbf{r})$ wave function is known as distorted waves describing elastic scattering. The expression "distorted wave" is meant to denote distortion away from the plane wave form due to the presence of the distorting potential $U(r)$ (see Fig. 2.1). Asymptotically, it has the form of an incident plane wave plus outgoing (scattered) spherical waves

$$\chi^{(+)}(\mathbf{k}, \mathbf{r}) \rightarrow e^{i\mathbf{k}\cdot\mathbf{r}} + f(\theta) \frac{1}{\mathbf{r}} e^{ikr}, \quad \mathbf{r} \rightarrow \infty \quad (2.2)$$

where $f(\theta)$ is the scattering amplitude. The (+) superscript stands for outgoing plane wave, while incoming spherical waves is the time-reverse of the $\chi^{(+)}$

$$\chi^{(-)}(\mathbf{k}, \mathbf{r}) = (\chi^{(+)}(-\mathbf{k}, \mathbf{r}))^* \quad (2.3)$$

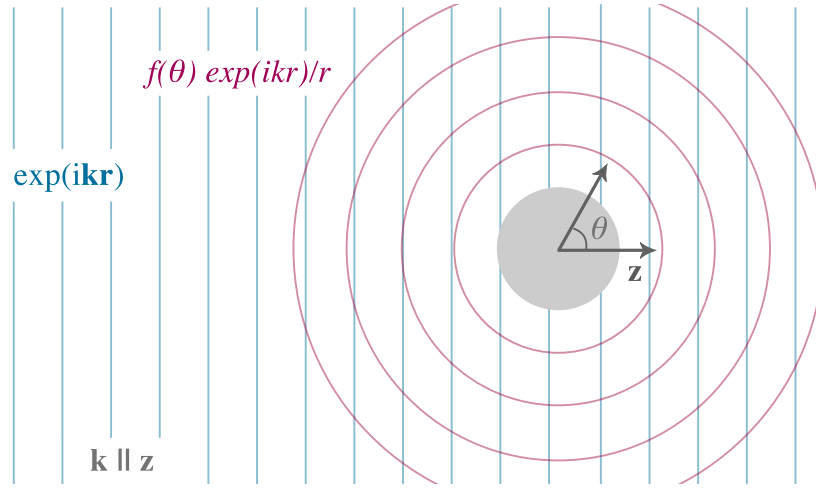


FIGURE 2.1: An incoming plane wave scattering off a body making a distorted wave

Using the partial wave expansion

$$\chi^{(+)}(\mathbf{k}, \mathbf{r}) = \frac{4\pi}{kr} \sum_{LM} i^L \chi_L(k, r) Y_{LM}(\hat{\mathbf{r}}) \left(Y_{LM}(\hat{\mathbf{k}})\right)^*, \quad (2.4)$$

A solution for Eq. (2.1) in the absence of any interaction potential, $U(r) = 0$, is given by

$$\chi^{(+)}(\mathbf{k}, \mathbf{r}) \rightarrow e^{i\mathbf{k}\cdot\mathbf{r}}, \quad \mathbf{r} \rightarrow \infty, \quad (2.5)$$

for radial part only is written as

$$\chi_L(k, r) \rightarrow kr j_L(kr), \quad r \rightarrow \infty, \quad (2.6)$$

where $j_L(kr)$ is the usual spherical Bessel function. The $\chi_L(k, r)$ radial function satisfies the radial Shrödinger equation

$$\left(\nabla_r + k^2 - \frac{L(L+1)}{r^2} - \frac{2\mu}{\hbar^2} U(r)\right) \chi_L(k, r) = 0, \quad (2.7)$$

where $k^2 = \frac{2\mu E}{\hbar^2}$.

In the case of the interaction potential has a more sophisticated form, including both Coulomb and nuclear short-range potentials, the radial Shrödinger equation (2.7) may be rewritten as

$$\left(\nabla_r + k^2 - \frac{2\eta k}{r} - \frac{L(L+1)}{r^2} - \frac{2\mu}{\hbar^2} U(r)\right) \chi_L(k, r) = 0, \quad (2.8)$$

where η is the usual Sommerfeld parameter with the Z charge numbers

$$\eta = \frac{Z_a Z_A e^2 \mu}{\hbar^2 k}$$

At the radius r_0 , where the nuclear potential is negligible, Eq. (2.8) has the solution, which can be expressed in terms of the H_L outgoing and H_L^* incoming Coulomb functions, as follow

$$\chi_L(k, r) \rightarrow \frac{i}{2} e^{i\sigma_L} (H_L(kr_0)^* - S_L H_L(kr_0)), \quad r \rightarrow r_0 \quad (2.9)$$

where σ_L is the Coulomb phase shift, and it is given with the Γ Gamma function as follow

$$\sigma_L = \text{Arg}(\Gamma(L + 1 + i\eta))$$

In practice, the radial Eq. (2.8) is solved by numerical integration from $r \approx 0$, then, matched the value and the slope of the result onto the form (2.9) at $r = r_0$. This procedure then gives a value for the S_L scattering matrix elements. Having the S_L matrix elements, the amplitude of the elastic scattering, analogous from Eq. (2.2), for the $\chi_L(k, r)$ wave function in the Eq. (2.8) is given by

$$f(\theta) = \frac{1}{2ik} \sum_L (2L + 1) e^{2i\sigma_L} (S_L - 1) P_L(\cos(\theta)) \quad (2.10)$$

where $P_L(x)$ is the Legendre polynomials, which are solutions to the Legendre differential equation. By means of the Rutherford scattering amplitude

$$f_C(\theta) = -\frac{\eta}{2k \sin^2(\frac{1}{2}\theta)} e^{(i\eta \ln(\sin^2(\frac{1}{2}\theta)) + 2i\sigma_0)} \quad (2.11)$$

the differential cross section of the elastic scattering has the form

$$\frac{d\sigma_\alpha}{d\Omega} = |f_C(\theta) + f(\theta)|^2. \quad (2.12)$$

The expression (2.12) allows thus to provide comparison with the obtained experimental data.

2.2 The coupled channels method for inelastic scattering

The elastic scattering of the projectile a by the nucleus A has been denoted by $\alpha = a + A$. Let $\alpha' = a + A^*$ be an inelastic channel, in which only the A

nucleus has an extra excitation. In the framework of the coupled channel (CC) approach the total wave function Ψ for the system may be written as

$$\Psi = \phi_\alpha(x) \chi_\alpha(\mathbf{r}_\alpha) + \phi_{\alpha'}(x) \chi_{\alpha'}(\mathbf{r}_{\alpha'}) \quad (2.13)$$

where \mathbf{r} is the channel coordinate for the partitions α or α' , x represents the corresponding internal coordinates. The total wave function can be part of the Shrödinger equation kind of

$$H\Psi = E\Psi \quad (2.14)$$

with the Hamiltonian appropriate particular for the α partition

$$H = H_\alpha + K_\alpha + V_\alpha. \quad (2.15)$$

where $H_\alpha \equiv H_a + H_A$ is the internal Hamiltonian for the nuclei a and A , K_α is the kinetic energy operator of relative motion and V_α is the interaction potential operator. The wave functions of ground $\phi_\alpha(x)$ and excited state $\phi_{\alpha'}(x)$, being eigenfunctions of the internal Hamiltonian H_α

$$\begin{aligned} H_\alpha \phi_\alpha(x) &= \varepsilon_\alpha \phi_\alpha(x) \\ H_\alpha \phi_{\alpha'}(x) &= \varepsilon_{\alpha'} \phi_{\alpha'}(x), \end{aligned} \quad (2.16)$$

have an orthonormality property of the form

$$\int dx (\phi_\alpha(x))^* \phi_{\alpha'}(x) = \delta_{\alpha\alpha'}. \quad (2.17)$$

Using the expression of total wave function (2.13), multiplying Eq. (2.14) from the left by the ϕ_α^* function, then, by the $\phi_{\alpha'}^*$ function, the two coupled equations can be defined in the following form

$$\begin{aligned} (E - \varepsilon_\alpha - K_\alpha - \langle \alpha | V_\alpha | \alpha \rangle) \chi_\alpha(\mathbf{r}) &= \langle \alpha | V_\alpha | \alpha' \rangle \chi_{\alpha'}(\mathbf{r}) \\ (E - \varepsilon_\alpha - K_\alpha - \langle \alpha' | V_\alpha | \alpha' \rangle) \chi_{\alpha'}(\mathbf{r}) &= \langle \alpha' | V_\alpha | \alpha \rangle \chi_\alpha(\mathbf{r}) \end{aligned} \quad (2.18)$$

where $\langle \alpha | V_\alpha | \alpha \rangle$, or $\langle \alpha' | V_\alpha | \alpha \rangle$, is the matrix element of V_α . In particular, the matrix element $\langle \alpha' | V_\alpha | \alpha \rangle$ is given by

$$\begin{aligned} \langle \alpha' | V_\alpha | \alpha \rangle &= \int dx \phi'_\alpha(x) V_\alpha(x, \mathbf{r}) \phi_\alpha(x) = \\ &= V_{\alpha'\alpha}(\mathbf{r}). \end{aligned} \quad (2.19)$$

An expansion of the coupling potential $V_{\alpha'\alpha}(\mathbf{r})$ into the λ multipoles can be given as follow

$$V_{\alpha'\alpha}(\mathbf{r}) = \sum_{\lambda\mu} V_{\alpha'\alpha}^{\lambda\mu}(r) Y_{\lambda\mu}(\hat{r}) \quad (2.20)$$

If the potential shape has a deformation, the nuclear potential can be constructed as

$$V_\alpha(x, \mathbf{r}) \equiv U(r - \delta(\hat{r}')) \quad (2.21)$$

where \hat{r}' denotes angular coordinates of (θ, ϕ) referred to the intrinsic reference frame. The function $\delta(\hat{r}')$ is normally expanded in multipoles

$$\delta(\hat{r}') = \sum_{\lambda} \delta_{\lambda} Y_{\lambda 0}(\hat{r}'). \quad (2.22)$$

In the collective model, the ground and excited states are characterized by their angular momenta I_i and I_f with projections M_i and M_f , respectively. For these state the relevant matrix element of the $V_{\alpha'\alpha}^{\lambda\mu}$ operator is described using the Wigner-Eckart theorem by

$$\langle I_i M_i | V_{\alpha'\alpha}^{\lambda\mu} | I_f M_f \rangle = \sqrt{2I_i + 1} \langle I_f M_f \lambda \mu | I_i M_i \rangle \langle I' | V_{\alpha'\alpha}^{\lambda} | I \rangle. \quad (2.23)$$

Using the definitions, (2.21) and (2.22), the reduced matrix element of radial multipoles from Eq. (2.23) can be rewritten as follow

$$\langle I_i | V_{\alpha'\alpha}^{\lambda\mu} | I_f \rangle = -\frac{\langle I_i | \delta_{\lambda} | I_f \rangle}{\sqrt{4\pi}} \frac{dU(r)}{dr} \quad (2.24)$$

where

$$\langle I_i | \delta_{\lambda} | I_f \rangle = \sqrt{2I_f + 1} \langle I_f M_f \lambda 0 | I_i M_i \rangle \langle \chi | \delta | \chi \rangle \delta_{M_i M_f}. \quad (2.25)$$

The matrix element $\langle \chi | \delta | \chi \rangle$ is the expectation value of the operator δ_{λ} in the internal state of the deformed nucleus. In the framework of the rotational model it can be given with the deformation length β_{λ} as follow

$$\langle \chi | \delta | \chi \rangle = R_0 \beta_{\lambda} \quad (2.26)$$

where R_0 is an average radius of the interaction potential.

The general asymptotic behaviour of the χ_{α} elastic channel can be taken from Eq. (2.2), while the inelastic channel $\chi_{\alpha'}$ may have

$$\chi_{\alpha'}(\mathbf{r}_{\alpha'}) \rightarrow f_{\alpha'}(\theta) \frac{e^{ikr_{\alpha'}}}{r}, \quad \mathbf{r}_{\alpha'} \rightarrow \infty \quad (2.27)$$

Note, that the plane wave expression doesn't present in this equation - only outgoing wave presents. A relevant differential cross section for the inelastic channel is obtained from the coefficient of the outgoing wave as follow

$$\frac{d\sigma_{\alpha'}(\theta)}{d\Omega} = \frac{k_{\alpha'}}{k_{\alpha}} |f_{\alpha'}(\theta)|^2. \quad (2.28)$$

The wave numbers k_{α} and $k_{\alpha'}$ follow from the energy conservation

$$E = \varepsilon_{\alpha} + \frac{\hbar^2 k_{\alpha}}{2\mu} = \varepsilon_{\alpha'} + \frac{\hbar^2 k_{\alpha'}}{2\mu}. \quad (2.29)$$

2.3 The coupled-reaction-channels method for the transfer reactions

Consider a model for the $a + A \rightarrow b + B$ nuclear reaction, in which entrance and exit channels are denoted as α and β respectively. The Ψ total wave function for this model may be given as

$$\Psi = \chi_{\alpha}(\mathbf{r}_{\alpha}) \phi_{\alpha}(x_{\alpha}) + \chi_{\beta}(\mathbf{r}_{\beta}) \phi_{\beta}(x_{\beta}). \quad (2.30)$$

with a model Hamiltonian H such that $(E - H)\Psi = 0$. From the projections of this equation onto the two channels,

$$\begin{aligned} \langle \chi_{\alpha} | (E - H) | \Psi \rangle &= 0 \\ \langle \chi_{\beta} | (E - H) | \Psi \rangle &= 0 \end{aligned} \quad (2.31)$$

with the two equivalent forms of H ,

$$\begin{aligned} H &= H_{\alpha} + K_{\alpha} + V_{\alpha} \\ H &= H_{\beta} + K_{\beta} + V_{\beta} \end{aligned} \quad (2.32)$$

one can get a pair of coupled equations for χ_{α} and χ_{β} :

$$\begin{aligned} [(E - \varepsilon_{\alpha}) - K_{\alpha} - \langle \alpha | V_{\alpha} | \alpha \rangle] \chi_{\alpha}(\mathbf{r}_{\alpha}) &= \langle \alpha | H - E | \beta \rangle \chi_{\beta} \\ [(E - \varepsilon_{\beta}) - K_{\beta} - \langle \beta | V_{\beta} | \beta \rangle] \chi_{\beta}(\mathbf{r}_{\beta}) &= \langle \beta | H - E | \alpha \rangle \chi_{\alpha}. \end{aligned} \quad (2.33)$$

These are *the coupled-reaction-channels* (CRC) equations. They are integro-differential equations, as may be seen more explicitly in the form

$$\begin{aligned} [(E - \varepsilon_\alpha) - K_\alpha - \langle \alpha | V_\alpha | \alpha \rangle] \chi_\alpha(\mathbf{r}_\alpha) &= \int d\mathbf{r}_\beta K_{\alpha\beta}(\mathbf{r}_\alpha, \mathbf{r}_\beta) \chi_\beta(\mathbf{r}_\beta) \\ [(E - \varepsilon_\beta) - K_\beta - \langle \beta | V_\beta | \beta \rangle] \chi_\beta(\mathbf{r}_\beta) &= \int d\mathbf{r}_\alpha K_{\beta\alpha}(\mathbf{r}_\beta, \mathbf{r}_\alpha) \chi_\alpha(\mathbf{r}_\alpha) \end{aligned} \quad (2.34)$$

where the kernels are

$$\begin{aligned} K_{\alpha\beta}(\mathbf{r}_\alpha, \mathbf{r}_\beta) &= J_{\alpha\beta} \int d\zeta_\alpha \phi_\alpha^*(x_\alpha) (H - E) \phi_\beta(x_\beta) \\ K_{\beta\alpha}(\mathbf{r}_\beta, \mathbf{r}_\alpha) &= J_{\beta\alpha} \int d\zeta_\beta \phi_\beta^*(x_\beta) (H - E) \phi_\alpha(x_\alpha). \end{aligned} \quad (2.35)$$

Here the internal coordinates have been transformed from the set x_α to the set $(\zeta_\alpha, \mathbf{r}_\beta)$, where the ζ_α are independent of \mathbf{r}_β . Also, $J_{\alpha\beta}$ is the Jacobian of this transformation. Then $J_{\beta\alpha}$ is the Jacobian for the analogous transformation from x_β to $(\zeta_\beta, \mathbf{r}_\alpha)$.

Since the off-diagonal matrix elements of V_α are small, they have little effect on the elastic scattering and may be neglected on the right side. This implies that the elastic scattering in the entrance α channel is described well by the potential $\langle \alpha | V_\alpha | \alpha \rangle$, and the potential $\langle \beta | V_\beta | \beta \rangle$ describes well the elastic scattering in the β channel. By doing this approximation, Eq. (2.33) may be rewritten as

$$\begin{aligned} [(E - \varepsilon_\alpha) - K_\alpha - \langle \alpha | V_\alpha | \alpha \rangle] \chi_\alpha(\mathbf{r}_\alpha) &\approx 0 \\ [(E - \varepsilon_\beta) - K_\beta - \langle \beta | V_\beta | \beta \rangle] \chi_\beta(\mathbf{r}_\beta) &\approx \langle \beta | H - E | \alpha \rangle \chi_\alpha \\ &\approx \langle \beta | V_\alpha | \alpha \rangle \chi_\alpha + \langle \beta | \alpha \rangle (H_\alpha - E_\alpha) \chi_\alpha \\ &\approx \langle \beta | V_\alpha | \alpha \rangle \chi_\alpha \end{aligned} \quad (2.36)$$

Here the prior interaction, that is the interaction of the α channel, is used. The non-orthogonal term $\langle \beta | \alpha \rangle (H_\alpha - E_\alpha) \chi_\alpha$ vanishes because of the χ_α is on-shell. The usual Green function techniques may then be used to solve these equations and give *the distorted wave Born approximation transition* (DWBA) amplitude. A detailed representation of the amplitude will be done in the next section.

2.4 Distorted Wave Born Approximation

Let consider the nuclear reaction of transfer ν particle from a A nucleus into a B nucleus:



In the case of weak coupling between intermediate channels, it is reasonable to evaluate the transition amplitude in Born Approximation.

In the rearrangement reactions there are few ways to describe the interaction between the different fragments, one for each partition. For example, if we choose to describe the scattering in terms of the nuclei of the entrance partition, the projectile-target interaction will be written as

$$V_{Ab} = V_{\nu b} + U_{ab}. \tag{2.38}$$

Here, $V_{\nu b}$ – a binding potential of the ν valence particle with the b core, and it is real potential, U_{ab} – a complex optical potential describing the scattering state of the $a + b$ system. In this representation, known as prior mode, the transition amplitude for the transfer process is given by

$$\begin{aligned} T_{prior} &= \langle \chi_{\beta}^{(-)} \phi_a \phi_B | V_{\nu b} + U_{ab} - U_{\alpha} | \chi_{\alpha}^{(+)} \phi_A \phi_b \rangle = \\ &= \int \int d\mathbf{r}_{\alpha} d\mathbf{r}_{\beta} \chi_{\beta}^{-}(\mathbf{r}_{\beta})^* I_{\beta\alpha}((\mathbf{r}_{\beta}, \mathbf{r}_{\alpha})) \chi_{\alpha}^{+}(\mathbf{r}_{\alpha}), \end{aligned} \tag{2.39}$$

where \mathbf{r}_{α} and \mathbf{r}_{β} – the radius vectors, illustrated in Fig.2.2, describing relative distance of the $b + A$ and $a + B$ systems respectively, U_{α} – the optical potential describing elastic scattering of α -channel, and $I_{\beta\alpha}$ is the kernel function having form

$$I_{\beta\alpha}((\mathbf{r}_{\beta}, \mathbf{r}_{\alpha})) = (\phi_a \phi_B | V_{\nu b} + U_{ab} - U_{\alpha} | \phi_A \phi_b). \tag{2.40}$$

Analogously, for the exit channel with $V_{aB} = V_{a\nu} + U_{ab}$ the transition amplitude turns to

$$T_{post} = \langle \chi_{\beta}^{(-)} \phi_a \phi_B | V_{a\nu} + U_{ab} - U_{\beta} | \chi_{\alpha}^{(+)} \phi_A \phi_b \rangle. \tag{2.41}$$

Here, U_{β} stands for the optical potential corresponding to β elastic channel.

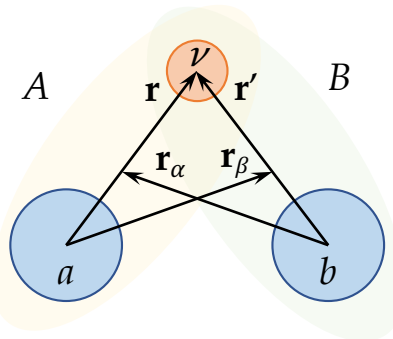


FIGURE 2.2: The arrangement of radial vectors in the DWBA on example of the $A + b \rightarrow a + B$ nuclear reaction. Here $A = a + \nu$ and $B = b + \nu$.

The differential cross section for the rearrangement nuclear reaction within the DWBA, in particular for prior form, may be written as

$$\frac{d\sigma}{d\Omega_{DWBA}} = \frac{\mu_\beta \mu_\alpha}{2\pi\hbar^2} \left(\frac{k_\beta}{k_\alpha} \right) |T_{prior}(\mathbf{k}_\beta, \mathbf{k}_\alpha)|^2 \quad (2.42)$$

For the post form the differential cross section is written analogously replacing the corresponding transition amplitude.

In accordance with the DWBA calculations the main ingredients are the internal wave functions for the initial (ϕ_A, ϕ_b) and final (ϕ_a, ϕ_B) nuclei. In this scheme, the valence particle ν is bound to the b core to give the composite B . In the simplest picture, the valence particle can be considered a pure single-particle state. This means that within this model there is only one possible configuration of the core and valence particle to give the nucleus B . Thus, the wave function for the nucleus B can be written as

$$\phi_B^{JM}(\xi, \mathbf{r}) = [\phi_b^I(\xi) \times \phi_{lsj}(\mathbf{r})]_{JM} \quad (2.43)$$

In a more sophisticated model, however, the state of the composite contains components of many single particle states coupled to all possible core states. Therefore, the wave function $\phi_B^{JM}(\xi, \mathbf{r})$ may be built as a superposition of the form

$$\phi_B^{JM}(\xi, \mathbf{r}) = \frac{1}{\sqrt{n_B}} \sum_{Ilj} \mathcal{A}_{lsj}^{IJ} [\phi_b^I(\xi) \times \phi_{lsj}(\mathbf{r})]_{JM} \quad (2.44)$$

where the coefficients \mathcal{A}_{lsj}^{IJ} are the so called coefficients of fractional parentage of

spectroscopic amplitudes. More information about the spectroscopic amplitudes will be introduced in the next section. The squared value of the amplitude is

$$S_{lsj}^{IJ} = |\mathcal{A}_{lsj}^{IJ}|^2, \quad (2.45)$$

which is called spectroscopic factors. The spectroscopic factors can be regarded as the probability of finding the valence particle ν in a single particle state l, s, j coupled to the core with spin I . The quantity n_B is the number of nucleons or clusters in the composite system.

Note that the kernel function $I_{\beta\alpha}(\mathbf{r}_\beta, \mathbf{r}_\alpha)$ involve the overlap between the composite and core wave functions. Using the Eq.2.44 the internal variable ξ in the integral can be explicitly performed giving just unity by normalization

$$(\phi_B^{JM}(\xi, \mathbf{r}), \phi_b^I(\xi)) \equiv \int d\xi \phi_B^{JM}(\xi, \mathbf{r}) \phi_b^I(\xi) = \frac{1}{\sqrt{n_B}} \sum_{Ilj} \mathcal{A}_{lsj}^{IJ} \phi_{lsj}(\mathbf{r}) \quad (2.46)$$

The bound wave function $\phi_{lsj}(\mathbf{r})$ obey the Shrödinger equation

$$(T + V_{\nu b}(\mathbf{r}) + \epsilon - E) \phi_{lsj}(\mathbf{r}) = 0 \quad (2.47)$$

where ϵ is the binding energy of the valence particle.

2.5 Spectroscopic Amplitudes within the Shell Model

Spectroscopic amplitudes for nuclear reactions can be obtained by calculations within the shell model. However, this approach is limited in calculating the amount of transferred particles. The calculation of matrix elements for the creation operator is suitable only in the case of the one-particle transfers, or at best two particle transfer. In nuclear reactions with the cluster transfer, one should use other theoretical approaches, or achieve certain values by fitting for the best reproduction of the observables.

Observables for the removal or addition of a nucleon from a specific initial state to a specific final state are related to the matrix elements of the creation and destruction operators. The creation operator a_{km}^+ is a tensor of rank j since it creates the single-particle state $|km\rangle$. Here, k stands for the set of single-particle quantum numbers nlj . The destruction operator a_{km} is not a tensor of

rank j , however,

$$\tilde{a}_{km} = (-1)^{j+m} [a_{k,-m}^+]^+ = (-1)^{j+m} a_{k,-m} \quad (2.48)$$

is a tensor of rank j . And its inverse is $a_{km} = (-1)^{j-m} \tilde{a}_{k,-m}$. Corresponding matrix elements of these operators can be written as

$$\langle k^{n-1} \omega' J' | | \tilde{a}_k | | k^n \omega J \rangle = (-1)^{j+J'-J} \langle k^n \omega J | | a_k^+ | | k^{n-1} \omega' J' \rangle \quad (2.49)$$

where ω – the harmonic oscillator parameter chosen to reproduce the observed mean-square charge radius, J – total spin of the n -particle state. All many-body matrix elements of a^+ can be reduced to these involving a single k -state.

Wave-function expansion relations and sum-rules for the states in the $n - 1$ particle system can be obtained by operating with the number operator

$$\hat{N}_k = \sum_m a_{km}^+ a_{km} \quad (2.50)$$

on the k^n configuration and then inserting a complete set of states with $n - 1$ particles

$$\begin{aligned} \hat{N}_k |k^n \omega JM\rangle &= \sum_m a_{km}^+ a_{km} |k^n \omega JM\rangle = n |k^n \omega J\rangle = \\ &= \sum_{m\omega' J' M'} a_{km}^+ |k^{n-1} \omega' J' M'\rangle \langle k^{n-1} \omega' J' M'| a_{km} |k^n \omega JM\rangle. \end{aligned} \quad (2.51)$$

The matrix element of $a_{k,m}$ can be reduced with the Wigner-Eckhart theorem

$$\begin{aligned} \langle k^{n-1} \omega' J' M' | a_{km} | k^n \omega JM \rangle &= (-1)^{j-m+J'-M'} \begin{pmatrix} J' & j & J \\ -M' & -m & M \end{pmatrix} \times \\ &\times \langle k^{n-1} \omega' J' | | a_{km} | | k^n \omega J \rangle. \end{aligned} \quad (2.52)$$

By Eq. 2.49 the reduced matrix element of \tilde{a} can be converted in a reduced matrix element of a^+ to obtain the final result:

$$\begin{aligned} \hat{N}_k |k^n \omega JM\rangle &= n |k^n \omega JM\rangle = \sum_{m\omega JM} (-1)^{-m-M'+J} \begin{pmatrix} J' & j & J \\ -M' & -m & M \end{pmatrix} \times \\ &\times a_{km}^+ |k^{n-1} \omega' J' M'\rangle \langle k^n \omega' J | | a_k^+ | | k^{n-1} \omega' J' M \rangle. \end{aligned} \quad (2.53)$$

Denoting the n -particle wave function by

$$|k^n \omega JM\rangle \equiv Z^+(k^n \omega JM) |\rangle \quad (2.54)$$

where Z^+ is the linear combination of a^+ operator which create the antisymmetric n -particle state, we can thus expand the k^n wave function in terms of those in the k^{n-1} basis:

$$|k^n\omega JM\rangle = (-1)^n \sum_{\omega' J'} \frac{\langle k^n\omega' J || a_k^+ || k^{n-1}\omega' J' M \rangle}{n\sqrt{2J+1}} [Z^+(k^{n-1}\omega' J') \times a_k^+]_{JM} | \rangle \quad (2.55)$$

A phase factor $(-1)^{n-1}$ arises from commuting a^+ with the $n-1$ particles in the state k^{n-1}

A sum rule for the matrix elements of a^+ can be obtained by multiplying both sides of Eq. 2.53 by $\langle k^n\omega'' J'' M'' |$ to obtain

$$\begin{aligned} n\delta_{JJ''}\delta_{MM''}\delta_{\omega\omega''} &= \sum_{m\omega' J' M'} (-1)^{-m-M'+J} \begin{pmatrix} J' & j & J \\ -M' & -m & M \end{pmatrix} \times \\ &\quad \times \langle k^n\omega'' J'' M'' | a_{km}^+ | k^{n-1}\omega' J' M' \rangle \langle k^n\omega J | a_k^+ | k^{n-1}\omega' J' \rangle = \\ &= \sum_{m\omega' J' M'} \begin{pmatrix} J' & j & J \\ -M' & -m & M \end{pmatrix} \begin{pmatrix} J'' & j & J' \\ -M'' & -m & M' \end{pmatrix} \times \\ &\quad \times \langle k^n\omega'' J'' | a_k^+ | k^{n-1}\omega' J' \rangle \langle k^n\omega J | a_k^+ | k^{n-1}\omega' J' \rangle = \\ &= \frac{\delta_{JJ''}\delta_{MM''}}{2J+1} \sum_{\omega' J'} \langle k^n\omega'' J'' | a_k^+ | k^{n-1}\omega' J' \rangle \langle k^n\omega J | a_k^+ | k^{n-1}\omega' J' \rangle. \end{aligned} \quad (2.56)$$

Then, one finds the sum-rule:

$$\sum_{\omega' J'} \langle k^n\omega'' J'' | a_k^+ | k^{n-1}\omega' J' \rangle \langle k^n\omega J | a_k^+ | k^{n-1}\omega' J' \rangle = n(2J+1)\delta_{\omega\omega''}\delta_{JJ''} \quad (2.57)$$

Thus:

$$\sum_{\omega' J'} |\langle k^n\omega J | a_k^+ | k^{n-1}\omega' J' \rangle|^2 = \sum_{\omega' J'} |\langle k^{n-1}\omega' J' | \tilde{a}_k | k^n\omega J \rangle|^2 = n(2J+1) \quad (2.58)$$

The matrix elements in which the sum over final states is normalized to unity are historically called coefficients of fractional parentage [49] (CFP) defined by:

$$\mathcal{A}_{lsj}^{JJ'} = \frac{\langle k^n\omega J | a_k^+ | k^{n-1}\omega' J' \rangle}{\sqrt{n(2J+1)}} \quad (2.59)$$

The reduced matrix elements of the creation and destruction operators are used to define the spectroscopic amplitudes associated with nuclear reactions. They are also the building blocks for the more complicated operators associated with one-body (such as electromagnetic and β -decay) and two-body transition

amplitudes.

2.6 Interaction potentials. The double folding model

The numerical calculations of the elastic scattering can be performed in the framework of the OM with the OM potential given by:

$$U(R) = -V^V(R) - iW^V(R) + V^{SO}(R)(\mathbf{l} \cdot \boldsymbol{\sigma}) + V^C(R), \quad (2.60)$$

where V^V , W^V , V^{SO} , and V^C are real volume, imaginary volume, spin-orbit and Coulomb potentials, respectively. The volume potentials of colliding two spherical nuclei may be represented as parametrized function. For example, in practice the Woods-Saxon potential is often used, and it has the form

$$\begin{aligned} V^V(r) &= V_0^V f_{r_V, a_V}(r), \\ W^V(r) &= V_0^W f_{r_W, a_W}(r), \\ f_{r_0, a_0}(r) &= \frac{1}{1 + \exp\left(\frac{r-r_0}{a_0}\right)}, \end{aligned} \quad (2.61)$$

where V_0 is depth of the potential, r_0 is average distance and a_0 is diffusion parameter.

The spin-orbit term of the OM potential has standard form

$$V^{SO}(r) = V_0^{SO} \left(\frac{\hbar}{m\pi c}\right)^2 \frac{1}{r} \frac{d}{dR} f_{R_{SO}, a_{SO}}(r). \quad (2.62)$$

The Coulomb term has been taken as the interaction of a point-charge with a uniformly charged sphere

$$V^C(r) = \begin{cases} \frac{Z_1 Z_2 e^2}{2r_C} \left(3 - \frac{r^2}{r_C^2}\right), & \text{for } r \leq r_C, \\ \frac{Z_1 Z_2 e^2}{r}, & \text{for } r > r_C. \end{cases}$$

The situation changes, when the colliding nuclei have sophisticated shape. Assume, that there are nuclear matter distribution of the projectile $\rho_a(r_a)$ and target $\rho_A(r_a)$, depending on internal their own radii. Folding the nucleon-nucleon interaction potential V_{nn} over the density distributions of nuclear matter, in the framework of the *Double folding model* an interaction potential may

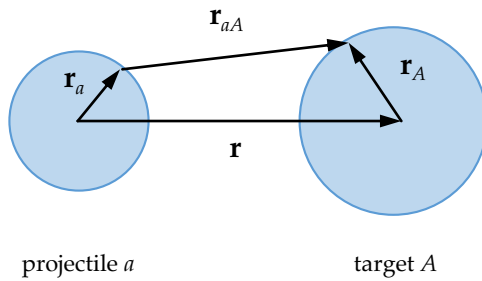


FIGURE 2.3: Radius vectors for the double folding model.

be constructed as follow

$$\begin{aligned} V^V(r) &= N_f V^{DF}(r) \\ V^{DF}(\mathbf{r}) &= \int \int d\mathbf{r}_a d\mathbf{r}_A \rho_a(\mathbf{r}_a) V_{nn}(r_{aA}) \rho_A(\mathbf{r}_A). \end{aligned} \quad (2.63)$$

where $r_{aA} = |\mathbf{r} + \mathbf{r}_A - \mathbf{r}_a|$ (see Fig. 2.3). The N_f normalization parameter is usually fitted in accordance with the dynamics of nuclear reaction of elastic scattering.

The DF potential may be calculated using the effective M3Y-Paris [50] nucleon-nucleon potential and the nuclear-matter-densities of projectile and target nuclei.

The V_{nn} effective nucleon-nucleon interactions usually are taken as a sum of the three Yukawa potentials, i.e. M3Y-potentials:

$$V_{nn}(r) = \sum_{i=1}^3 N_i \frac{\exp(-\mu_i r)}{\mu_i r}. \quad (2.64)$$

The parameters N_i , μ_i of the M3Y-Paris effective NN-potential [50], often used in the double folding calculations, are given in Tab.2.1.

The dependence $g(E)$ of the folding potential on the collision energy and an additional dependence on the nuclear matter density in the region of their overlap $F(\rho)$ have been phenomenologically established. The folding potential is usually taken as the real part of the optical potential, adjusting its depth to better reproduce the experimental data. The imaginary part of the optical potential is selected in the form of the Woods-Saxon potential, or the same folding potential, while varying its depth.

TABLE 2.1: Parameters of the M3Y-Paris [50] NN-potential used in double-folding calculations.

i	N_i , MeV	Direct T=0	Exchange T=0	Direct T=1	Exchange T=1	μ_i , fm $^{-1}$
1	11061.60		-1524.25	313.62	-4118.9	4.0000
2	-2537.5		-518.75	223.5	1054.75	2.5000
3	0.0		-7.84	0.0	2.62	0.7072

The potential depending on the collision energy of the projectile, undergoes a change by multiplying a factor

$$g(E) = 1 - 0.003 \frac{E}{A}. \quad (2.65)$$

An additional dependence of the V_{nn} potential on the total density of colliding nuclei in the region of their overlap may given as

$$F(\rho) = C (1 + \alpha \exp(-\beta \rho) - \gamma \rho(\mathbf{r})). \quad (2.66)$$

with the parameters

$$C = 0.2658 \quad \alpha = 3.8033 \quad \beta = 1.4099 \quad \gamma = 4.0 \quad (2.67)$$

For the particles t , ${}^3\text{He}$, α , which have simple structure, the density distribution of nuclear matter can be represented as parametrized Gaussian function as follow

$$\rho(r) = \rho_0 \exp(-\alpha_0 r^2) \quad (2.68)$$

where the parameters ρ_0 and α_0 are defined in condition to reproduce the rms matter radii

$$\alpha_0 = \frac{3}{2\langle r_m^2 \rangle}, \quad \rho_0 = a \left(\frac{\alpha_0}{\pi} \right)^{3/2} \quad (2.69)$$

here a – atomic number of projectile.

The density distributions in (2.63) are normalized so that

$$\int \rho_A(\mathbf{r}) d\mathbf{r} = A \quad \int \rho_a(\mathbf{r}) d\mathbf{r} = a \quad (2.70)$$

where A, a are the number of nucleons in the respective nuclei.

As regards target nuclei, having cluster structure, the density distribution of nuclear matter are calculated by means of the three body wave function, and its details are set out in the Section 1.5 .

Chapter 3

Results and discussions

3.1 The three-body wave function

The chosen three-body wave function are obtained by variational method, and its parameters for ground state of ${}^6\text{He}$, ${}^6\text{Li}$ and ${}^9\text{Be}$ are listed in Application B. The process of minimization of eigen-energy of the three-body systems was done with the RSC potential [51] for nucleon-nucleon interaction, the SBB potential [52] for α - N interaction and the BFW potential [53] for α - α interaction. In Tab. 3.1 the used and obtained data of variational calculations are listed¹.

The obtained results of eigen-energies of the three-body systems in the ground state are equal to -0.228 MeV for ${}^6\text{He}$, -3.258 MeV for ${}^6\text{Li}$ and -1.417 MeV for ${}^9\text{Be}$. These theoretical data are differ from experimental data slightly. For example slightly difference has ${}^9\text{Be}$, its experimental established energy in the three-body system is $E_{exp} = -1.417$ MeV. The significant differences between variational eigen-energy were in ${}^6\text{He}$ and ${}^6\text{Li}$. Corresponding value of the energy are $E_{exp} = -0.975$ MeV for ${}^6\text{He}$, $E_{exp} = -3.700$ MeV for ${}^6\text{Li}$. Such kind of discrepancy of variational calculations with experimental data are probably in the non-completeness of the basis function. The basis function taken in this work has no symmetrization, and doesn't enfold an alternative coordinate space.

¹The obtained data of the variational calculations are not the subject of our research, since the results, perhaps better ones, have already been published and discussed. The purpose of the section result of the three-body wave function is to familiarize with what wave function we are dealing with, and its features will be needed in further discussions.

TABLE 3.1: Results of the search for the minimum energy of three-body systems found by means of the variational approach: ^6He , ^6Li and ^9Be . The obtained minimum energy E_{min} , used set of quantum numbers $\gamma \equiv \lambda l L S$, the dimension D and the probability P of each γ are listed.

^6He			^6Li			^9Be		
$E_{min} = -0.228$			$E_{min} = -3.258$			$E_{min} = -1.417$		
γ	D	P	γ	D	P	γ	D	P
$\lambda l L S$								
0 0 0 0	9×9	0.884	0 0 0 1	8×8	0.898	0 1 1 1	7×7	0.403
1 1 1 1	9×9	0.102	2 0 2 1	7×7	0.073	2 1 1 1	7×7	0.328
2 2 0 0	5×5	0.010	1 1 1 0	7×7	0.021	2 1 2 1	7×7	0.235
3 3 1 1	5×5	0.004	2 2 0 1	5×5	0.005	2 3 1 1	6×6	0.017
			2 2 1 1	5×5	0.002	2 3 2 1	5×5	0.004
						4 3 1 1	4×4	0.009
						4 3 2 1	4×4	0.003

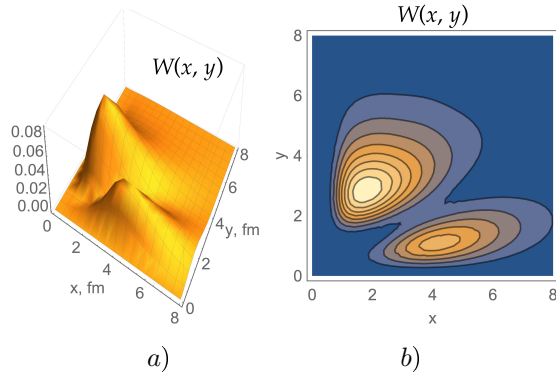


FIGURE 3.1: The correlation function $W(x, y)$ of the three-body wave function of the ground state of ${}^6\text{He}$ in the *a*) 3D-Plot and *b*) contour-plot.

In Figures 3.1, 3.2 and 3.3 the correlation density of the three-body wave function are illustrated in the 3D-Plot for ${}^6\text{He}$, ${}^6\text{Li}$ and ${}^9\text{Be}$. For the purpose of good visibility the contour-plot are given along.

In the Figures 3.1 and 3.2, two main geometric configurations can be distinguished, cigar-shaped within coordinates $(4.0, 1.0)$, and helicopter-shaped within coordinates $(1.8, 3.0)$, both for ${}^6\text{He}$ and ${}^6\text{Li}$ nuclei. The striking highlight of such geometrical configurations is clear evidence of the cluster structure. In particular, we see that in ${}^6\text{He}$, the effect of pairing two nucleons stands out against the background of comparison with ${}^6\text{Li}$. Similar results were described in works [31], and were obtained in the method using hyperspherical harmonics [19].

The Fig. 3.3 shows the locality of the wave function, which indicates the bound state of the ground state of ${}^9\text{Be}$. Moreover, the maximum of the correlation density function is shown at the coordinates $(3.0, 2.0)$, that is $x \simeq 3$, $y \simeq 2$. This allows us to make the assumption that basically the pair of α -particles are relatively farther than the distance of the valence neutron from the center of

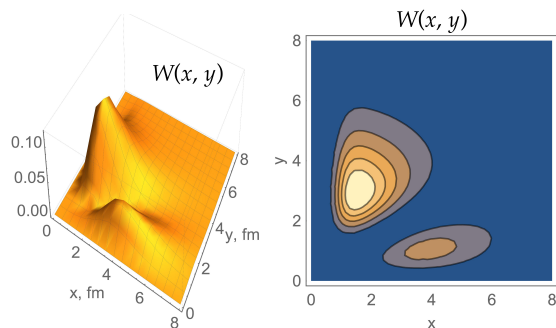


FIGURE 3.2: The same caption as in the Fig.3.1, but for ${}^6\text{Li}$.

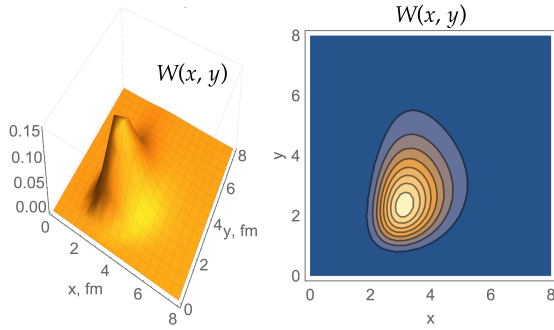


FIGURE 3.3: The same caption as in the Fig.3.1, but for ${}^9\text{Be}$.

mass of the pair.

3.2 The density distribution function of nuclear matter

On the basis of the three-body wave function in Eq.1.1, the distribution function of the density of nuclear matter was calculated using Equations 1.36, 1.37 and 1.39 for ${}^6\text{He}$, ${}^6\text{Li}$ and ${}^9\text{Be}$ in the ground states. The calculation results are shown in the Figures 3.4, 3.5 and 3.6. The plotted the density functions of ${}^6\text{He}$, ${}^6\text{Li}$ and ${}^9\text{Be}$ are normalized to their own atomic masses.

A distinctive feature of the obtained results is in the extended tail of the density function for ${}^6\text{He}$ in Fig.3.4. This is caused by the nucleons in the three-body system. In particular, the density function of the alpha particle $\rho_{\alpha}^{(k)}(R)$ inside ${}^6\text{He}$ tends to zero rapidly as the radius R increases. The density function of two neutrons $\rho_N^{(p)}(R) + \rho_N^{(q)}(R)$ starts near zero, reaching a maximum near

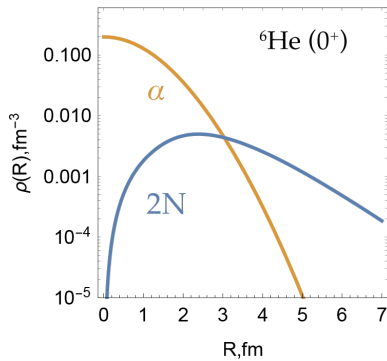


FIGURE 3.4: The density distribution function of nuclear matter $\rho(R) = \rho_{\alpha}^{(k)} + \rho_N^{(p)} + \rho_N^{(q)}$ illustrated with the densities of the ${}^6\text{He}$ constituents.

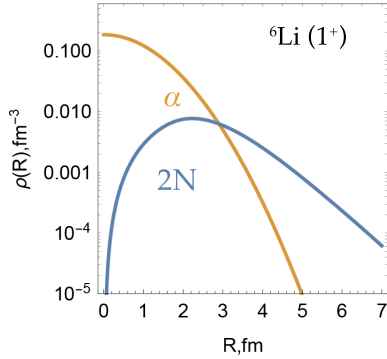


FIGURE 3.5: The same caption as in Fig. 3.4, but for ${}^6\text{Li}$.

$R \simeq 2.5$, and decreases more slowly than the density function of the alpha particle. What is obvious is that the start of the value of the density function $\rho_N^{(p)}(R) + \rho_N^{(q)}(R)$ near zero means that these two neutrons lie in the p -shell. Thus, we see that the main contribution to the density function starting from $R \simeq 3.0$ is due to two neutrons.

A similar structure of the nucleus ${}^6\text{Li}$ is seen in Fig. 3.5. The density function of the alpha particle $\rho_\alpha^{(k)}(R)$ inside ${}^6\text{Li}$ is visible, rapidly tending to zero as the radius R increases. And the density function of the two nucleons $\rho_N^{(p)}(R) + \rho_N^{(q)}(R)$, starting around zero, reaches a maximum near $R \simeq 2.5$, and decreases more slowly than the density function of the α -particle $\rho_\alpha^{(k)}(R)$. The beginning of the value of the density function $\rho_N^{(p)}(R) + \rho_N^{(q)}(R)$ near zero means that these two nucleons lie in the p -shell. In fact, we see, again as in the case with ${}^6\text{He}$, that the main contribution to the density function is due to two nucleons starting from $R \simeq 3.0$.

The density function $\rho(R)$ of ${}^9\text{Be}$ has a different shape than the other two

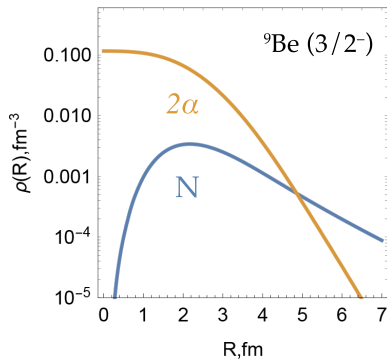


FIGURE 3.6: The density distribution function of nuclear matter $\rho(R) = \rho_N^{(k)} + \rho_\alpha^{(p)} + \rho_\alpha^{(q)}$ illustrated with the densities of the ${}^9\text{Be}$ constituents.

previous nuclei (see Fig.3.6). The alpha particle density function has become much more voluminous. The nuclear matter density distribution function $\rho_\alpha^{(p)} + \rho_\alpha^{(q)}$ tends to zero faster than the valence neutron density function $\rho_N^{(k)}$ with increasing distance R . Starting from the $R \simeq 5.0$ distance, the valence neutron density function $\rho_N^{(k)}$ prevails in the nuclear matter contribution. The spectator in the (k, pq) scheme has such distribution function starting near zero, which is characteristic of p -shell nucleons.

The formulas obtained by us for calculating the distribution function of the density of nuclear matter in the framework of the three-body model were tested using the parameters of the wave function of the ground state of ${}^9\text{Be}$ and ${}^6\text{Li}$ nuclei presented from the sources [32, 54]. In particular, for verification, calculations were made for the rms charge radius. The results obtained $\langle R_{ch}^2 \rangle^{\frac{1}{2}} = 2.54 \text{ fm}$ and $\langle R_{ch}^2 \rangle^{\frac{1}{2}} = 2.34 \text{ fm}$ for ${}^6\text{Li}$ and ${}^9\text{Be}$ nuclei, respectively, are in excellent agreement with the data indicated in those sources, which means that the chosen method is correct. And also, in addition to the fact that all formulas have been carefully checked at every stage, this excludes the presence of errors in the calculation formulas.

The density function of nuclear matter is an excellent subject for studying rms matter radii. Given the function $\rho(R)$, we can represent the formula for calculating the rms matter radii $\langle R_m^2 \rangle$ as

$$\langle R_m^2 \rangle = \frac{\int_0^\infty dR R^4 \rho(R)}{\int_0^\infty dR R^2 \rho(R)}. \quad (3.1)$$

The results of calculated rms matter radii are presented in Tab.3.2 with the values of the binding energy BE_{min} for the three-body system obtained by the variational method for nuclei. The general picture of the obtained radii shows an overestimation in comparison with other sources [55–57]. For example, the radius of the ${}^6\text{He}$ nucleus obtained in our calculations shows 2.97 fm , while the another source gives 0.35 fm less. The difference with another radius in the

TABLE 3.2: Comparisons of the binding energies obtained by means of variational approach BE_{min} with the experimental data BE_{exp} and the rms matter radii $\langle R_m^2 \rangle^{\frac{1}{2}}$ with other sources.

	${}^6\text{He } (0^+)$	${}^6\text{Li } (1^+)$	${}^9\text{Be } (\frac{3}{2}^-)$
BE_{min}	0.228	3.258	1.417
BE_{exp}	0.97	3.70	1.57
$\langle R_m^2 \rangle^{\frac{1}{2}}, \text{ fm}$	2.97	2.69	2.78
	2.62 [55]	2.45 [56]	2.62 [57]

case of ${}^6\text{Li}$ is 0.24 fm , and for ${}^9\text{Be}$ 0.16 fm . That is, if you list the nuclei from the table from left to right, the difference in radii decreases. If we look at the obtained theoretical calculations of the binding energy BE_{min} and compare with the experimental data, there is an opposite tendency in the energy differences – the difference decreases – 0.742 MeV , 0.442 MeV , 0.153 MeV . Thus, it can be assumed that the greater the underestimation in the binding energy, the more overestimation in the rms matter radii.

In accordance with this proposal, the dependence of the binding energy with the $\langle R_m^2 \rangle^{1/2}$ was studied using the example of ${}^6\text{He}$. In order to obtain the binding energy close to the experimental data, the depth of the $\alpha - N$ interaction potential, which has a Gaussian shape, was increased from 47 MeV to 49 MeV . Thus, it was possible to reproduce the experimental value of the binding energy. However, the obtained rms radius $\langle R_m^2 \rangle^{1/2} = 2.93 \text{ fm}$ decreased by only 0.04 fm .

The reason for the discrepancy between our results obtained from calculations of the rms matter radii with other sources could not be explained. Perhaps, the problem lies in the basis function, which has not been symmetrized or antisymmetrized. Moreover, the basis function is not complete, that it should have enclosed the entire basis space. Nevertheless, knowing the very weak dependence of the density distribution function on the binding energy of the three-body systems, we can use this wave function in calculations to construct interaction potentials within the framework of the folding model.

In the process of calculating the rms matter radii, it was found that elements from the set γ , that have a contribution to the wave function below 0.1 (see Tab.3.1), do not affect the obtained values. Therefore, such elements of the γ were excluded from the density function calculations.

3.3 The $\alpha + {}^6\text{He}$ nuclear reactions

3.3.1 Elastic scattering

Theoretical calculations of the differential cross section of the elastic colliding of the ${}^6\text{He} + \alpha$ system has been carried out within the framework of the OM. The calculations were done by means of *FRESCO*² code [58]. As the interaction potential of the ${}^6\text{He} + \alpha$ system were taken the double folding potential. The potential was built using the three-body wave function of the ground state of

²further, when it comes to calculations within the framework of the OM, CC and CRC methods, it will mean that all calculations were carried out using the FRESCO code [58].

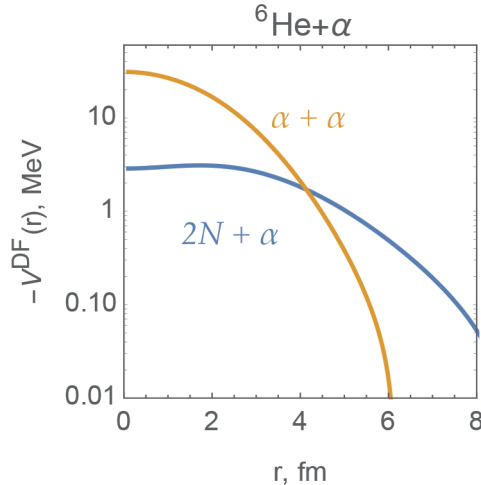


FIGURE 3.7: The folding potential $V^{DF}(r)$ in the framework of the three-body model. The potential is for the interaction of the α particle with the constituents of ${}^6\text{He}$.

${}^6\text{He}$. The interactions of its α -cluster and two nucleon with the α -projectile are presented in Fig. 3.7. The calculated double folding potential has a specific structure. It is worth noting that the potential of the α cluster with the projectile decreases rapidly as the distance r increases, while the potential of interaction of two nucleons with the projectile decreases slowly.

The potential obtained within the framework of the double folding model based on the three-body wave function was used to calculate the differential cross section for elastic scattering ${}^6\text{He}$ by alpha particles at energy $E_{lab} = 151 \text{ MeV}$. The results obtained using different potentials, including the double folding potentials, are shown in Fig.3.8.

In addition to the folding potential, two other potentials (WS1 and WS2) are presented as the Woods-Saxon potential taken from [59]. The parameters of the potentials used in the calculations of the theoretical curves within the optical model and the corresponding χ^2 are presented in Tab. 3.3. Comparison of theoretical curves with the experimental data is in good agreement, if we do not take into account the backward angles caused by another interaction mechanism, which will be discussed in the next section. The difference in cross sections with different potentials is insignificant, except for the folding potential, which does not describe the first experimental point.

The advantage of folding potential in comparison with others consists of a less number of adjustable parameters to the experimental data. If these parameters in the both phenomenological potential WS1 and potential WS2 are six, then folding potential depends on only two parameters. The overhead

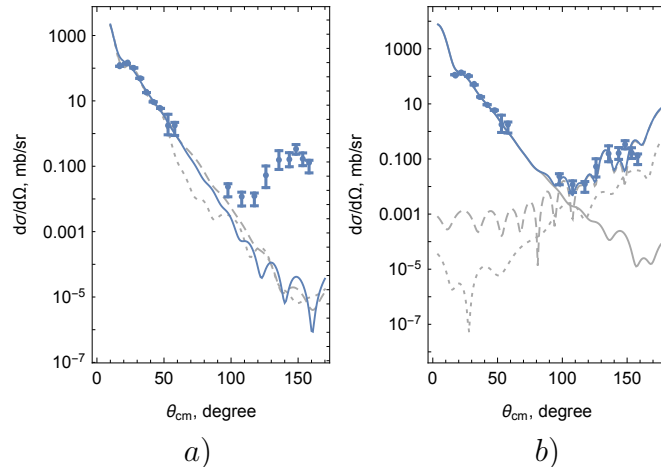


FIGURE 3.8: *a)* The differential cross section of the elastic scattering of ${}^6\text{He}$ by α -particles at $E_{lab} = 151\text{MeV}$ with the different potentials: the double folding potential (blue solid), the WS2 (gray dashed) [59] and WS1 (gray dotted) [59]. *b)* The cross sections of the elastic transfer reaction in terms of the transfer mechanisms: elastic scattering (solid gray), simultaneous transfer of $2N$ (gray dashed), sequential transfer of $2N$ (dotted) and total coherent sum (solid blue). Experimanetal data taken from [59].

in this case is a small concession in the χ^2 test.

3.3.2 Elastic transfer

In Fig. 3.8.*a*) theoretical curves were presented to describe the experimental data on elastic scattering. The calculations made within the framework of the optical model showed a good result. However, this is only at the front scattering angles. The backscattering angles are far from the description of optical calculations. Therefore, in order to explain this difference, we propose mechanisms for the transfer of two nucleons: sequential and simultaneous transfer. A schematic representation of the mechanisms can be seen in Fig. 3.9. Thus, the differential cross section of these mechanisms can be written as follows

$$\frac{d\sigma}{d\Omega}(\theta) = |f(\theta)_{OM} + f_{sim}(\pi - \theta) + f_{seq}(\pi - \theta)|^2 \quad (3.2)$$

Calculations for obtaining the differential cross section of the elastic transfer were carried out within the framework of the CRC method. Potential for the input and output channels was taken the double folding potential, and the potential for the intermediate channel was taken the optical potential with global optical parametrizations for α particles [60]. Trial calculations have shown that the results depend very little on the selected potential for the intermediate channel. The results of calculations for elastic transfer made in the framework of

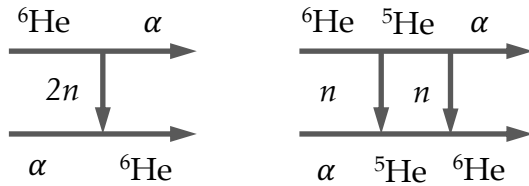


FIGURE 3.9: Schematic representation of the elastic transfer nuclear reaction, on the left - the simultaneous transfer of two nucleons, on the right - the sequential transfer of two nucleons.

CRC are shown in Fig. 3.8.b). The sequential transfer of two nucleons is shown by gray dotted curves, their simultaneous transfer by dashed gray curves, the elastic scattering cross section by solid gray curves, and, finally, their coherent sum is shown as a blue solid curve. The wave function of the bound states was chosen by fitting the potential depth to the binding energy of the composite systems. In particular, the binding energy of one neutron with ${}^6\text{He}$ was 1.8 MeV, neutron with ${}^5\text{He}$ – 0.1 MeV, and two neutrons with α – 0.9 MeV.

As mentioned in the previous section, the elastic collision mechanism prevails at the forward scattering angles. Beginning at an angle of 90 degrees, the contribution to the cross section is mainly due to the simultaneous transfer of two nucleons. It is worth noting here that two neutrons have the $nlj\ 2S_0$ configuration, which, possibly, leads to an oscillatory cross section. Ten times less is the contribution of the sequential transfer of neutrons, having the $1P_{\frac{3}{2}}$ configuration. Note that the spectroscopic amplitudes for two neutrons in ${}^6\text{He}$, one neutron in ${}^5\text{He}$ and in ${}^6\text{He}$ were taken to be equal to unity for the beginning. The results showed a difference in cross-sections for sequential and simultaneous transmissions of about ten. For the best reproduction of the experimental data, the spectroscopic amplitude of two neutrons was taken $\mathcal{A}_{2S_0}^{00} = 1.3$, while the others remained unchanged.

Thus, it was possible to achieve good agreement between the calculated differential cross section, using the double-folding potential and the proposed

TABLE 3.3: The parameters of the potentials used in OM calculations for both $\alpha + {}^6\text{He}$ and $\alpha + {}^6\text{Li}$ nuclear reactions. For more details, see the text

	$-V_0$, MeV	R_v , fm	a_v , fm	$-W_0$, MeV	R_w , fm	a_w , fm	χ^2/N
DF- ${}^6\text{He}$		$N_r=1.4$			$N_i=0.5$		7.32
DF- ${}^6\text{Li}$		$N_r=2.0$			$N_i=1.8$		11.61
WS1- ${}^6\text{He}$	102.5	1.78	0.920	13.0	3.85	0.5	5.75
WS2- ${}^6\text{He}$	102.5	1.54	0.904	7.0	4.28	0.569	6.31
WS1- ${}^6\text{Li}$	102.5	1.78	0.820	11.8	4.11	0.950	15.43

transfer mechanisms, with the experimental data.

3.4 The $\alpha + {}^6\text{Li}$ nuclear reactions

3.4.1 Elastic scattering

To calculate the elastic scattering cross section, we used the potential obtained by the folding model method based on the three body model. Therefore, it is possible to look at the structure of the interaction of alpha particles, which are a projectile, with a deuteron and an alpha particle inside the nucleus ${}^6\text{Li}$ (see, Fig. 3.10). The function of the interaction potential of the projectile with the internal alpha particle rapidly tends to zero, while the function of the interaction potential of the projectile with the internal deuteron slowly decreases. It should also be noted that, starting from the distance $r \simeq 4.0$, the main contribution is due to the interaction of the projectile with the internal deuteron.

The results of calculating the differential cross section of elastic collision of the $\alpha + {}^6\text{Li}$ system are shown in Fig. 3.11 a). The cross section based on the folding potential ($\text{DF-}{}^6\text{Li}$), represented by the blue curve, is in better agreement than the potential ($\text{WS1-}{}^6\text{Li}$) taken from [59], which is shaped like the Woods-Saxon potential. The proof comes from the value of the χ^2 test for each potential. The potential parameters and χ^2 values are listed in Tab. 3.3. The ${}^6\text{Li}$ structure is very similar to the ${}^6\text{He}$ structure. Therefore, as in the case of ${}^6\text{He}$, the calculations made in the framework of the OM are well described

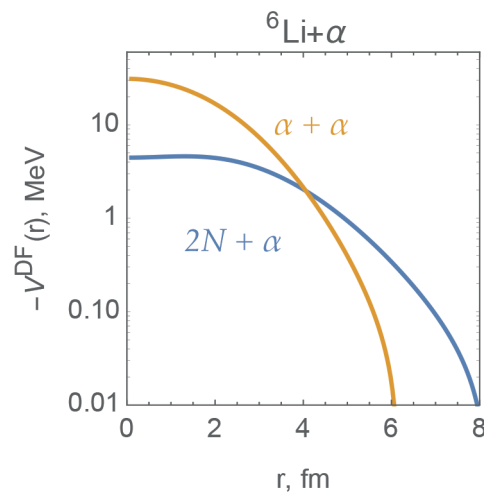


FIGURE 3.10: The folding potential $V^{DF}(r)$ in the framework of the three-body model. The potential is for the interaction of the α particle with the constituents of ${}^6\text{Li}$.

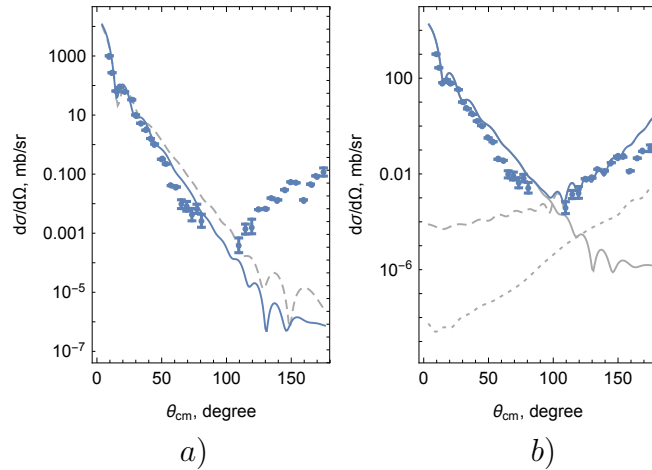


FIGURE 3.11: *a)* The differential cross section of the elastic scattering of ${}^6\text{Li}$ by α -particles at $E_{lab} = 166\text{MeV}$ with the different potentials: the double folding potential DF- ${}^6\text{Li}$ (blue solid), the WS1- ${}^6\text{Li}$ (gray dashed) [59]. *b)* The cross sections of the elastic transfer reaction are represented in terms of the transfer mechanisms: elastic scattering (solid gray), simultaneous transfer of d (gray dashed), sequential transfer of $2N$ (dotted) and their coherent sum (solid blue). Experimanetal data taken from [59].

only at the forward scattering angles. Differential cross sections belonging to the backward angles have the character of another mechanism - the transfer of d inside ${}^6\text{Li}$. How exactly this subsystem is transferred will be discussed in the next section devoted to elastic transfer for the $\alpha + {}^6\text{He}$ reaction.

Potential WS1- ${}^6\text{Li}$ describes the experimental data not so much better than it was expected from the source taken [59]. It is possible that an error was overlooked at the typing stage for the publisher. It should be noted that omissions in our calculations for elastic scattering $\alpha + {}^6\text{Li}$ are excluded, since the approach perfectly reproduces the theoretical curves of the potential WS1- ${}^6\text{He}$ and WS2- ${}^6\text{He}$ for elastic scattering $\alpha + {}^6\text{He}$ exactly the same as it looks in its own source.

It should be noted that the corresponding double folding potential for the elastic scattering $\alpha + {}^6\text{Li}$ reaction depends only on two parameters adjusted to the experimental data.

3.4.2 Elastic transfer

An increase in the cross section for the elastic scattering $\alpha + {}^6\text{Li}$ reaction starting from 90° suggests the existence of additional reaction mechanisms. In this case, in order to register the same particle as the elastically scattered projectile, a deuteron particle must be transferred to the target at angles above 90° .

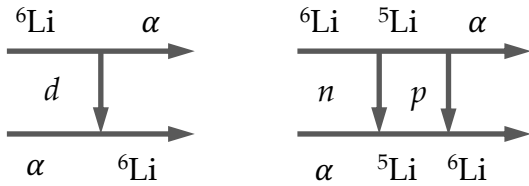


FIGURE 3.12: Schematic representation of the elastic transfer nuclear reaction, on the left - the simultaneous transfer of two nucleons, on the right - the sequential transfer of two nucleons.

That is, the incident particle ${}^6\text{Li}$ transfers its deuteron to the α -target. Then, the remaining alpha particle of ${}^6\text{Li}$ continues its path, while the newly formed nucleus ${}^6\text{Li}$ flies in the opposite direction according to the law of momentum conservation. In particular, the presence of a deuteron transfer mechanism is not excluded. These transfer mechanisms are shown schematically in Fig 3.12.

As in the case of ${}^6\text{He}$, calculations for obtaining the differential cross section of the elastic transfer were carried out within the framework of the CRC method. For the input and output channels the double folding potential was taken, and for the intermediate channel the optical potential with global optical parametrizations for α particles [60] was chosen. Preliminary calculations have shown that the cross sections depend weakly on the selected potential for the intermediate channel. The sequential transfer of two nucleons is shown by gray dotted curves, their simultaneous transfer by dashed gray curves, the elastic scattering cross section by solid gray curves, and, finally, their coherent sum is shown as a blue solid curve. The wave function of the bound states was chosen by fitting the potential depth to the binding energy of the composite systems. In particular, the binding energy of one neutron with ${}^5\text{Li}$ was 5.663 MeV, as neutron with ${}^5\text{He}$ taken 0.9 MeV, and as d with α taken 1.474 MeV. The differential cross section for this reaction is determined using the same formula 3.2.

The results of calculations for elastic transfer are shown in Fig. 3.11.b). The mechanism of elastic collision in the reaction of $\alpha + {}^6\text{Li}$ prevails over other mechanisms at the forward scattering angles. However, starting from 90° we see that the main contribution to the cross section is caused by the simultaneous transfer of two nucleons of ${}^6\text{Li}$, that is, the deuteron. The difference from the reaction $\alpha + {}^6\text{He}$, where two nucleons are transferred, the reaction $\alpha + {}^6\text{Li}$ consists reaction of the deuteron transfer, which has spin $S(d) = 1$, therefore, and also in the spin structure of the composite nucleus ${}^6\text{Li} = \alpha + d$. That is, according to the law of conservation of moments and parity, a deuteron can be

transferred by $2S1$ and $2D1$ configurations.

Calculations on the cross section showed that the cross section with the $2S1$ wave has an oscillatory character, as in the case with the elastic transfer reaction $\alpha + {}^6\text{He}$, then with the $2D1$ wave the cross section takes a smooth form. The spectroscopic amplitude for the $2S1$ configuration of the deuteron in ${}^6\text{Li}$ was taken $\mathcal{A}_{2S1}^{10} \simeq 0.7$, and for the $2D1$ configuration of the transferred deuteron $\mathcal{A}_{2D1}^{10} \simeq 0.5$, considering that this wave has a much smaller contribution to the structure ${}^6\text{Li}$ (see, Tab. 3.1). Therefore, the resulting section is more or less smooth compared to the case with the elastic transfer reaction $\alpha + {}^6\text{He}$. As for the sequential transfer of the d system, it has a contribution much less than the simultaneous transfer by one order of magnitude. This is when first neutron is transferred then proton. And the reverse order of transfer is greatly underestimated due to the Coulomb repulsion of proton with the α -projectile.

3.5 The $d + {}^9\text{Be}$ nuclear reactions

3.5.1 The elastic channel

The DF potential was calculated using the effective M3Y-Paris nucleon-nucleon potential and the nuclear-matter-densities of projectile and target nuclei. In order to calculate the ${}^9\text{Be}$ matter distribution we applied the $\alpha+\alpha+n$ three-body model (for more details, see Ref. [61]), while the matter density distribution of the deuteron projectile was chosen to be of the form

$$\rho\left(\frac{1}{2}r\right) = \int |\Psi(\mathbf{r})|^2 d\Omega_r. \quad (3.3)$$

For convenience, in the OM and CC (CRC) calculations the potentials have been fitted by means of the sum of three Woods-Saxon potentials:

$$V^V(R) = \sum_{i=1}^3 V^i f^{R_i, a_i}(R), \quad (3.4)$$

$$f^{R_V, a_V}(R) = \frac{1}{1 + \exp \frac{R - R_V}{a_V}}. \quad (3.5)$$

The parameters of the imaginary part of the optical potential were obtained by fitting the theoretical cross sections to the experimental data at 19.5 MeV and 35 MeV incident energies. As a starting point, the same parameterizations of the real part were used. The obtained potential parameters after fitting are

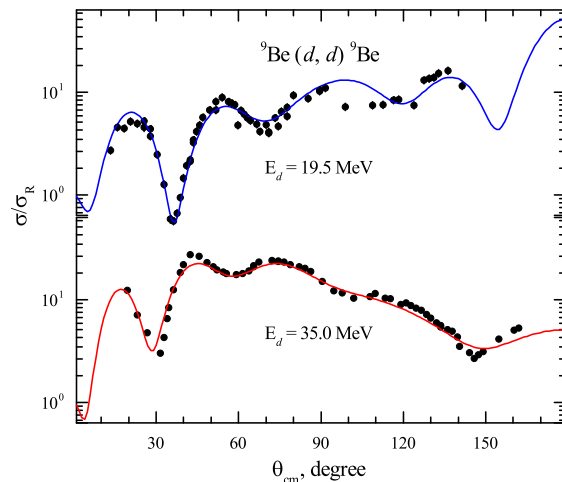


FIGURE 3.13: The angular distribution of elastic scattering data of d from ${}^9\text{Be}$ at laboratory energy 19.5 MeV in comparison with theoretical calculations within the OM (solid curve).

listed in Table 3.4 for both 19.5 MeV and 35.0 MeV incident energies.

The comparison of the results of the theoretical calculations with the measured data for elastic scattering at 19.5 MeV and 35.0 MeV energies are plotted in Fig. 3.13. The cross sections obtained in the framework of the OM with the DF potential are shown as solid curves. Theoretical results obtained by means of the OM give an excellent agreement, $\chi^2 \approx 2.5$, with the experimental data. The parameters of parameterized double-folding potential are listed in Table 3.4.

3.5.2 Inelastic scattering

The CC and DWBA approaches have been applied to analyse the measured inelastic scattering data corresponding to the ${}^9\text{Be}(5/2^-, 2.43 \text{ MeV})$ excitation. Calculations were performed employing the FRESCO code [58] and the DWUCK5 code [62] which are available in the NRV knowledge-base [63].

In order to describe the measured experimental data one has to consider the ${}^9\text{Be}$ target having a quadrupole deformation. Thus, the ${}^9\text{Be}$ spectrum consists of the rotational band including the $3/2^-$ ground state, $5/2^-$ state at 2.43 MeV and $7/2^-$ state at 6.38 MeV. Couplings to these states were taken into account within the coupled-channel approach. The spin reorientations were also taken into account. The coupling interaction has the usual form:

$$V_\lambda(R) = -\beta_\lambda R_V \left| \frac{dV^V}{dR} \right| - i\beta_\lambda R_W \left| \frac{dW^D}{dR} \right|, \quad (3.6)$$

where β_λ is the deformation parameter of λ multipole describing the target-nucleus form. Here, we neglect as usual the contribution of the Coulomb interaction.

TABLE 3.4: Parameterized double-folding potentials of the $d+{}^9\text{Be}$ system used in the OM, CC and DWBA calculations.

E_d , MeV	i MeV	V_0 , fm	r_v^a , fm	a_v , fm	W_0 , MeV	r_w^a , fm	a_w , fm	V_0^{SO} , MeV	N_R ,	r_C^a , fm	χ^2/N
19.5	16.18	0.328	0.308	3.99	25.50 (17.5 ^b)	0.328	0.127	3.275	1.22	0.809	2.490
	270.97	0.746	0.831	0.746		0.766					
	30.605	1.491	1.724	0.924		1.491	2.238				
35.0	15.941	0.328	0.308	7.07	22.50 (17.5 ^b)	0.612	0.108	3.275	1.17	0.809	2.503
	268.68	0.746	0.831	0.838		0.731					
	30.58	1.491	1.724	0.999		1.377	1.856				

^a Radii are defined as $R_i = r_i (A_P^{1/3} + A_T^{1/3})$.

^b The values are used in CRC calculations.

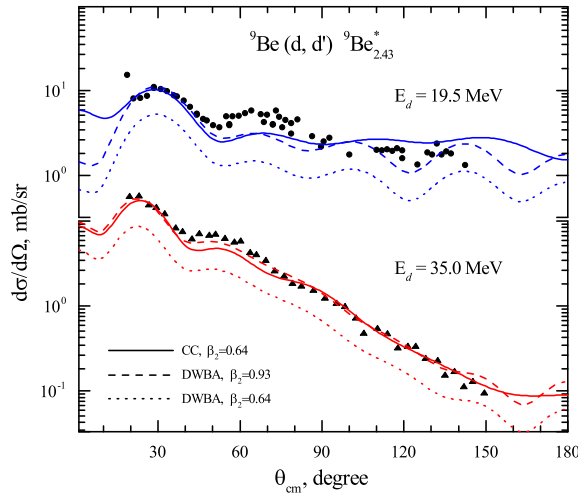


FIGURE 3.14: The cross sections of inelastic scattering ${}^9\text{Be}(d, d') {}^9\text{Be}^*$ ($E_{exc}=2.43 \text{ MeV}$) at laboratory energies 19.5 MeV (full circle) and 35 MeV (full triangle). Theoretical curves are described in the text.

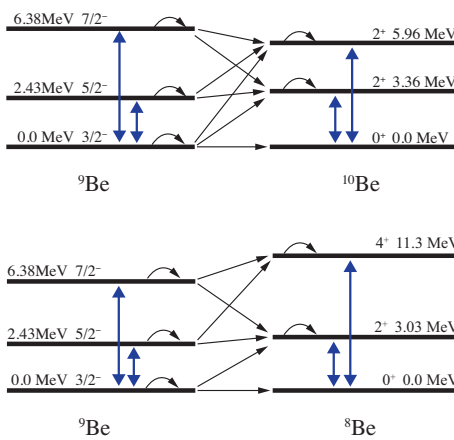


FIGURE 3.15: The target coupling schemes in the ${}^9\text{Be}(d, p){}^{10}\text{Be}$ (upper) and the ${}^9\text{Be}(d, t){}^8\text{Be}$ (lower) nuclear reactions. The bold two-headed arrows indicate $E\lambda$ transitions. The spin re-orientation effects are indicated as back-pointing arrows.

The calculated cross sections for inelastic scattering to the $5/2^-$ state at 2.43 MeV are shown in Fig. 3.14. The solid curves correspond to the results obtained within the CC approach, while the dashed and dotted curves were obtained within the DWBA approach using different values of the deformation parameter β_2 . The used potential parameters are listed in Table ??.

All the results in Fig. 3.14 are in good agreement with the experimental data, except for the cross sections around 60° at 19.5 MeV incident energy. The quadrupole deformation parameter $\beta_2 = 0.64$ extracted within the coupled-channel model is consistent with the previous studies [64, 65].

In the case of DWBA calculations, one uses the DF potential (see Table 3.4) for both the entrance and the exit channels. The DWBA angular distributions very well reproduce the structure of experimental data but clearly underestimate them when the deformation parameter $\beta_2 = 0.64$ is used (see the dotted curves in Fig. 3.14). In order to get the best fit the deformation parameter must be increased up to $\beta_2 = 0.93$, which is quite close to the values reported in previous studies (see, for example, [66, 67]).

Thus, one may confirm that channel coupling and the effects of spin reorientation enhance the cross section that results in the reduction of the deformation parameter. However, the DWBA approach takes into account only first-order contributions to the transition amplitude. In particular, it also describes only general features of the angular distributions and overestimates the deformation parameter in order to compensate the difference between the experimental data and the DWBA cross sections.

3.5.3 One-nucleon transfer reactions

The one-neutron pick-up ${}^9\text{Be}(d, t){}^8\text{Be}$ and stripping ${}^9\text{Be}(d, p){}^{10}\text{Be}$ reactions were analyzed here within the framework of the Coupled Reaction Channels (CRC).

The double-folding potential given in Table 3.4 was used in the CRC calculations for the entrance channel and the global optical parameterizations from Ref. [68, 69] were used for the exit channels. The coupling schemes of target and daughter nuclei for the ${}^9\text{Be}(d, p){}^{10}\text{Be}$ and ${}^9\text{Be}(d, t){}^8\text{Be}$ reactions are illustrated in Fig. 3.15. The states of ${}^{10}\text{Be}$, 2_1^+ and 2_2^+ , as well as the low-lying excited states of ${}^8\text{Be}$, 2^+ and 4^+ , were included in the coupling scheme. Also, the schemes take into account the spin reorientations of states on the condition $J \neq 0$.

In order to construct the bound-state wave functions of the transferred particle in the entrance and exit channels, the common method, i.e. fitting the

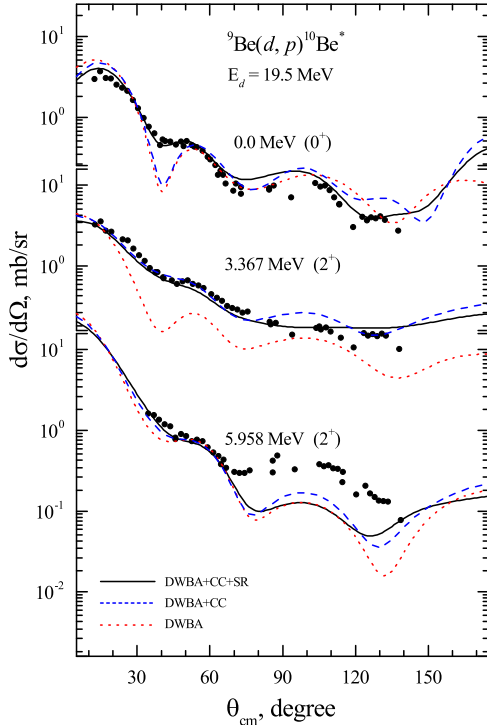


FIGURE 3.16: Differential cross sections for the ${}^9\text{Be}(d, p){}^{10}\text{Be}^*$ reactions at 19.5 MeV leading to different final states (labelled in the figure) in ${}^{10}\text{Be}$. The experimental data are shown in comparison with theoretical results obtained within the CRC method.

depth of the corresponding Woods-Saxon potential to the known binding energy, was employed. The reduced radius and diffuseness in this case are set to be $r = 1.25$ fm and $a = 0.65$ fm, respectively. If the transfer takes place to a final unbound state, the depth of the potential for this state was adjusted to yield a binding energy equal to -0.1 MeV in accordance with the procedure used in Ref. [65].

If the core and the composite nuclei have internal excitation energies, a renewed binding energy BE^* of the transferred particle is expressed by the formula:

$$BE^* = BE - E_{com}^* + E_{core}^* \quad (3.7)$$

where BE – the binding energy of the transferred particle, E_{com}^* , E_{core}^* – excitation energies of the composite and core nuclei, respectively.

The spectroscopic amplitude \mathcal{S} for the addition of a particle to a core with angular momentum J_{core} to form a composite with J_{com} is related to the matrix element of the creation operator \hat{a}^\dagger :

$$\mathcal{S}_{Nlj} = \frac{\langle J_{com} \| \hat{a}_{Nlj}^\dagger \| J_{core} \rangle}{\sqrt{2J_{com} + 1}} \quad (3.8)$$

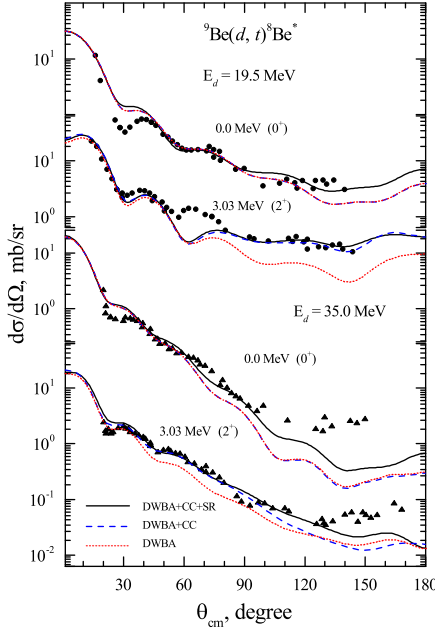


FIGURE 3.17: Differential cross sections for the ${}^9\text{Be}(d, t){}^8\text{Be}^*$ reactions at 19.5 and 35 MeV leading to different final states (labelled in the figure) in ${}^8\text{Be}$. The experimental data are shown in comparison with theoretical results obtained within the CRC method.

where Nlj is the set of particle quantum numbers. The spectroscopic amplitudes for one particle states were calculated by means of the *ANTOINE* code [70] using the effective Cohen-Kurath interaction for p -shell nuclei [71]. The calculated spectroscopic amplitudes for the one-nucleon transfer reactions are listed in Table 3.5.

Angular distributions of the ${}^9\text{Be}(d, p){}^{10}\text{Be}$ nuclear reaction at $E_d=19.5$ MeV are shown in comparison with the theoretical curves calculated in the framework of the CRC method in Fig. 3.16.

In order to study the couplings of the input channels, the outputs were fixed using the deformation parameter of ${}^8\text{Be}$ from Ref. [74], and for ${}^{10}\text{Be}$ from Ref. [65]. The direct transition from the ground state is indicated by the dotted line (DWBA). The contributions of the transitions from excited states (CC), and from spin reorientations (SR) are indicated by dashed and solid lines, respectively. During the analysis, it was found that spin reorientation has a significant contribution in the $p + {}^{10}\text{Be}_{gs}$ channel, especially in the range of 40-60 degrees.

It is interesting to note that we managed to describe within the CRC method the differential cross section of the ${}^9\text{Be}(d, p){}^{10}\text{Be}_{gs}$ reaction at all scattering angles, including the range 40° - 60° , where they were not covered in Refs. [66, 75].

TABLE 3.5: Spectroscopic amplitudes used in CRC calculations for the Composite = Core + Nucleon system. The one-nucleon spectroscopic amplitudes have been calculated by means of the *ANTOINE* code [70]. The alpha spectroscopic amplitudes were taken from [72, 73].

Com	2J ₁	Core	2J ₂	N	2J	SA	Com	2J ₁	Core	2J ₂	N	2J	SA
⁹ Be	3	⁸ Be	0	n	3	-0.761	⁹ Be	3	⁸ Li	2 ₁	p	1	-0.444
⁹ Be	3	⁸ Be	4	n	3	0.816	⁹ Be	3	⁸ Li	6	p	3	-0.592
⁹ Be	3	⁸ Be	4	n	1	-0.242	⁹ Be	3	⁸ Li	2 ₂	p	3	-0.236
⁹ Be	5	⁸ Be	4	n	3	0.986	⁹ Be	3	⁸ Li	2 ₂	p	1	0.036
⁹ Be	5	⁸ Be	4	n	1	-0.417	⁹ Be	5	⁸ Li	4	p	3	0.593
⁹ Be	5	⁸ Be	8	n	3	-0.374	⁹ Be	5	⁸ Li	4	p	1	0.515
⁹ Be	7	⁸ Be	4	n	3	-0.457	⁹ Be	5	⁸ Li	2 ₁	p	3	-0.672
⁹ Be	7	⁸ Be	8	n	3	0.919	⁹ Be	5	⁸ Li	6	p	3	-0.571
⁹ Be	7	⁸ Be	8	n	1	-0.429	⁹ Be	5	⁸ Li	6	p	1	-0.171
⁸ Be	0	⁷ Li	3	p	3	-1.204	⁹ Be	5	⁸ Li	2 ₂	p	3	0.200
⁸ Be	0	⁷ Li	1	p	1	0.736	⁹ Be	7	⁸ Li	4	p	3	-0.323
⁸ Be	4	⁷ Li	3	p	3	-0.748	⁹ Be	7	⁸ Li	6	p	3	-0.899
⁸ Be	4	⁷ Li	3	p	1	-0.612	⁹ Be	7	⁸ Li	6	p	1	-0.564
⁸ Be	4	⁷ Li	1	p	3	0.667	⁷ Li	3	⁶ Li	2	n	3	0.657
⁸ Be	4	⁷ Li	7	p	3	0.624	⁷ Li	3	⁶ Li	2	n	1	-0.538
⁸ Be	4	⁷ Li	5 ₂	p	3	0.079	⁷ Li	3	⁶ Li	6	n	3	0.744
⁸ Be	4	⁷ Li	5 ₂	p	3	-0.146	⁷ Li	3	⁶ Li	4	n	3	-0.032
⁸ Be	8	⁷ Li	7	p	3	0.864	⁷ Li	3	⁶ Li	4	n	1	0.399
⁸ Be	8	⁷ Li	7	p	1	0.687	⁷ Li	1	⁶ Li	2	n	3	-0.925
⁸ Be	8	⁷ Li	5 ₂	p	3	0.374	⁷ Li	1	⁶ Li	2	n	1	0.197
⁸ Li	4	⁷ Li	3	n	3	-0.988	⁷ Li	1	⁶ Li	4	n	3	-0.555
⁸ Li	4	⁷ Li	3	n	1	0.237	⁷ Li	7	⁶ Li	6	n	3	-0.936
⁸ Li	4	⁷ Li	1	n	3	0.430	⁷ Li	7	⁶ Li	6	n	1	0.645
⁸ Li	4	⁷ Li	7	n	3	-0.496	⁷ Li	7	⁶ Li	4	n	3	-0.456
⁸ Li	4	⁷ Li	5	n	3	-0.665	⁷ Li	5 ₂	⁶ Li	2	n	3	-0.650
⁸ Li	4	⁷ Li	5 ₂	n	1	-0.275	⁷ Li	5 ₂	⁶ Li	6	n	3	0.732
⁸ Li	2 ₁	⁷ Li	3	n	3	0.567	⁷ Li	5 ₂	⁶ Li	6	n	1	0.549
⁸ Li	2 ₁	⁷ Li	3	n	1	0.351	⁷ Li	5 ₂	⁶ Li	4	n	3	0.200
⁸ Li	2 ₁	⁷ Li	1	n	3	0.905	⁷ Li	5 ₂	⁶ Li	4	n	1	-0.114
⁸ Li	2 ₁	⁷ Li	1	n	1	0.331	⁶ Li	2	d	2	α	0	0.907
⁸ Li	2 ₁	⁷ Li	5 ₂	n	3	0.767	⁶ Li	2	d	2	α	4	0.077
⁸ Li	6	⁷ Li	3	n	3	0.581	⁶ Li	6	d	2	α	4	0.943
⁸ Li	6	⁷ Li	5 ₂	n	3	-0.660	⁶ Li	6	d	2	α	8	0.028
⁸ Li	6	⁷ Li	5 ₂	n	1	-0.541	⁶ Li	4	d	2	α	4	0.929
⁸ Li	6	⁷ Li	7	n	3	0.973	⁹ Be	3	⁵ He	3	α	0	-0.925
⁸ Li	6	⁷ Li	7	n	1	-0.404	⁹ Be	5	⁵ He	3	α	4	0.784
⁸ Li	2 ₂	⁷ Li	3	n	3	-0.617	⁹ Be	5	⁵ He	3	α	4	0.974
⁸ Li	2 ₂	⁷ Li	3	n	1	-0.841	⁹ Be	5	⁵ He	3	α	8	-0.260
⁸ Li	2 ₂	⁷ Li	1	n	3	0.178	⁹ Be	7	⁵ He	3	α	4	0.882
⁸ Li	2 ₂	⁷ Li	1	n	1	0.331	⁹ Be	7	⁵ He	3	α	8	-0.737
⁸ Li	2 ₂	⁷ Li	5	n	3	0.231	⁷ Li	3	t	1	α	1	0.970
⁹ Be	3	⁸ Li	4	p	3	-0.947	⁷ Li	1	t	1	α	1	0.961
⁹ Be	3	⁸ Li	4	p	1	-0.319	⁷ Li	7	t	1	α	3	0.952
⁹ Be	3	⁸ Li	2 ₁	p	3	0.454	⁷ Li	5 ₂	t	1	α	3	0.223

An appreciable contribution of the $3/2^- \rightarrow 2_1^+$, $5/2^- \rightarrow 2_1^+$, $7/2^- \rightarrow 2_1^+$ transitions was observed in the $p + {}^{10}\text{Be}_{3.37}$ channel in the entire range of scattering angles. In the cross section of the $p + {}^{10}\text{Be}_{5.96}$ channel, the theoretical calculation underestimates the experimental data starting from 70° . Possibly, other higher excited states of ${}^9\text{Be}$ should be taken into account.

Figure 3.17 displays the cross sections of the ${}^9\text{Be}(d, t){}^8\text{Be}$ nuclear reaction at both 19.5 MeV and 35 MeV incident energies. As in the case of the (d, p) reactions, the (d, t) reactions also show the strong channel-coupling effects. We see a manifestation of spin-reorientation effects in the $t + {}^8\text{Be}_{gs}$ channels and a significant contribution of the $3/2^- \rightarrow 2^+$, $5/2^- \rightarrow 2^+$, $7/2^- \rightarrow 2^+$ transitions in the $t + {}^8\text{Be}_{3.03}$ channel. Disagreements around 30° in the $t + {}^8\text{Be}_{gs}$ channel for both 19.5 MeV and 35 MeV incident energies and around 60° in the $t + {}^8\text{Be}_{3.03}$ channel for 19.5 MeV incident energy are possibly caused by the uncertainty in the $t + {}^8\text{Be}$ interaction potential.

Theoretical calculations made within the CRC method show, in general, good agreement with the experimental data for both (d, p) and (d, t) reactions. The analysis showed strong coupling effects in both entrance and exit channels. The effects of such couplings were also emphasized in Refs. [65, 76].

3.5.4 Cluster-transfer reaction

Differential cross sections for the nuclear reaction ${}^9\text{Be}(d, \alpha){}^7\text{Li}$ are of particular interest. This is due to the specific behaviour of the cross section at large scattering angles, which indicates a ${}^5\text{He}$ cluster transfer. In addition, the cross section calculated within the DWBA approach underestimates the data even at forward scattering angles. Therefore, in order to understand the difference between theory and experiment, the following transfer mechanisms are suggested (see Fig. 3.18):

- direct transfer of heavy clusters d and ${}^5\text{He}$;
- sequential two-step transfer of $n-p$, $p-n$, $n-\alpha$ and $\alpha-n$;

The resulting differential cross section for the ${}^9\text{Be}(d, \alpha){}^7\text{Li}$ reaction has the form of a coherent sum of two amplitudes

$$\frac{d\sigma}{d\Omega}(\theta) = |f_I(\theta) + f_{II}(\theta)|^2, \quad (3.9)$$

where the amplitude

$$f_I(\theta) = f_{{}^5\text{He}}(\pi - \theta) + f_{n-\alpha}(\pi - \theta) + f_{\alpha-n}(\pi - \theta) \quad (3.10)$$

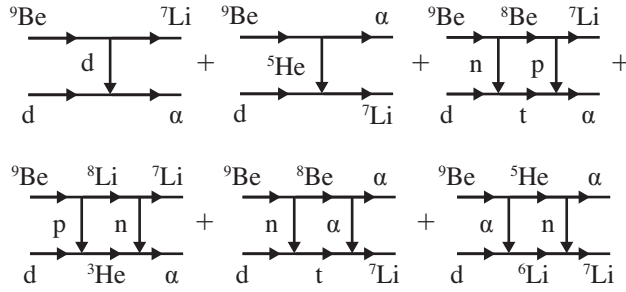


FIGURE 3.18: The scheme illustrates the reaction mechanisms taken into account in CRC calculations of the cross sections for ${}^9\text{Be}(d, \alpha){}^7\text{Li}$ reaction.

describes the transfer of the heavy ${}^5\text{He}$ -cluster and sequential two-step transfer of $n-\alpha$ and $\alpha-n$, and the amplitude

$$f_{II}(\theta) = f_d(\theta) + f_{n-p}(\theta) + f_{p-n}(\theta) \quad (3.11)$$

corresponds to the deuteron pick-up and sequential two-step transfer of $n-p$ and $p-n$.

The DF potential (see Table 3.4) for the entrance channel and global optical potential parameterizations from Refs. [69, 77, 78] for intermediate and exit channels were used in the analysis. The prior form for the first coupling and the post form for the second coupling were chosen for two-step transfer reactions in order to avoid the non-orthogonal terms in the calculations of transition amplitudes.

The spectroscopic amplitudes of the d and ${}^5\text{He}$ clusters were taken from Ref. [79], while the alpha-cluster spectroscopic amplitudes given in Table 3.5 were provided by Dr. A. Volya within the method reported in Ref. [73].

The calculated cross sections are shown in Fig. 3.19 with the α -particle angular distributions formed in the ${}^9\text{Be}(d, \alpha){}^7\text{Li}^*$ reaction at incident energies of 19.5 and 35 MeV and corresponding to the low-lying excitation of the ${}^7\text{Li}$ nucleus in the exit channels. The transfer of the deuteron (dash-dotted curve) provides the dominant contribution in all the channels. Despite the fact that the spectroscopic amplitude of the deuteron $S_{1D_3} = 0.558$ in the ${}^9\text{Be}$ nucleus is not of great importance, a noticeable cross section is due to the large value of the deuteron spectroscopic amplitude $S_{1S_1} = 1.732$ of ${}^4\text{He}$.

The angular distribution of deuteron transfer has a significant cross section also at the backward scattering angles, which is mainly caused by the contribution of the D wave. This symmetrical behaviour of the cross section of D waves is very similar to the cross section of evaporation residues. Tanaka *et*

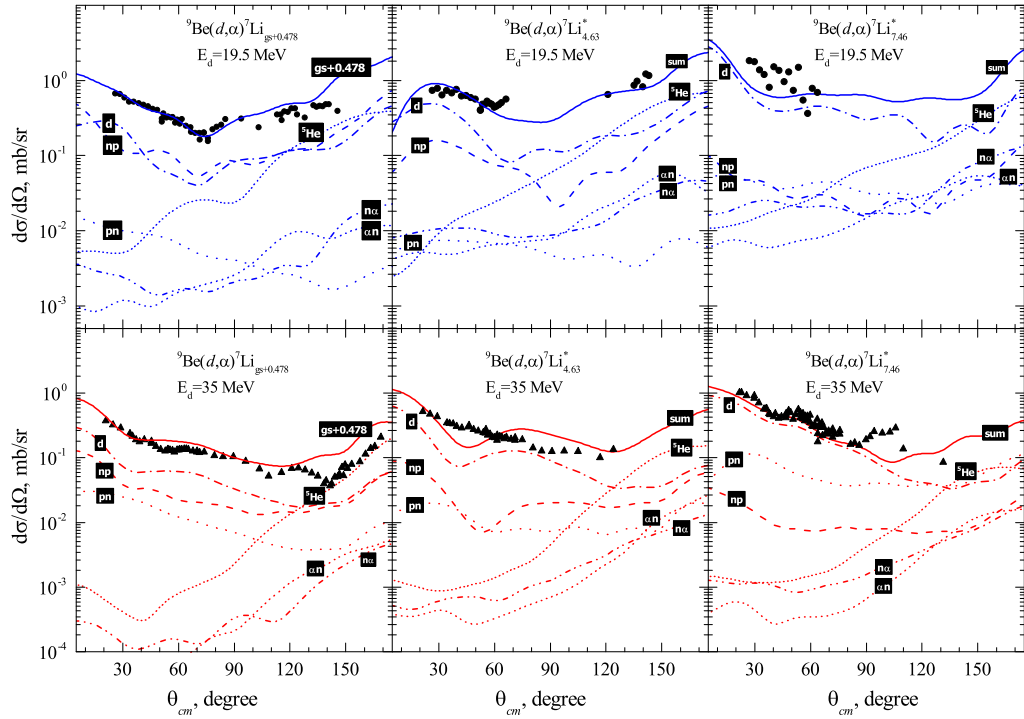


FIGURE 3.19: Differential cross sections for the ${}^9\text{Be}(d,\alpha){}^7\text{Li}$ reactions measured at 19.5 MeV and 35 MeV energy with the ${}^7\text{Li}$ observed in the ground or low-lying excited states in the exit channels.

al [80] analyzed the role of the compound process in ${}^9\text{Be}(d,\alpha){}^7\text{Li}$ reaction and claimed the domination of the compound nucleus channels at the energies of 12.17 MeV and 14.43 MeV. However, in Ref. [66] the negligible contribution of the compound-nucleus mechanism was shown at 7 MeV using the DWBA analysis. In this regard, our theoretical results based on the CRC method show that there is no need to take into account the mechanism through the compound-nucleus formation at energies of 19.5 and 35.0 MeV.

Starting from scattering angle $\theta_{c.m.} = 120^\circ$, the transfer of the ${}^5\text{He}$ cluster, labeled as ${}^5\text{He}$ in Fig. 3.19, has a predominant contribution in all channels. It should be noted that a similar result was reported earlier in Ref. [66]. One-step transfer of the ${}^5\text{He}$ cluster was also indicated as a dominant process by Jarczyk *et al* [81] in studying the ${}^{12}\text{C}({}^{11}\text{B}, {}^6\text{Li}){}^{17}\text{O}$ and ${}^{12}\text{C}(d, {}^7\text{Li}){}^7\text{Be}$ reactions.

Using the CRC method, we are able to estimate the contribution of the sequential transfer of ${}^5\text{He}$, which was not studied before. Corresponding cross sections are shown in Fig. 3.19 as curves labeled $n\alpha$ and αn . It turned out that the $n\alpha$ and αn transfer processes provide indeed a contribution more than one order of magnitude smaller in comparison with the one-step ${}^5\text{He}$ transfer. Nevertheless, it should be noted that the contribution of the $n\alpha$ and the αn

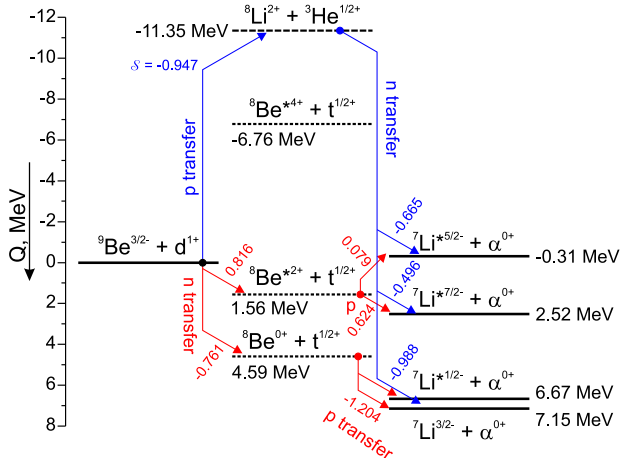


FIGURE 3.20: The scheme illustrates the energy balance of the different intermediate stages for the two-step mechanisms of ${}^9\text{Be}(d, \alpha){}^7\text{Li}$ transfer reaction. The Q -values for the different intermediate channels are shown near the corresponding lines. The numbers near the arrows correspond to the spectroscopic amplitudes of the heaviest reaction participants. For example, spectroscopic amplitude for the ${}^9\text{Be} = {}^8\text{Li} + p$ configuration is equal $S = -0.947$.

transfer channels increases with the increase in the ${}^7\text{Li}$ excitation energy, where they should not be ignored.

The two-step n - p transfer is another mechanism providing a noticeable contribution to the cross section. It is due to the prominent cluster structure of the ${}^9\text{Be}$ nucleus having the weakly bound neutron. This structural feature explains also the weakness of the p - n sequential transfer contribution to the cross section corresponding to the ${}^7\text{Li}(\text{g.s.})$ in the exit channel. However, with increasing the ${}^7\text{Li}$ excitation energy these two mechanisms are interchanged in the significance of their contributions, as depicted by the curves in Fig. 3.19, and the p - n transfer begins to play a leading role, providing, in particular, almost 10 times larger contribution in the case of reaction at $E_{\text{lab}} = 35$ MeV with ${}^7\text{Li}^*(7.46)$ MeV in exit channel.

In Fig. 3.20, the possible scenarios for the n - p and p - n sequential transfer for the reaction under consideration are shown in respect to the Q -values. One may see that all the steps of the n - p sequential transfer have positive Q -values, while the p - n transfer goes through the intermediate channel ${}^8\text{Li} + {}^3\text{He}$ that has a considerably negative Q -value. Together with the large values of the spectroscopic amplitudes (shown near to the arrows in Fig. 3.20), this explains the leading role of the $(d, t; t, \alpha)$ mechanism in populating the ground state of ${}^7\text{Li}$ in the exit channel.

The situation becomes quite different in the case of the ${}^7\text{Li}^*(5/2^-)$ in the exit

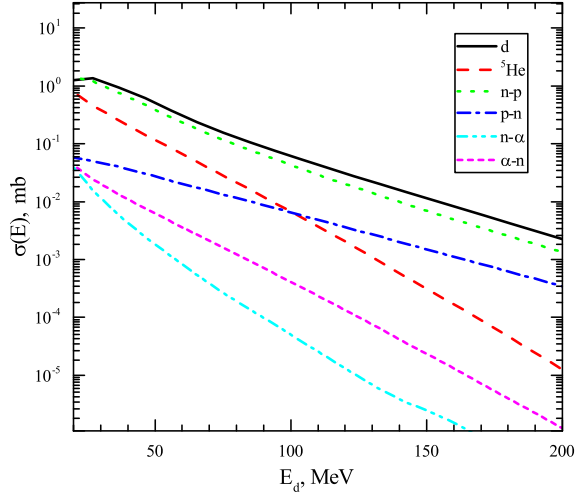


FIGURE 3.21: Contributions of the different mechanisms to the cross section of the ${}^9\text{Be}(d, \alpha){}^7\text{Li}_{g.s.}$ reaction. See Fig. 3.18 for explanation of the curve notations.

channel. First, the population of this state through the $n-p$ transfer involves the ${}^9\text{Be} = {}^8\text{Be}^*(2^+) + n$ intermediate configuration where the ${}^8\text{Be}$ cluster has to be in the 2^+ excited state. Note that the ${}^8\text{Be}(0^+)$ ground state is inappropriate because of angular-momentum-coupling mismatch in the entrance and exit configurations. Second, the extremely small spectroscopic amplitude of the ${}^8\text{Be}^*(2^+) = {}^7\text{Li}^*(5/2^-) + p$ configuration, which is $\mathcal{S} = 0.079$, influences the transfer amplitude. These two factors lead to the suppression of the contribution of $(d, t; t, \alpha)$ mechanism in population of the ${}^7\text{Li}^*(5/2^-)$ state in the exit channel. Therefore, the $p-n$ sequential transfer prevails over the $n-p$ one.

Figure 3.21 shows the contributions of all the mechanisms mentioned above to the total cross section of the ${}^9\text{Be}(d, \alpha){}^7\text{Li}_{g.s.}$ reaction (see Fig. 3.18) as a function of the deuteron energy. One may conclude that mainly four mechanisms contribute to the cross section of this reaction. The transfer of the deuteron-cluster is the predominant channel at all collision energies. The sequential $n-p$ and $p-n$ transfers play a significant role at the high energies. The ${}^5\text{He}$ -cluster transfer gives almost 20% of the cross section at low energies and outdoes the sequential $p-n$ transfer in this energy domain. This allows us to claim that the configurations $n+{}^8\text{Be}$ and $\alpha + {}^5\text{He}$ provide noticeable contributions to the ground-state wave function of the ${}^9\text{Be}$ nucleus. These conclusions agree well with the previous experimental studies [13, 14].

Chapter 4

Key findings and Conclusion

Appendix A

Some aspects from the quantum theory of angular momenta

A total angular momentum \mathbf{j} are decomposed into two angular momenta \mathbf{j}_1 and \mathbf{j}_2 by means of the Clebsch-Gordan coefficient. For example, to quote a basis $|jm\rangle$ with the angular momentum j with its z -component m , the Clebsch-Gordan coefficient can be represented as follow

$$|jm\rangle = \sum_{m_1 m_2} \langle j_1 m_1 j_2 m_2 | jm \rangle |j_1 m_1\rangle |j_2 m_2\rangle, \quad (\text{A.1})$$

For non-zero values of the coefficient (A.1) vectors \mathbf{j}_1 , \mathbf{j}_2 and \mathbf{j} must satisfy the rule of triangle:

$$\begin{aligned} |j_1 - j_2| &\leq j \leq j_1 + j_2 \\ |j - j_2| &\leq j_1 \leq j + j_2 \\ |j_1 - j| &\leq j_2 \leq j_1 + j \end{aligned}$$

and the condition

$$m = m_1 + m_2.$$

If there are three vectors \mathbf{j}_1 , \mathbf{j}_2 and \mathbf{j}_3 , one can get a total angular momentum \mathbf{j} in two ways

$$\mathbf{j} = (\mathbf{j}_1 + \mathbf{j}_2) + \mathbf{j}_3 = \mathbf{j}_{12} + \mathbf{j}_3 \quad (\text{A.2})$$

$$= \mathbf{j}_1 + (\mathbf{j}_2 + \mathbf{j}_3) = \mathbf{j}_1 + \mathbf{j}_{23} \quad (\text{A.3})$$

The Basis $|(j_1 j_2) j_{12}, j_3; jm\rangle$ and the basis $|j_1, (j_2 j_3); jm\rangle$ corresponding to Eq. (A.2) and Eq. (A.3) are related through a factor $U(j_1 j_2 j_3; j_{12} j_{23})$, which

is the Racah coefficient:

$$|(j_1 j_2) j_{12}, j_3; jm\rangle = \sum_{j_{23}} U(j_1 j_2 j_3; j_{12} j_{23}) |j_1, (j_2 j_3); jm\rangle. \quad (\text{A.4})$$

Four angular momenta, \mathbf{j}_1 , \mathbf{j}_2 , \mathbf{j}_3 and \mathbf{j}_4 , are added into the total momentum \mathbf{j} by

$$\mathbf{j} = (\mathbf{j}_1 + \mathbf{j}_2) + (\mathbf{j}_3 + \mathbf{j}_4) = \mathbf{j}_{12} + \mathbf{j}_{34} \quad (\text{A.5})$$

$$= (\mathbf{j}_1 + \mathbf{j}_3) + (\mathbf{j}_2 + \mathbf{j}_4) = \mathbf{j}_{13} + \mathbf{j}_{24} \quad (\text{A.6})$$

Two basis $|j_1 j_2(j_{12}), j_3 j_4(j_{34}); jm\rangle$ and $|j_1 j_3(j_{13}), j_2 j_4(j_{24}); jm\rangle$, constructed respectively on the scheme Eq. A.5 and Eq. A.6, are related as follow

$$|j_1 j_2(j_{12}), j_3 j_4(j_{34}); jm\rangle = \sum_{j_{13}, j_{24}} \begin{bmatrix} j_1 & j_2 & j_{12} \\ j_3 & j_4 & j_{34} \\ j_{13} & j_{24} & j \end{bmatrix} |j_1 j_3(j_{13}), j_2 j_4(j_{24}); jm\rangle \quad (\text{A.7})$$

where transformation coefficient with square brackets is called a unitary 9j-symbol.

A spacial spherical harmonics is expressed like

$$\mathcal{Y}_{lm}(\mathbf{r}) = r^l Y_{lm}(\hat{r}) \quad (\text{A.8})$$

where $Y_{lm}(\hat{r})$ – spherical function, which is a eigenfunction of angular part the $\Delta_{\hat{r}}$ Laplace operator. For $\mathbf{r} = a\mathbf{r}_1 + b\mathbf{r}_2$ a decomposition of the spacial spherical harmonics $\mathcal{Y}_{lm}(\mathbf{r})$ leads to the following equality

$$\begin{aligned} \mathcal{Y}_{lm}(\mathbf{r} = a\mathbf{r}_1 + b\mathbf{r}_2) &= \sum_{l_1, l_2, m_1, m_2} a^{l_1} b^{l_2} \langle l_1 m_1 | l_2 m_2 | lm \rangle \mathcal{D}(l, l_1, l_2) \times \\ &\quad \times \mathcal{Y}_{l_1 m_1}(\mathbf{r}_1) \mathcal{Y}_{l_2 m_2}(\mathbf{r}_2) \\ &= \sum_{l_1, l_2} a^{l_1} b^{l_2} \mathcal{D}(l, l_1, l_2) [\mathcal{Y}_{l_1}(\mathbf{r}_1) \times \mathcal{Y}_{l_2}(\mathbf{r}_2)]_{lm} \end{aligned} \quad (\text{A.9})$$

with the condition $l = l_1 + l_2$, and $\mathcal{D}(l, l_1, l_2)$ is given by

$$\mathcal{D}(l, l_1, l_2) = \sqrt{\frac{4\pi(2l+1)!}{(2l_1+1)!(2l_2+1)!}} \quad (\text{A.10})$$

Spherical harmonics with the argument are coupled as follow

$$[Y_{l_1}(\hat{r}) \times Y_{l_2}(\hat{r})]_{lm} = \mathcal{C}(l_1, l_2, l) Y_{lm}(\hat{r}) \quad (\text{A.11})$$

where the $\mathcal{C}(l_1, l_2, l)$ coefficient reads as

$$\mathcal{C}(l_1, l_2, l) = \sqrt{\frac{(2l_1 + 1)(2l_2 + 1)}{4\pi(2l + 1)}} \langle l_1 0 \ l_2 0 \ | \ l 0 \rangle \quad (\text{A.12})$$

It would be useful also note a coupling between two spherical hyper harmonics kind of

$$\left[Y_{l_{12}}^{(l_1 l_2)}(\hat{\mathbf{r}}_1, \hat{\mathbf{r}}_2) \times Y_{l_{34}}^{(l_3 l_4)}(\hat{\mathbf{r}}_1, \hat{\mathbf{r}}_2) \right]_{lm} = \sum_{l_{13} l_{24}} E_{l_{13} l_{24}}^{l_1 l_2 l_{12} l_2 l_4 l_{34} l} Y_{lm}^{(l_{13} l_{24})}(\hat{\mathbf{r}}_1, \hat{\mathbf{r}}_2) \quad (\text{A.13})$$

where the coupling coefficient $E_{l_{13} l_{24}}^{l_1 l_2 l_{12} l_2 l_4 l_{34} l}$ is given as

$$E_{l_{13} l_{24}}^{l_1 l_2 l_{12} l_2 l_4 l_{34} l} = \begin{bmatrix} l_1 & l_2 & l_{12} \\ l_3 & l_4 & l_{34} \\ l_{13} & l_{24} & l \end{bmatrix} \mathcal{C}(l_1, l_3, l_{13}) \mathcal{C}(l_2, l_4, l_{24}). \quad (\text{A.14})$$

Appendix B

Parameters of the three body wave function

B.1 Helium-6

TABLE B.1: The three-body wave function parameters found by means of variational approach for the ground state of ${}^6\text{He}$

i	$\alpha_i^{(k)}$	$\beta_i^{(k)}$	C_i
$\gamma \equiv 0 \ 0 \ 0$			
1	0.03872262	0.09444994	-0.1737337132E-04
2	0.03872262	0.28926931	-0.7746568943E-01
3	0.03872262	0.50341072	0.1537953138E+00
4	0.03872262	0.75592149	-0.2068222047E+00
5	0.03872262	1.07956780	0.1915099409E+00
6	0.03872262	1.54178260	-0.1186045848E+00
7	0.03872262	2.31514050	0.4377908070E-01
8	0.03872262	4.02900180	-0.8511508780E-02
9	0.03872262	12.33951600	0.8124669663E-03
10	0.11859473	0.09444994	0.1914598067E+00
11	0.11859473	0.28926931	-0.4142283997E-01
12	0.11859473	0.50341072	-0.9504287755E+00
13	0.11859473	0.75592149	0.5100204701E+00
14	0.11859473	1.07956780	0.4351961872E+00
15	0.11859473	1.54178260	-0.5512501566E+00
16	0.11859473	2.31514050	0.2353573699E+00
17	0.11859473	4.02900180	-0.3888384752E-01
18	0.11859473	12.33951600	0.2142226702E-02

Continued on next page

Table B.1 – continued from previous page

i	$\alpha_i^{(k)}$	$\beta_i^{(k)}$	C_i
19	0.20638850	0.09444994	-0.7243857878E+00
20	0.20638850	0.28926931	0.1811320023E+01
21	0.20638850	0.50341072	-0.2829679245E+00
22	0.20638850	0.75592149	0.6392623958E-01
23	0.20638850	1.07956780	-0.1629089089E+01
24	0.20638850	1.54178260	0.1304993071E+01
25	0.20638850	2.31514050	-0.4928065738E+00
26	0.20638850	4.02900180	0.1996819496E-01
27	0.20638850	12.33951600	0.1060241013E-01
28	0.30991295	0.09444994	0.1599423834E+01
29	0.30991295	0.28926931	-0.5264844147E+01
30	0.30991295	0.50341072	0.7012917232E+01
31	0.30991295	0.75592149	-0.4714686948E+01
32	0.30991295	1.07956780	-0.4796509839E+00
33	0.30991295	1.54178260	0.2065489512E+01
34	0.30991295	2.31514050	-0.8987555045E+00
35	0.30991295	4.02900180	0.4500233344E+00
36	0.30991295	12.33951600	-0.8218053258E-01
37	0.44260156	0.09444994	-0.1956103683E+01
38	0.44260156	0.28926931	0.7193813517E+01
39	0.44260156	0.50341072	-0.1163049706E+02
40	0.44260156	0.75592149	0.6193322640E+01
41	0.44260156	1.07956780	0.7415949805E+01
42	0.44260156	1.54178260	-0.8938587045E+01
43	0.44260156	2.31514050	0.3391887206E+01
44	0.44260156	4.02900180	-0.1168066181E+01
45	0.44260156	12.33951600	0.1744136293E+00
46	0.63210054	0.09444994	0.1402383982E+01
47	0.63210054	0.28926931	-0.5136700789E+01
48	0.63210054	0.50341072	0.8665026533E+01
49	0.63210054	0.75592149	-0.2933774272E+01
50	0.63210054	1.07956780	-0.8943836753E+01
51	0.63210054	1.54178260	0.8717580886E+01
52	0.63210054	2.31514050	-0.3215399907E+01

Continued on next page

Table B.1 – continued from previous page

i	$\alpha_i^{(k)}$	$\beta_i^{(k)}$	C_i
53	0.63210054	4.02900180	0.1165125187E+01
54	0.63210054	12.33951600	-0.1665816218E+00
55	0.94916212	0.09444994	-0.5455065421E+00
56	0.94916212	0.28926931	0.1973142226E+01
57	0.94916212	0.50341072	-0.3305486410E+01
58	0.94916212	0.75592149	0.5936725650E+00
59	0.94916212	1.07956780	0.4339113002E+01
60	0.94916212	1.54178260	-0.4005833236E+01
61	0.94916212	2.31514050	0.1671843031E+01
62	0.94916212	4.02900180	-0.6442299484E+00
63	0.94916212	12.33951600	0.8553541645E-01
64	1.65181150	0.09444994	0.1291465276E+00
65	1.65181150	0.28926931	-0.3358554818E+00
66	1.65181150	0.50341072	0.6888942468E+00
67	1.65181150	0.75592149	-0.1350120966E+00
68	1.65181150	1.07956780	-0.1153775517E+01
69	1.65181150	1.54178260	0.1271270643E+01
70	1.65181150	2.31514050	-0.7908870481E+00
71	1.65181150	4.02900180	0.2382269089E+00
72	1.65181150	12.33951600	-0.2472769828E-01
73	5.05895900	0.09444994	-0.1003954377E+00
74	5.05895900	0.28926931	-0.1270223362E+00
75	5.05895900	0.50341072	-0.3653418537E+00
76	5.05895900	0.75592149	0.6548391778E+00
77	5.05895900	1.07956780	-0.1837812114E+00
78	5.05895900	1.54178260	0.2724244480E+00
79	5.05895900	2.31514050	0.5022837020E-01
80	5.05895900	4.02900180	-0.1318577464E-01
81	5.05895900	12.33951600	-0.5334531276E-03
$\gamma \equiv 1\ 1\ 1\ 1$			
1	0.03872262	0.09444994	-0.1209912997E-03
2	0.03872262	0.28926931	-0.2752286691E-03
3	0.03872262	0.50341072	0.8313112741E-03

Continued on next page

Table B.1 – continued from previous page

i	$\alpha_i^{(k)}$	$\beta_i^{(k)}$	C_i
4	0.03872262	0.75592149	-0.1569396728E-02
5	0.03872262	1.07956780	0.1841931183E-02
6	0.03872262	1.54178260	-0.1329878249E-02
7	0.03872262	2.31514050	0.5732118509E-03
8	0.03872262	4.02900180	-0.1407523317E-03
9	0.03872262	12.33951600	0.2464625078E-04
10	0.11859473	0.09444994	0.3780785946E-03
11	0.11859473	0.28926931	-0.1000393773E-01
12	0.11859473	0.50341072	0.1426933985E-01
13	0.11859473	0.75592149	-0.2639755490E-01
14	0.11859473	1.07956780	0.3639070623E-01
15	0.11859473	1.54178260	-0.3096578932E-01
16	0.11859473	2.31514050	0.1507393647E-01
17	0.11859473	4.02900180	-0.4078109925E-02
18	0.11859473	12.33951600	0.7893561124E-03
19	0.20638850	0.09444994	-0.1675476628E-02
20	0.20638850	0.28926931	0.3933745812E-01
21	0.20638850	0.50341072	-0.1092045673E+00
22	0.20638850	0.75592149	0.1542197135E+00
23	0.20638850	1.07956780	-0.1840525972E+00
24	0.20638850	1.54178260	0.1475223686E+00
25	0.20638850	2.31514050	-0.6976541581E-01
26	0.20638850	4.02900180	0.1855170403E-01
27	0.20638850	12.33951600	-0.3521003985E-02
28	0.30991295	0.09444994	0.4106806042E-02
29	0.30991295	0.28926931	-0.9266191014E-01
30	0.30991295	0.50341072	0.2815735552E+00
31	0.30991295	0.75592149	-0.4603450597E+00
32	0.30991295	1.07956780	0.5000169839E+00
33	0.30991295	1.54178260	-0.3928705377E+00
34	0.30991295	2.31514050	0.1830077652E+00
35	0.30991295	4.02900180	-0.4774102277E-01
36	0.30991295	12.33951600	0.7847255538E-02
37	0.44260156	0.09444994	-0.5723743876E-02

Continued on next page

Table B.1 – continued from previous page

i	$\alpha_i^{(k)}$	$\beta_i^{(k)}$	C_i
38	0.44260156	0.28926931	0.1267185089E+00
39	0.44260156	0.50341072	-0.4013118748E+00
40	0.44260156	0.75592149	0.6809541150E+00
41	0.44260156	1.07956780	-0.7658315705E+00
42	0.44260156	1.54178260	0.5861381351E+00
43	0.44260156	2.31514050	-0.2712619146E+00
44	0.44260156	4.02900180	0.7108163202E-01
45	0.44260156	12.33951600	-0.1022953848E-01
46	0.63210054	0.09444994	0.4677586570E-02
47	0.63210054	0.28926931	-0.1014186442E+00
48	0.63210054	0.50341072	0.3298241305E+00
49	0.63210054	0.75592149	-0.5616842239E+00
50	0.63210054	1.07956780	0.6411713372E+00
51	0.63210054	1.54178260	-0.4946856323E+00
52	0.63210054	2.31514050	0.2242477697E+00
53	0.63210054	4.02900180	-0.6092825450E-01
54	0.63210054	12.33951600	0.8592838651E-02
55	0.94916212	0.09444994	-0.2194397884E-02
56	0.94916212	0.28926931	0.4740184928E-01
57	0.94916212	0.50341072	-0.1572767288E+00
58	0.94916212	0.75592149	0.2605021995E+00
59	0.94916212	1.07956780	-0.2950306986E+00
60	0.94916212	1.54178260	0.2325275547E+00
61	0.94916212	2.31514050	-0.1002393441E+00
62	0.94916212	4.02900180	0.2887819798E-01
63	0.94916212	12.33951600	-0.4542642070E-02
64	1.65181150	0.09444994	0.5992856734E-03
65	1.65181150	0.28926931	-0.1164675896E-01
66	1.65181150	0.50341072	0.4636939204E-01
67	1.65181150	0.75592149	-0.5909598945E-01
68	1.65181150	1.07956780	0.7349403097E-01
69	1.65181150	1.54178260	-0.6253335023E-01
70	1.65181150	2.31514050	0.2300764414E-01
71	1.65181150	4.02900180	-0.6869029310E-02

Continued on next page

Table B.1 – continued from previous page

i	$\alpha_i^{(k)}$	$\beta_i^{(k)}$	C_i
72	1.65181150	12.33951600	0.1279464637E-02
73	5.05895900	0.09444994	-0.8739688325E-04
74	5.05895900	0.28926931	0.2659208242E-02
75	5.05895900	0.50341072	-0.4297540353E-02
76	5.05895900	0.75592149	0.1984703845E-01
77	5.05895900	1.07956780	-0.1802355036E-01
78	5.05895900	1.54178260	0.1173642602E-01
79	5.05895900	2.31514050	-0.7529136326E-02
80	5.05895900	4.02900180	0.1375626183E-02
81	5.05895900	12.33951600	-0.2653098521E-03
$\gamma \equiv 2\ 2\ 0\ 0$			
1	0.07010120	0.17098674	0.8287413344E-05
2	0.07010120	0.55006725	-0.2315910360E-03
3	0.07010120	1.07956780	0.2205912189E-03
4	0.07010120	2.11877100	-0.1546351743E-03
5	0.07010120	6.81612260	0.1309976070E-03
6	0.22551676	0.17098674	0.1592019751E-03
7	0.22551676	0.55006725	0.1457399081E-02
8	0.22551676	1.07956780	-0.6213676741E-02
9	0.22551676	2.11877100	0.5178724836E-02
10	0.22551676	6.81612260	-0.4694996433E-02
11	0.44260156	0.17098674	-0.3630365442E-03
12	0.44260156	0.55006725	0.5589096347E-03
13	0.44260156	1.07956780	0.9499448616E-02
14	0.44260156	2.11877100	-0.1099890159E-01
15	0.44260156	6.81612260	0.1241336217E-01
16	0.86865448	0.17098674	0.3996664351E-03
17	0.86865448	0.55006725	-0.4801971131E-03
18	0.86865448	1.07956780	-0.9127801910E-02
19	0.86865448	2.11877100	0.6666082171E-02
20	0.86865448	6.81612260	-0.1471088050E-01
21	2.79447630	0.17098674	-0.3154650054E-03
22	2.79447630	0.55006725	-0.8889072435E-04

Continued on next page

Table B.1 – continued from previous page

i	$\alpha_i^{(k)}$	$\beta_i^{(k)}$	C_i
23	2.79447630	1.07956780	0.1109393782E-01
24	2.79447630	2.11877100	-0.2003915591E-01
25	2.79447630	6.81612260	0.1595658076E-01
$\gamma \equiv 3\ 3\ 1\ 1$			
1	0.07010120	0.17098674	-0.2579335841E-06
2	0.07010120	0.55006725	-0.2765357271E-05
3	0.07010120	1.07956780	0.6139330639E-05
4	0.07010120	2.11877100	-0.7938375153E-05
5	0.07010120	6.81612260	0.1167298934E-04
6	0.22551676	0.17098674	0.5917355271E-06
7	0.22551676	0.55006725	-0.6483646762E-04
8	0.22551676	1.07956780	0.8695083699E-05
9	0.22551676	2.11877100	-0.4800513075E-05
10	0.22551676	6.81612260	0.6570347080E-06
11	0.44260156	0.17098674	-0.1470428346E-05
12	0.44260156	0.55006725	0.1350176334E-03
13	0.44260156	1.07956780	-0.2583695882E-03
14	0.44260156	2.11877100	0.1700235229E-03
15	0.44260156	6.81612260	-0.2196174841E-03
16	0.86865448	0.17098674	0.2122290583E-05
17	0.86865448	0.55006725	-0.1948661774E-03
18	0.86865448	1.07956780	0.3856831336E-03
19	0.86865448	2.11877100	-0.3277457806E-03
20	0.86865448	6.81612260	0.4749778522E-03
21	2.79447630	0.17098674	-0.3460810077E-05
22	2.79447630	0.55006725	0.3075671947E-03
23	2.79447630	1.07956780	-0.6343122836E-03
24	2.79447630	2.11877100	0.6129185220E-03
25	2.79447630	6.81612260	-0.7981418030E-03

B.2 Lithium-6

TABLE B.2: The three-body wave function parameters found by means of variational approach for the ground state of ${}^6\text{Li}$

i	$\alpha_i^{(k)}$	$\beta_i^{(k)}$	C_i
$\gamma \equiv 0 \ 0 \ 0 \ 1$			
1	0.04011531	0.10896291	-0.1803892906E-03
2	0.04011531	0.33559821	0.3207207170E-01
3	0.04011531	0.59133984	-0.3287679135E-01
4	0.04011531	0.90793256	0.1666301953E-02
5	0.04011531	1.34805360	0.2701001430E-01
6	0.04011531	2.06977730	-0.2223424493E-01
7	0.04011531	3.64704510	0.6998916361E-02
8	0.04011531	11.23264600	-0.9092908423E-03
9	0.12355238	0.10896291	-0.1229642431E+00
10	0.12355238	0.33559821	0.4717347384E+00
11	0.12355238	0.59133984	-0.4651643626E+00
12	0.12355238	0.90793256	0.9962817084E+00
13	0.12355238	1.34805360	-0.1276226929E+01
14	0.12355238	2.06977730	0.7795864921E+00
15	0.12355238	3.64704510	-0.2215678668E+00
16	0.12355238	11.23264600	0.2737675477E-01
17	0.21770511	0.10896291	0.2891126276E+00
18	0.21770511	0.33559821	-0.2411541395E+01
19	0.21770511	0.59133984	0.4451709775E+01
20	0.21770511	0.90793256	-0.5916104705E+01
21	0.21770511	1.34805360	0.6633130630E+01
22	0.21770511	2.06977730	-0.3973171424E+01
23	0.21770511	3.64704510	0.1148495732E+01
24	0.21770511	11.23264600	-0.1428310234E+00
25	0.33426051	0.10896291	-0.5014236271E+00
26	0.33426051	0.33559821	0.4520521450E+01
27	0.33426051	0.59133984	-0.1112526104E+02
28	0.33426051	0.90793256	0.1674630659E+02
29	0.33426051	1.34805360	-0.1709289595E+02
30	0.33426051	2.06977730	0.9959388720E+01

Continued on next page

Table B.2 – continued from previous page

i	$\alpha_i^{(k)}$	$\beta_i^{(k)}$	C_i
31	0.33426051	3.64704510	-0.2904926089E+01
32	0.33426051	11.23264600	0.3617330676E+00
33	0.49629358	0.10896291	0.3691148992E+00
34	0.49629358	0.33559821	-0.4642975913E+01
35	0.49629358	0.59133984	0.1274670370E+02
36	0.49629358	0.90793256	-0.2118020809E+02
37	0.49629358	1.34805360	0.2169847161E+02
38	0.49629358	2.06977730	-0.1253059589E+02
39	0.49629358	3.64704510	0.3772546645E+01
40	0.49629358	11.23264600	-0.4754319741E+00
41	0.76200024	0.10896291	-0.1809029181E+00
42	0.76200024	0.33559821	0.2500421767E+01
43	0.76200024	0.59133984	-0.7609285593E+01
44	0.76200024	0.90793256	0.1339612438E+02
45	0.76200024	1.34805360	-0.1393810450E+02
46	0.76200024	2.06977730	0.8191177607E+01
47	0.76200024	3.64704510	-0.2652360165E+01
48	0.76200024	11.23264600	0.3460395761E+00
49	1.34268030	0.10896291	-0.3393395929E-01
50	1.34268030	0.33559821	-0.8838357055E+00
51	1.34268030	0.59133984	0.2777870668E+01
52	1.34268030	0.90793256	-0.5070333148E+01
53	1.34268030	1.34805360	0.5647602756E+01
54	1.34268030	2.06977730	-0.3354616735E+01
55	1.34268030	3.64704510	0.1188442606E+01
56	1.34268030	11.23264600	-0.1651377670E+00
57	4.13536210	0.10896291	0.1870036658E+00
58	4.13536210	0.33559821	0.4191765900E+00
59	4.13536210	0.59133984	-0.7254042356E+00
60	4.13536210	0.90793256	0.9549950353E+00
61	4.13536210	1.34805360	-0.1622631305E+01
62	4.13536210	2.06977730	0.8926129595E+00
63	4.13536210	3.64704510	-0.3158854492E+00

Continued on next page

Table B.2 – continued from previous page

i	$\alpha_i^{(k)}$	$\beta_i^{(k)}$	C_i
64	4.13536210	11.23264600	0.4519872066E-01
$\gamma \equiv 2\ 0\ 2\ 1$			
1	0.04589142	0.12465222	-0.4544993203E-05
2	0.04589142	0.38711777	0.1753871978E-03
3	0.04589142	0.69514632	-0.2908374912E-03
4	0.04589142	1.10631900	0.1937616620E-03
5	0.04589142	1.76069660	-0.5504100412E-04
6	0.04589142	3.16167810	-0.2590345143E-05
7	0.04589142	9.81885300	0.3537294375E-05
8	0.14251960	0.12465222	-0.8283263110E-03
9	0.14251960	0.38711777	0.2882961865E-02
10	0.14251960	0.69514632	-0.7044119057E-02
11	0.14251960	1.10631900	0.1208480243E-01
12	0.14251960	1.76069660	-0.8850892215E-02
13	0.14251960	3.16167810	0.3211420819E-02
14	0.14251960	9.81885300	-0.5615393109E-03
15	0.25592205	0.12465222	0.3778904276E-02
16	0.25592205	0.38711777	-0.1265670820E-01
17	0.25592205	0.69514632	0.5268784537E-01
18	0.25592205	1.10631900	-0.7447374680E-01
19	0.25592205	1.76069660	0.5134143603E-01
20	0.25592205	3.16167810	-0.1939583611E-01
21	0.25592205	9.81885300	0.3609459940E-02
22	0.40729761	0.12465222	-0.1850338246E-01
23	0.40729761	0.38711777	0.1964881039E-01
24	0.40729761	0.69514632	-0.9278266295E-01
25	0.40729761	1.10631900	0.1667969445E+00
26	0.40729761	1.76069660	-0.1109233499E+00
27	0.40729761	3.16167810	0.4768747213E-01
28	0.40729761	9.81885300	-0.9728947184E-02
29	0.64821044	0.12465222	0.2452749104E-01
30	0.64821044	0.38711777	-0.2206628080E-01
31	0.64821044	0.69514632	0.1119515408E+00

Continued on next page

Table B.2 – continued from previous page

i	$\alpha_i^{(k)}$	$\beta_i^{(k)}$	C_i
32	0.64821044	1.10631900	-0.1861487916E+00
33	0.64821044	1.76069660	0.7751512522E-01
34	0.64821044	3.16167810	-0.4867592996E-01
35	0.64821044	9.81885300	0.1231423886E-01
36	1.16398970	0.12465222	-0.7562685391E-01
37	1.16398970	0.38711777	-0.8661044694E-03
38	1.16398970	0.69514632	-0.1641712051E+00
39	1.16398970	1.10631900	0.4712722505E+00
40	1.16398970	1.76069660	-0.2597092534E+00
41	1.16398970	3.16167810	0.8507230018E-01
42	1.16398970	9.81885300	-0.1807666847E-01
43	3.61486630	0.12465222	-0.1151873725E+00
44	3.61486630	0.38711777	-0.4136720190E-01
45	3.61486630	0.69514632	-0.9558240386E-01
46	3.61486630	1.10631900	0.4532504074E+00
47	3.61486630	1.76069660	-0.1845375904E+00
48	3.61486630	3.16167810	0.1043736131E+00
49	3.61486630	9.81885300	-0.1537030856E-01
$\gamma \equiv 1\ 1\ 1\ 0$			
1	0.04589142	0.12465222	-0.4866938229E-04
2	0.04589142	0.38711777	-0.1458515802E-03
3	0.04589142	0.69514632	0.3281186122E-03
4	0.04589142	1.10631900	-0.4226021938E-03
5	0.04589142	1.76069660	0.2998171719E-03
6	0.04589142	3.16167810	-0.1127048329E-03
7	0.04589142	9.81885300	0.2936410508E-04
8	0.14251960	0.12465222	-0.2504898128E-04
9	0.14251960	0.38711777	-0.5265548964E-02
10	0.14251960	0.69514632	0.4963256286E-02
11	0.14251960	1.10631900	-0.5769305333E-02
12	0.14251960	1.76069660	0.4424222636E-02
13	0.14251960	3.16167810	-0.2011073744E-02
14	0.14251960	9.81885300	0.5788519952E-03

Continued on next page

Table B.2 – continued from previous page

i	$\alpha_i^{(k)}$	$\beta_i^{(k)}$	C_i
15	0.25592205	0.12465222	0.1851282670E-04
16	0.25592205	0.38711777	0.8034383746E-02
17	0.25592205	0.69514632	-0.3170206581E-01
18	0.25592205	1.10631900	0.2216280794E-01
19	0.25592205	1.76069660	-0.1433958645E-01
20	0.25592205	3.16167810	0.7072212353E-02
21	0.25592205	9.81885300	-0.2351274853E-02
22	0.40729761	0.12465222	0.2014357651E-05
23	0.40729761	0.38711777	-0.1019895539E-01
24	0.40729761	0.69514632	0.4134925630E-01
25	0.40729761	1.10631900	-0.4900724944E-01
26	0.40729761	1.76069660	0.2061304370E-01
27	0.40729761	3.16167810	-0.1128969179E-01
28	0.40729761	9.81885300	0.4373172358E-02
29	0.64821044	0.12465222	-0.7329403869E-05
30	0.64821044	0.38711777	0.6398513513E-02
31	0.64821044	0.69514632	-0.3750326707E-01
32	0.64821044	1.10631900	0.4142645560E-01
33	0.64821044	1.76069660	-0.1634689117E-01
34	0.64821044	3.16167810	0.7968526649E-02
35	0.64821044	9.81885300	-0.3264161578E-02
36	1.16398970	0.12465222	0.4470438404E-04
37	1.16398970	0.38711777	0.8876501864E-03
38	1.16398970	0.69514632	0.2859676625E-01
39	1.16398970	1.10631900	-0.2243748552E-01
40	1.16398970	1.76069660	0.8253615321E-02
41	1.16398970	3.16167810	-0.4010945593E-02
42	1.16398970	9.81885300	0.1415435440E-02
43	3.61486630	0.12465222	0.1027736424E-04
44	3.61486630	0.38711777	0.1488674478E-02
45	3.61486630	0.69514632	0.1023799446E-03
46	3.61486630	1.10631900	0.7482735185E-02
47	3.61486630	1.76069660	-0.4434008119E-02
48	3.61486630	3.16167810	0.1560196173E-02

Continued on next page

Table B.2 – continued from previous page

i	$\alpha_i^{(k)}$	$\beta_i^{(k)}$	C_i
49	3.61486630	9.81885300	-0.8083446767E-03
$\gamma \equiv 2\ 2\ 0\ 1$			
1	0.06450960	0.17522372	-0.9922676129E-06
2	0.06450960	0.56369770	0.1221705852E-03
3	0.06450960	1.10631900	-0.1523134894E-03
4	0.06450960	2.17127340	0.1088605050E-03
5	0.06450960	6.98502340	-0.9061751882E-04
6	0.20752850	0.17522372	-0.1090065045E-03
7	0.20752850	0.56369770	-0.2692287200E-03
8	0.20752850	1.10631900	0.3087213448E-02
9	0.20752850	2.17127340	-0.2277606332E-02
10	0.20752850	6.98502340	0.2119734920E-02
11	0.40729761	0.17522372	0.2079958375E-03
12	0.40729761	0.56369770	-0.2667376133E-02
13	0.40729761	1.10631900	-0.8877499020E-03
14	0.40729761	2.17127340	-0.1511321584E-03
15	0.40729761	6.98502340	-0.2069870206E-02
16	0.79936658	0.17522372	-0.2263976040E-03
17	0.79936658	0.56369770	0.1939224400E-02
18	0.79936658	1.10631900	-0.3396150888E-03
19	0.79936658	2.17127340	0.1016127706E-01
20	0.79936658	6.98502340	-0.2185699277E-02
21	2.57157590	0.17522372	0.1298152166E-03
22	2.57157590	0.56369770	-0.7626896248E-03
23	2.57157590	1.10631900	-0.8197544068E-02
24	2.57157590	2.17127340	-0.7645842537E-03
25	2.57157590	6.98502340	0.7937033880E-02
$\gamma \equiv 2\ 2\ 1\ 1$			
1	0.06450960	0.17522372	-0.3339597522E-05
2	0.06450960	0.56369770	-0.1132330265E-04
3	0.06450960	1.10631900	0.2267914059E-04
4	0.06450960	2.17127340	-0.2352307209E-04

Continued on next page

Table B.2 – continued from previous page

i	$\alpha_i^{(k)}$	$\beta_i^{(k)}$	C_i
5	0.06450960	6.98502340	0.1834281885E-04
6	0.20752850	0.17522372	-0.5748859294E-05
7	0.20752850	0.56369770	-0.4563431809E-03
8	0.20752850	1.10631900	0.4295222452E-03
9	0.20752850	2.17127340	-0.3213521201E-03
10	0.20752850	6.98502340	0.2805387071E-03
11	0.40729761	0.17522372	0.3533052459E-05
12	0.40729761	0.56369770	0.2970520213E-03
13	0.40729761	1.10631900	-0.1260175766E-02
14	0.40729761	2.17127340	0.6248126780E-03
15	0.40729761	6.98502340	-0.6892394941E-03
16	0.79936658	0.17522372	-0.2664777462E-04
17	0.79936658	0.56369770	-0.9840418266E-03
18	0.79936658	1.10631900	0.2070404093E-02
19	0.79936658	2.17127340	-0.6012080564E-03
20	0.79936658	6.98502340	0.1244787678E-02
21	2.57157590	0.17522372	-0.4021970008E-04
22	2.57157590	0.56369770	-0.2991833581E-03
23	2.57157590	1.10631900	-0.7585129820E-02
24	2.57157590	2.17127340	-0.1618767394E-02
25	2.57157590	6.98502340	-0.1750811298E-02
$\gamma \equiv 2\ 2\ 2\ 1$			
1	0.08101653	0.22006054	-0.1929412768E-05
2	0.08101653	0.73921874	-0.2006956937E-04
3	0.08101653	1.65572340	0.1507761142E-04
4	0.08101653	5.56184130	-0.3426758073E-04
5	0.27214757	0.22006054	0.3125675258E-04
6	0.27214757	0.73921874	-0.1565966223E-03
7	0.27214757	1.65572340	0.3834815879E-03
8	0.27214757	5.56184130	0.1940567272E-03
9	0.60956396	0.22006054	-0.4781842976E-05
10	0.60956396	0.73921874	-0.4525121801E-03
11	0.60956396	1.65572340	-0.1060836916E-01

Continued on next page

Table B.2 – continued from previous page

i	$\alpha_i^{(k)}$	$\beta_i^{(k)}$	C_i
12	0.60956396	5.56184130	0.5677338934E-02
13	2.04762340	0.22006054	-0.1457667771E-03
14	2.04762340	0.73921874	-0.9277348020E-03
15	2.04762340	1.65572340	-0.8276319924E-02
16	2.04762340	5.56184130	-0.8204815867E-02
$\gamma \equiv 0 \ 2 \ 2 \ 1$			
1	0.10913507	0.29643729	0.1620767206E-03
2	0.10913507	1.10631900	0.7256729573E-02
3	0.10913507	4.12883880	-0.4323400140E-02
4	0.40729761	0.29643729	-0.1575387211E-02
5	0.40729761	1.10631900	-0.1957717882E-01
6	0.40729761	4.12883880	0.9438138297E-02
7	1.52005540	0.29643729	0.1390639775E-02
8	1.52005540	1.10631900	0.6800024355E-02
9	1.52005540	4.12883880	-0.1569399655E-01

B.3 Beryllium-9

TABLE B.3: The three-body wave function parameters found by means of variational approach for the ground state of ${}^9\text{Be}$

i	$\alpha_i^{(k)}$	$\beta_i^{(k)}$	C_i
$\gamma \equiv 0 \ 1 \ 1 \ 1$			
1	0.09222844	0.03467231	-0.5749151068E-03
2	0.09222844	0.10767772	-0.3838851470E-02
3	0.09222844	0.19335659	-0.3343703114E-02
4	0.09222844	0.30772526	0.6152031912E-03
5	0.09222844	0.48974194	0.3127639817E-02
6	0.09222844	0.87942826	-0.2202594466E-02
7	0.09222844	2.73113720	0.7301101473E-04
8	0.28642305	0.03467231	-0.1402006121E-03
9	0.28642305	0.10767772	-0.7091214738E-02
10	0.28642305	0.19335659	0.2305680350E-02
11	0.28642305	0.30772526	-0.1742778302E+00
12	0.28642305	0.48974194	-0.3187167848E-01
13	0.28642305	0.87942826	0.3039506091E-01
14	0.28642305	2.73113720	0.9514809808E-02
15	0.51432908	0.03467231	-0.8527376132E-03
16	0.51432908	0.10767772	0.7747996702E-02
17	0.51432908	0.19335659	-0.4446218448E-01
18	0.51432908	0.30772526	0.4402942877E+00
19	0.51432908	0.48974194	-0.2046128930E+00
20	0.51432908	0.87942826	-0.4056323274E+00
21	0.51432908	2.73113720	-0.7813977210E-01
22	0.81855004	0.03467231	0.5375067316E-02
23	0.81855004	0.10767772	0.2796107394E-01
24	0.81855004	0.19335659	0.1235796374E+00
25	0.81855004	0.30772526	-0.4224621555E+00
26	0.81855004	0.48974194	0.6577748985E+00
27	0.81855004	0.87942826	0.9996163672E+00
28	0.81855004	2.73113720	0.1445247127E+00
29	1.30271490	0.03467231	-0.5298458930E-02

Continued on next page

Table B.3 – continued from previous page

i	$\alpha_i^{(k)}$	$\beta_i^{(k)}$	C_i
30	1.30271490	0.10767772	-0.3527622920E-01
31	1.30271490	0.19335659	-0.1045218882E+00
32	1.30271490	0.30772526	0.2291556567E+00
33	1.30271490	0.48974194	-0.5780951776E+00
34	1.30271490	0.87942826	-0.8020981495E+00
35	1.30271490	2.73113720	-0.6308805304E-01
36	2.33928160	0.03467231	0.1647190294E-02
37	2.33928160	0.10767772	0.1114473473E-01
38	2.33928160	0.19335659	0.3518997183E-01
39	2.33928160	0.30772526	-0.9067262584E-01
40	2.33928160	0.48974194	0.1819309090E+00
41	2.33928160	0.87942826	0.1997706489E+00
42	2.33928160	2.73113720	-0.1672610367E-01
43	7.26483260	0.03467231	-0.1754592338E-03
44	7.26483260	0.10767772	-0.8593955119E-03
45	7.26483260	0.19335659	-0.6094809212E-02
46	7.26483260	0.30772526	0.2033436508E-01
47	7.26483260	0.48974194	-0.2275729417E-01
48	7.26483260	0.87942826	-0.8355648909E-02
49	7.26483260	2.73113720	0.7660503690E-02
$\gamma \equiv 2\ 1\ 1\ 1$			
1	0.09222844	0.03467231	-0.1924771157E-05
2	0.09222844	0.10767772	-0.2356249922E-04
3	0.09222844	0.19335659	-0.2411396428E-04
4	0.09222844	0.30772526	-0.3277817525E-03
5	0.09222844	0.48974194	0.3510077596E-03
6	0.09222844	0.87942826	-0.1042721976E-03
7	0.09222844	2.73113720	0.7300483783E-05
8	0.28642305	0.03467231	-0.1811185889E-04
9	0.28642305	0.10767772	-0.9263076412E-03
10	0.28642305	0.19335659	-0.1355643769E-02
11	0.28642305	0.30772526	-0.1275242738E-02
12	0.28642305	0.48974194	-0.6633639490E-02

Continued on next page

Table B.3 – continued from previous page

i	$\alpha_i^{(k)}$	$\beta_i^{(k)}$	C_i
13	0.28642305	0.87942826	0.4570012890E-02
14	0.28642305	2.73113720	-0.6773126034E-03
15	0.51432908	0.03467231	-0.2451069527E-04
16	0.51432908	0.10767772	0.2390967055E-02
17	0.51432908	0.19335659	-0.5125262756E-02
18	0.51432908	0.30772526	-0.5418800266E-02
19	0.51432908	0.48974194	-0.2109364349E-01
20	0.51432908	0.87942826	-0.2515442562E-01
21	0.51432908	2.73113720	0.6601216814E-02
22	0.81855004	0.03467231	0.2286563138E-04
23	0.81855004	0.10767772	-0.5363732756E-02
24	0.81855004	0.19335659	0.2315350945E-01
25	0.81855004	0.30772526	-0.1755538546E-01
26	0.81855004	0.48974194	0.5532754524E-01
27	0.81855004	0.87942826	-0.3382279171E-01
28	0.81855004	2.73113720	-0.1186306105E-01
29	1.30271490	0.03467231	0.1042128190E-03
30	1.30271490	0.10767772	0.6603541558E-02
31	1.30271490	0.19335659	-0.1579342851E-01
32	1.30271490	0.30772526	0.3817737886E-01
33	1.30271490	0.48974194	-0.1880665950E-01
34	1.30271490	0.87942826	0.6354958107E-01
35	1.30271490	2.73113720	-0.1023900583E-01
36	2.33928160	0.03467231	-0.1138017603E-03
37	2.33928160	0.10767772	-0.3549492629E-02
38	2.33928160	0.19335659	-0.2172338237E-02
39	2.33928160	0.30772526	-0.1716855378E-01
40	2.33928160	0.48974194	-0.2158352491E-01
41	2.33928160	0.87942826	-0.2664998049E-02
42	2.33928160	2.73113720	0.1795868885E-01
43	7.26483260	0.03467231	0.5481566912E-04
44	7.26483260	0.10767772	0.1616977160E-02
45	7.26483260	0.19335659	0.2999057062E-02
46	7.26483260	0.30772526	0.5941831686E-02

Continued on next page

Table B.3 – continued from previous page

i	$\alpha_i^{(k)}$	$\beta_i^{(k)}$	C_i
47	7.26483260	0.48974194	0.2509228284E-01
48	7.26483260	0.87942826	-0.2888442185E-01
49	7.26483260	2.73113720	-0.1306911414E-01
$\gamma \equiv 2\ 1\ 2\ 1$			
1	0.09222844	0.03467231	-0.3010378678E-05
2	0.09222844	0.10767772	-0.3755683361E-04
3	0.09222844	0.19335659	-0.1320445807E-04
4	0.09222844	0.30772526	-0.4112501943E-04
5	0.09222844	0.48974194	0.6953669839E-04
6	0.09222844	0.87942826	-0.2860739308E-04
7	0.09222844	2.73113720	0.5423290871E-05
8	0.28642305	0.03467231	-0.1103139569E-04
9	0.28642305	0.10767772	-0.5090367741E-03
10	0.28642305	0.19335659	-0.7148466875E-03
11	0.28642305	0.30772526	-0.3929303844E-02
12	0.28642305	0.48974194	-0.3977209961E-04
13	0.28642305	0.87942826	0.9213700358E-03
14	0.28642305	2.73113720	-0.1948617319E-03
15	0.51432908	0.03467231	-0.4733213692E-04
16	0.51432908	0.10767772	-0.2857738750E-03
17	0.51432908	0.19335659	-0.2777454876E-02
18	0.51432908	0.30772526	0.3561667784E-02
19	0.51432908	0.48974194	-0.2946736188E-01
20	0.51432908	0.87942826	-0.8666890705E-02
21	0.51432908	2.73113720	0.2748423502E-02
22	0.81855004	0.03467231	0.5631914170E-04
23	0.81855004	0.10767772	-0.7971505555E-03
24	0.81855004	0.19335659	0.5371812194E-02
25	0.81855004	0.30772526	-0.2551441441E-01
26	0.81855004	0.48974194	0.4680352343E-01
27	0.81855004	0.87942826	-0.3854700723E-01
28	0.81855004	2.73113720	-0.1222388447E-01
29	1.30271490	0.03467231	0.6206550924E-04

Continued on next page

Table B.3 – continued from previous page

i	$\alpha_i^{(k)}$	$\beta_i^{(k)}$	C_i
30	1.30271490	0.10767772	0.3834269660E-02
31	1.30271490	0.19335659	0.4162933824E-03
32	1.30271490	0.30772526	0.4735754022E-01
33	1.30271490	0.48974194	-0.1389393548E-01
34	1.30271490	0.87942826	0.8961263346E-01
35	1.30271490	2.73113720	0.8808594255E-02
36	2.33928160	0.03467231	-0.7647542798E-04
37	2.33928160	0.10767772	-0.2890372198E-02
38	2.33928160	0.19335659	-0.3276057155E-02
39	2.33928160	0.30772526	-0.2749917292E-01
40	2.33928160	0.48974194	-0.4710540922E-02
41	2.33928160	0.87942826	-0.5466921396E-01
42	2.33928160	2.73113720	0.2818082044E-02
43	7.26483260	0.03467231	0.3333979438E-04
44	7.26483260	0.10767772	0.1155051008E-02
45	7.26483260	0.19335659	0.1905609943E-02
46	7.26483260	0.30772526	0.9732835265E-02
47	7.26483260	0.48974194	0.2074495567E-02
48	7.26483260	0.87942826	0.1851242373E-01
49	7.26483260	2.73113720	-0.4869370430E-02
$\gamma \equiv 2\ 3\ 1\ 1$			
1	0.10776416	0.04051280	-0.1718969469E-07
2	0.10776416	0.12746398	-0.1350667625E-05
3	0.10776416	0.23612589	-0.1105295982E-04
4	0.10776416	0.40103536	-0.9776430048E-06
5	0.10776416	0.74291449	0.7818043812E-05
6	0.10776416	2.33740540	-0.1657183025E-05
7	0.33905453	0.04051280	0.5619336286E-07
8	0.33905453	0.12746398	0.5297325790E-06
9	0.33905453	0.23612589	0.2429380314E-04
10	0.33905453	0.40103536	-0.7202852868E-03
11	0.33905453	0.74291449	-0.5017077937E-03
12	0.33905453	2.33740540	0.7685878901E-04

Continued on next page

Table B.3 – continued from previous page

i	$\alpha_i^{(k)}$	$\beta_i^{(k)}$	C_i
13	0.62809554	0.04051280	-0.2882973360E-06
14	0.62809554	0.12746398	-0.1419326948E-04
15	0.62809554	0.23612589	-0.1971653098E-03
16	0.62809554	0.40103536	0.1367614996E-02
17	0.62809554	0.74291449	-0.2329445855E-03
18	0.62809554	2.33740540	-0.1038875830E-02
19	1.06675520	0.04051280	0.5215988170E-06
20	1.06675520	0.12746398	0.2838726456E-04
21	1.06675520	0.23612589	0.5215310433E-03
22	1.06675520	0.40103536	-0.1687394348E-02
23	1.06675520	0.74291449	0.2978139773E-02
24	1.06675520	2.33740540	0.5095314999E-02
25	1.97615460	0.04051280	-0.4079628548E-06
26	1.97615460	0.12746398	-0.1393485092E-04
27	1.97615460	0.23612589	-0.5466031490E-03
28	1.97615460	0.40103536	0.1777350931E-02
29	1.97615460	0.74291449	-0.3110115061E-02
30	1.97615460	2.33740540	-0.6388951126E-02
31	6.21750490	0.04051280	0.2858299794E-06
32	6.21750490	0.12746398	-0.2515569774E-05
33	6.21750490	0.23612589	0.4286470482E-03
34	6.21750490	0.40103536	-0.1506471110E-02
35	6.21750490	0.74291449	0.1647806248E-02
36	6.21750490	2.33740540	0.3849236254E-02
$\gamma \equiv 2\ 3\ 2\ 1$			
1	0.12964559	0.04873889	0.1693294553E-07
2	0.12964559	0.15679385	0.1049895108E-05
3	0.12964559	0.30772526	0.1228675253E-04
4	0.12964559	0.60394482	0.2771362931E-05
5	0.12964559	1.94290080	-0.2211980330E-04
6	0.41707208	0.04873889	0.3551996642E-07
7	0.41707208	0.15679385	0.1075704259E-04
8	0.41707208	0.30772526	0.8745751123E-04

Continued on next page

Table B.3 – continued from previous page

i	$\alpha_i^{(k)}$	$\beta_i^{(k)}$	C_i
9	0.41707208	0.60394482	0.9594057967E-03
10	0.41707208	1.94290080	0.8746328794E-03
11	0.81855004	0.04873889	0.6352400316E-07
12	0.81855004	0.15679385	-0.1942454226E-04
13	0.81855004	0.30772526	0.1609826431E-04
14	0.81855004	0.60394482	-0.1726785289E-02
15	0.81855004	1.94290080	-0.4042936946E-04
16	1.60649490	0.04873889	-0.1710826173E-06
17	1.60649490	0.15679385	0.2301228629E-05
18	1.60649490	0.30772526	-0.1979072562E-03
19	1.60649490	0.60394482	0.9738317810E-03
20	1.60649490	1.94290080	-0.3203561255E-02
21	5.16812160	0.04873889	0.1116340388E-06
22	5.16812160	0.15679385	0.1167778442E-04
23	5.16812160	0.30772526	0.1738791058E-03
24	5.16812160	0.60394482	-0.3609843531E-03
25	5.16812160	1.94290080	0.5494840873E-02
$\gamma \equiv 4\ 3\ 1\ 1$			
1	0.16281973	0.06121036	0.1321914819E-08
2	0.16281973	0.20561544	-0.4736845147E-06
3	0.16281973	0.46054339	-0.3319521179E-05
4	0.16281973	1.54703930	0.3553888116E-05
5	0.54693765	0.06121036	-0.6503262677E-07
6	0.54693765	0.20561544	0.1654995181E-05
7	0.54693765	0.46054339	-0.1640576015E-03
8	0.54693765	1.54703930	-0.4829795892E-03
9	1.22504670	0.06121036	0.1390571831E-06
10	1.22504670	0.20561544	-0.2891665504E-05
11	1.22504670	0.46054339	0.3281309143E-03
12	1.22504670	1.54703930	0.8592636208E-03
13	4.11512900	0.06121036	-0.1154820611E-06
14	4.11512900	0.20561544	0.2842324272E-05
15	4.11512900	0.46054339	-0.2326745567E-03

Continued on next page

Table B.3 – continued from previous page

i	$\alpha_i^{(k)}$	$\beta_i^{(k)}$	C_i
16	4.11512900	1.54703930	-0.5225362461E-03
$\gamma \equiv 4\ 3\ 2\ 1$			
1	0.16281973	0.06121036	-0.1950076982E-09
2	0.16281973	0.20561544	-0.2964169729E-06
3	0.16281973	0.46054339	-0.1306289078E-05
4	0.16281973	1.54703930	0.1006880888E-05
5	0.54693765	0.06121036	-0.2314866478E-07
6	0.54693765	0.20561544	-0.1222001577E-06
7	0.54693765	0.46054339	-0.1063250475E-03
8	0.54693765	1.54703930	-0.1370765485E-03
9	1.22504670	0.06121036	0.4339252791E-07
10	1.22504670	0.20561544	0.1146087127E-05
11	1.22504670	0.46054339	0.2039624307E-03
12	1.22504670	1.54703930	0.3150677285E-03
13	4.11512900	0.06121036	-0.2831722723E-07
14	4.11512900	0.20561544	-0.1086792529E-05
15	4.11512900	0.46054339	-0.1370131651E-03
16	4.11512900	1.54703930	-0.2779272754E-03

Bibliography

1. Donoghue, J. F., Golowich, E. & Holstein, B. R. *Dynamics of the standard model* (Cambridge university press, 2014).
2. Griffiths, D. *Introduction to elementary particles* (John Wiley & Sons, 2020).
3. Ramond, P. *Journeys beyond the standard model* (Perseus Books Cambridge, 1999).
4. Ter-Akopian, G. *et al.* Radioactive ion beam research made in Dubna. *Nuclear Physics A* **734**, 295–302 (2004).
5. Yano, Y. The RIKEN RI beam factory project: A status report. *Nuclear Instruments and Methods in Physics Research Section B: Beam Interactions with Materials and Atoms* **261**, 1009–1013 (2007).
6. Gade, A & Sherrill, B. NSCL and FRIB at Michigan State University: Nuclear science at the limits of stability. *Physica Scripta* **91**, 053003 (2016).
7. Hong, B. *et al.* Plan for nuclear symmetry energy experiments using the LAMPS system at the RIB facility RAON in Korea. *The European Physical Journal A* **50**, 49 (2014).
8. Fukuda, N *et al.* Identification and separation of radioactive isotope beams by the BigRIPS separator at the RIKEN RI Beam Factory. *Nuclear Instruments and Methods in Physics Research Section B: Beam Interactions with Materials and Atoms* **317**, 323–332 (2013).
9. Rutherford, E. VIII. Uranium radiation and the electrical conduction produced by it. *The London, Edinburgh, and Dublin Philosophical Magazine and Journal of Science* **47**, 109–163 (1899).
10. Stuewer, R. H. in *The kaleidoscope of science* 147–186 (Springer, 1986).
11. Poenaru, D., Gherghescu, R. & Greiner, W. Cluster decay of superheavy nuclei. *Physical Review C* **85**, 034615 (2012).
12. Canto, L., Gomes, P., Donangelo, R & Hussein, M. Fusion and breakup of weakly bound nuclei. *Physics reports* **424**, 1–111 (2006).

13. Brown, T. A. D. *et al.* Decay studies for states in ${}^9\text{Be}$ up to 11 MeV: Insights into the $\text{n}+{}^8\text{Be}$ and $\alpha+{}^5\text{He}$ cluster structure. *Phys. Rev.* **C76**, 054605 (2007).
14. Papka, P. *et al.* Decay path measurements for the 2.429 MeV state in ${}^9\text{Be}$: Implications for the astrophysical $\alpha + \alpha + \text{n}$ reaction. *Phys. Rev.* **C75**, 045803 (2007).
15. Descouvemont, P. & Baye, D. ${}^{12}\text{Be}$ molecular states in a microscopic cluster model. *Physics Letters B* **505**, 71–74 (2001).
16. Tohsaki, A., Horiuchi, H., Schuck, P. & Röpke, G. Alpha Cluster Condensation in C 12 and O 16. *Physical Review Letters* **87**, 192501 (2001).
17. Kanada-En'yo, Y., Horiuchi, H. & Ono, A. Structure of Li and Be isotopes studied with antisymmetrized molecular dynamics. *Physical Review C* **52**, 628 (1995).
18. Pudliner, B., Pandharipande, V., Carlson, J., Pieper, S. C. & Wiringa, R. B. Quantum Monte Carlo calculations of nuclei with $A < \sim 7$. *Physical Review C* **56**, 1720 (1997).
19. Zhukov, M. *et al.* Bound state properties of Borromean halo nuclei: ${}^6\text{He}$ and ${}^{11}\text{Li}$. *Physics reports* **231**, 151–199 (1993).
20. Navrátil, P., Quaglioni, S., Stetcu, I. & Barrett, B. R. Recent developments in no-core shell-model calculations. *Journal of Physics G: Nuclear and Particle Physics* **36**, 083101 (2009).
21. Forssén, C., Navrátil, P., Ormand, W. & Caurier, E. Large basis ab initio shell model investigation of Be 9 and Be 11. *Physical Review C* **71**, 044312 (2005).
22. Navratil, P. & Ormand, W. E. Ab initio shell model with a genuine three-nucleon force for the p-shell nuclei. *Physical Review C* **68**, 034305 (2003).
23. Navratil, P. & Ormand, W. E. Ab initio shell model calculations with three-body effective interactions for p-shell nuclei. *Physical review letters* **88**, 152502 (2002).
24. Horiuchi, H. Generator coordinate treatment of composite particle reaction and molecule-like structures. *Progress of Theoretical Physics* **43**, 375–389 (1970).
25. Tang, Y.-C., LeMere, M. & Thompson, D. Resonating-group method for nuclear many-body problems. *Physics Reports* **47**, 167–223 (1978).

26. Wheeler, J. A. On the mathematical description of light nuclei by the method of resonating group structure. *Physical Review* **52**, 1107 (1937).
27. Nesterov, A., Arickx, F., Broeckhove, J. & Vasilevsky, V. Three-cluster description of properties of light neutron-and proton-rich nuclei in the framework of the algebraic version of the resonating group method. *Physics of Particles and Nuclei* **41**, 716–765 (2010).
28. Brink, D. & Bloch, C. *Proceedings of the International School of Physics “enrico fermi” Course XXXVI* 1966.
29. Arai, K., Suzuki, Y. & Lovas, R. Structure of ${}^6\text{He}$ with an extended three-cluster model. *Physical Review C* **59**, 1432 (1999).
30. Descouvemont, P. Halo structure of ${}^{14}\text{Be}$ in a microscopic ${}^{12}\text{Be} + \text{n} + \text{n}$ cluster model. *Physical Review C* **52**, 704 (1995).
31. Kukulin, V. & Krasnopol’sky, V. A stochastic variational method for few-body systems. *Journal of Physics G: Nuclear Physics* **3**, 795 (1977).
32. Voronchev, V., Kukulin, V., Pomerantsev, V., Razikov, K. D. & Ryzhikh, G. Study of the Structure and Properties of Nuclei with $A = 9$ (${}^9\text{Be}$ - ${}^9\text{B}$) in Terms of Multicluster Dynamic Model $2\alpha + \text{N}$. *Yad. Fiz.* **57**, 1964–1980 (1994).
33. Kukulin, V., Krasnopol’Sky, V., Voronchev, V. & Sazonov, P. Detailed study of the cluster structure of light nuclei in a three-body model:(II). The spectrum of low-lying states of nuclei with $A = 6$. *Nuclear Physics A* **453**, 365–388 (1986).
34. Kukulin, V., Krasnopol’sky, V., Voronchev, V. & Sazonov, P. Detailed study of the cluster structure of light nuclei in a three-body model:(I). Ground state of ${}^6\text{Li}$. *Nuclear Physics A* **417**, 128–156 (1984).
35. Kukulin, V. & Pomerantsev, V. The orthogonal projection method in scattering theory. *Annals of Physics* **111**, 330–363 (1978).
36. Feshbach, H. The optical model and its justification. *Annual Review of Nuclear Science* **8**, 49–104 (1958).
37. Satchler, G. & Tobocman, W. Gamma Rays from Deuteron Stripping Reactions. *Physical Review* **118**, 1566 (1960).
38. Golovkov, M., Kulikauskas, V., Voronchev, V., Krasnopol’skii, V. & Kukulin, V. Cross sections for low-energy deuteron reactions in ${}^6\text{Li}$. *Soviet Journal of Nuclear Physics* **34**, 480–481 (1981).

39. Glozman, L. Y., Kukulin, V. & Neudatchin, V. A study of the ${}^6\text{Li}$ (π^+ , pp) ${}^4\text{He}$ reaction within the three-body problem. *Nuclear Physics A* **430**, 589–604 (1984).
40. Zhusupov, M., Ibreaeva, E., Kukulin, V. & Peresypkin, V. Elastic and inelastic scattering of protons and antiprotons by the ${}^6\text{Li}$ nucleus at intermediate energies. *Physics of Atomic Nuclei* **57**, 1937–1948 (1994).
41. Kukulin, V. I. & Voronchev, V. T. Pinch-based thermonuclear D^3He fusion driven by a femtosecond laser. *Phys. At. Nucl.* **73**, 1376 (2010).
42. Seksembayev, Z., Kukulin, V. & Sakhiev, S. Study of a dense hot plasma's burning in Z-pinch devices with inertial-magnetic confinement. *Phys. Scr.* **93**, 085602 (2018).
43. Kakenov, M., Kukulin, V., Pomerantsev, V. & Bayakhmetov, O. Properties of dibaryons in nuclear medium. *The European Physical Journal A* **56**, 1–18 (2020).
44. Blokhintsev, L., Kukulin, V., Sakharuk, A., Savin, D. & Kuznetsova, E. Determination of the α + d vertex constant (asymptotic coefficient) from the He 4+ d phase-shift analysis. *Physical Review C* **48**, 2390 (1993).
45. Tursunov, E., Kadyrov, A., Turakulov, S. & Bray, I. Theoretical study of the $\alpha + \text{d} \rightarrow \text{Li } 6 + \gamma$ astrophysical capture process in a three-body model. *Physical Review C* **94**, 015801 (2016).
46. Suzuki, Y., Suzuki, M. & Varga, K. *Stochastic variational approach to quantum-mechanical few-body problems* (Springer Science & Business Media, 1998).
47. Kukulin, V., Voronchev, V. & Razikov, K. D. *Dynamic multicenter model of light nuclei. Main formalism* tech. rep. (Moskovskij Gosudarstvennyj Univ., 1990).
48. Satchler, G. R. & Love, W. G. Folding model potentials from realistic interactions for heavy-ion scattering. *Physics Reports* **55**, 183–254 (1979).
49. De Shalit, A. & Talmi, I. *Nuclear shell theory* 1963.
50. Anantaraman, N., Toki, H. & Bertsch, G. An effective interaction for inelastic scattering derived from the Paris potential. *Nuclear Physics A* **398**, 269–278 (1983).
51. Day, B. Three-body correlations in nuclear matter. *Physical Review C* **24**, 1203 (1981).

52. Sack, S, Biedenharn, L. & Breit, G. The Elastic Scattering of Protons by Alpha Particles. *Physical Review* **93**, 321 (1954).
53. Buck, B, Friedrich, H & Wheatley, C. Local potential models for the scattering of complex nuclei. *Nuclear Physics A* **275**, 246–268 (1977).
54. Pomerantsev, V. Private communication.
55. Antonov, A. *et al.* Charge and matter distributions and form factors of light, medium, and heavy neutron-rich nuclei. *Physical Review C* **72**, 044307 (2005).
56. Egelhof, P *et al.* in *Exotic Nuclei and Atomic Masses* 61–67 (Springer, 2003).
57. Hirai, M, Kumano, S, Saito, K. & Watanabe, T. Clustering aspects in nuclear structure functions. *Physical Review C* **83**, 035202 (2011).
58. Thompson, I. J. Coupled reaction channels calculations in nuclear physics. *Comp. Phys. Rep.* **7**, 167 –212 (1988).
59. Oganessian, Y. T., Zagrebaev, V. & Vaagen, J. Dynamics of two-neutron transfer reactions with the Borromean nucleus ${}^6\text{He}$. *Physical Review C* **60**, 044605 (1999).
60. Avrigeanu, V, Hodgson, P. & Avrigeanu, M. Global optical potentials for emitted alpha particles. *Physical Review C* **49**, 2136 (1994).
61. Urazbekov, B. A., Denikin, A. S., Sakhiev, S. K. & Burtebaev, N. T. Manifestation of the cluster structure of the ${}^9\text{Be}$ nucleus in direct nuclear reactions. *Bull. Rus. Acad. Sci. Phys.* **80**, 247 (2016).
62. Kunz, P. D. *Computer code DWUCK5* unpublished. <https://www.oecd-nea.org/tools/abstract/detail/nesc9872>.
63. Karpov, A. *et al.* NRV web knowledge base on low-energy nuclear physics. *Nucl. Instr. and Meth. Phys. Res. t* **A859**, 112 –124. <http://nrv.jinr.ru> (2017).
64. Lukyanov, S. *et al.* Study of internal structures of 9 , ${}^{10}\text{Be}$ and ${}^{10}\text{B}$ in scattering of ${}^4\text{He}$ from ${}^9\text{Be}$. *Journal of Physics G: Nuclear and Particle Physics* **41**, 035102 (2014).
65. Harakeh, M., Van Popta, J, Saha, A & Siemssen, R. Strong coupled-channels effects in the ${}^9\text{Be} (\alpha, t) {}^{10}\text{B}$ reaction. *Nuclear Physics A* **344**, 15–40 (1980).
66. Szczurek, A. *et al.* Mechanism of Reactions Induced by 7 MeV Deuterons on ${}^9\text{Be}[(d, p), (d, d), (d, t), (d, {}^4\text{He})]$. *Z. Phys. A* **333**, 271 (1989).

67. Votava, H. J., Clegg, T. B., Ludwig, E. J. & Thompson, W. J. Proton Scattering from ${}^9\text{Be}$ between 6 and 30 MeV and the Structure of ${}^9\text{Be}$. *Nucl. Phys.* **A204**, 529 (1973).
68. Koning, A. J. & Delaroche, J. P. Local and global nucleon optical models from 1 keV to 200 MeV. *Nucl. Phys.* **A713**, 231 (2003).
69. Li, X., Liang, C. & Cai, C. Global triton optical model potential. *Nucl. Phys.* **A789**, 103 (2007).
70. Caurier, E., Martínez-Pinedo, G., Nowacki, F., Poves, A. & Zuker, A. P. The shell model as a unified view of nuclear structure. *Rev. Mod. Phys.* **77**, 427–488 (2 2005).
71. Cohen, S. & Kurath, D. Effective Interactions for the 1p Shell. *Nucl. Phys.* **73**, 1 (1965).
72. Volya, A. *Private communication*.
73. Kravvaris, K. & Volya, A. Study of Nuclear Clustering from an Ab Initio Perspective. *Phys. Rev. Lett.* **119**, 062501 (2017).
74. Della Rocca, V. & Iachello, F. Cluster shell model: I. Structure of ${}^9\text{Be}$, ${}^9\text{B}$. *Nucl. Phys.* **A973**, 1 (2018).
75. Galanina, L. I. & Zelenskaya, N. S. Mechanisms of sequential particle transfer and characteristics of light neutron-excess and oriented nuclei. *Phys. Part. Nucl.* **43**, 147 (2012).
76. Rudchik, A. T. *et al.* Elastic and inelastic scattering of ${}^{15}\text{N}$ ions by ${}^9\text{Be}$ at 84 MeV. *Nucl. Phys.* **A947**, 161 (2016).
77. Avrigeanu, V., Hodgson, P. E. & Avrigeanu, M. Global Optical Potentials for Emitted Alpha Particles. *Phys. Rev.* **C49**, 2136 (1994).
78. Cook, J. Global Optical-Model Potentials for the Elastic Scattering of ${}^{6,7}\text{Li}$ Projectiles. *Nucl. Phys.* **A388**, 153 (1982).
79. Kwasniewicz, E. & Jarczyk, L. Five-Nucleon Spectroscopic Amplitudes for 1p-Shell Nuclei. *Nucl. Phys.* **A441**, 77 (1985).
80. Tanaka, S. The ${}^9\text{Be}(\text{d}, \text{t}){}^8\text{Be}$ and ${}^9\text{Be}(\text{d}, \alpha){}^7\text{Li}$ Reaction in the Energy Range from 12.17 MeV to 14.43 MeV. *J. Phys. Soc. Jpn.* **44**, 1405 (1978).
81. Jarczyk, L. *et al.* Five-Nucleon Simultaneous and Sequential Transfer in the ${}^{12}\text{C}({}^{11}\text{B}, {}^6\text{Li}){}^{17}\text{O}$ and ${}^{12}\text{C}(\text{d}, {}^7\text{Li}){}^7\text{Be}$ Reactions. *Phys. Rev.* **C54**, 1302 (1996).